universität wien

MASTERARBEIT / MASTER'S THESIS

Titel der Masterarbeit / Title of the Master's Thesis

„Effect of pore network geometry on the efficiency of microbial soil organic matter decomposition“

verfasst von / submitted by

Magdalena Rath, Bakk.phil BSc

angestrebter akademischer Grad / in partial fulfilment of the requirements for the degree of

Master of Science (MSc)

Wien, 2023 / Vienna, 2023

Studienkennzahl lt. Studienblatt / degree programme code as it appears on the student record sheet:	A 066 910
Studienrichtung lt. Studienblatt / degree programme as it appears on the student record sheet:	Computational Science
Betreut von / Supervisor:	Assoz. Prof. Dr. Christina Kaiser
Mitbetreut von / Co-Supervisor:	Dr. Ksenia Guseva

Acknowledgements

First of all, i would like to thank my supervisor Christina Kaiser for giving me the opportunity to work on this fascinating topic and guiding me through the challenges in such a supportive way. I also want to thank Ksenia for her great support and many helpful advices.
Further I thank Amadeus who's everlasting support and encouragement helped me through all the difficult times in the last years. Thank you!

Contents

Part I

General Introduction

Microbial decomposition of soil organic matter is one of the major drivers of nutrient and carbon (C) cycling in terrestrial ecosystems. Autotrophs, like plants, take up carbon from the atmosphere via photosynthesis and store it in their cells. The carbon is used to build up cell components and to store energy in form of sugars. On the other hand they emit carbon into the atmosphere in form of CO_2 via respiration. The net amount of carbon taken up by plants is subsequently added to the soils as dead organic material from plants and other living organisms. Microorganisms that are allocated in the soils produce extracellular enzymes to break down the plant material and use the carbon contained to built up their cell components and metabolic products. They also emit carbon into the atmosphere by respiration (Heimann and Reichstein, 2008). Is the system in an equilibrium state, the C flux from the soil to the atmosphere roughly equals the net photosynthesis flux(Crowther et al., 2016).
With $3500 - 4800Pg$ C contained in the soils of the earth, this C pool is larger than that of the atmosphere ($828Pg$) and of living plants ($450 - 650Pg$) (Ciais et al., 2013). Given these facts, it is not a surprise that it is widely unchallenged that soils play a crucial role in climate change. And indeed, the observed short-term responses of carbon losses to soil warming are without question far-reaching in many studies (Crowther et al., 2016). How exactly the interdependent processes of C cycling, C storage and climate change impact each other is part of scientific debate though. It is not understood in detail what effects of earth warming and altered rainfall patterns on the terrestrial C cycle are to be expected globally. A lack of data and understanding of mechanisms limits accuracy of spatial and temporal extrapolation of local short-term observations. Also if a change in soil management may be able to enhance C storage in soils and therefore may compensate the increased emission due to the consumption of fossil fuels is unclear. (Baveye et al., 2018; Heimann and Reichstein, 2008; Crowther et al., 2016) The precise prediction of processes in relation to terrestrial decomposition of organic matter is of high importance for some of the most urgent issues of today and requires profound understanding of the system and its interrelations.

Various ecological interactions influencing the efficiency of decomposition have been studied in detail. Computational models are a broadly used tool in soil science to investigate questions that are difficult to address experimentally. There are macroscale models which as an example brought insight in the biogeochemical processes involved (Schimel and Weintraub, 2003) and the impact of microbial community composition on C-cycling rates (Schimel and Schaeffer, 2012). Specifically the effort in the improvement of macroscopic models of soil organic matter (SOM) turnover for integration in large-scale carbon-cycling or earth system models has been immense (Pot et al., 2022).

These theoretical models are all concerned with the large scale fluxes of carbon and are based on the assumptions that all components are well mixed on smaller scales and bulk soil characteristics describe the microbial environment at every point in the soil matrix adequately. But in fact, soils are highly heterogeneous habitats built up hierarchically from soil aggregates - the structural unit of soils - which provide a complex pore system within and between the aggregates. Microaggregates in the size range of $20 - 250\mu m$ combine to

macroaggregates ($> 250\mu m$). The soil pores can be seen as microsites for storing air, water, nutrients and microbes that are connected in local biogeochemical cycles. The physical and chemical conditions are highly heterogeneous between the microsites. (Menon et al., 2020) How this heterogeneity affects the system, and how to scale up the processes is a subject of ongoing debates in the field.
The 3-dimensional structure of the pore space causes the emergence of spatially isolated distinct microbial microcolonies that are influenced by distinct environmental factors. Depending on the water content in the soil, diffusion allows for transfer of substrate and metabolites between soil pores. Or, at unsaturated conditions, exchange of solubles between pores is impeded. Water flow depends on water content and pore size and connectivity. Flow paths determine the pattern of soluble carbon distribution and their transport rates. The diffusion of gases, like O_2 similarly depends on pore size and connectivity, but strongly decreases with increased water saturation. (König et al., 2020; Wilpiszeski et al., 2019) As a consequence, O_2 concentrations strongly vary between soil pores in spatial proximity. Similarly, redox conditions and pH present a heterogeneous spatial pattern at the micro-scale. (König et al., 2020) Spatial segregation is also known as driver of microbial diversity in disconnected habitats like soil pores under unsaturated conditions. In an experiment with two distinct soil textures Carson et al. (2010) could prove that lower connectivity of the soil pores enhances the diversity of microbes. Also the evolutionary processes of soil microbes are determined by the compartmentalization of the habitat(Rillig et al., 2017) and the spatial structure of soil pore space regulates microbial community composition (Wilpiszeski et al., 2019). This leads to distinct biotic interactions between the microsites in addition to the abiotic interactions described above.
To reflect the immense spatial heterogeneity of the habitat the necessity of a micro-scale perspective to gain insight in biological mechanism relevant for decomposition of organic matter has been pointed out many times (Baveye et al., 2018; Pot et al., 2022; König et al., 2020; Golparvar et al., 2021). Since crucial chemical, physical and biological conditions at the micro-scale are not precisely described by bulk soil measurements it is of great importance to include the spatial heterogeneity in models of microbial degradation.

In the beginning, there were major hurdles that stood in the way of scientific progress in integration of the spatial heterogeneity in ecological soil models. The opacity of soil and the complexity of interrelated biological and environmental factors were strong burdens for the experimental study of interplay between soil structure and microbial activity. Some of the technical difficulties have been overcome in recent years. Baveye et al. (2018)
Only since 20 years ago significant advances have enabled methods that provide increasingly reliable information about the geometry of pores and solids in soils at resolutions as small as $0.05\mu m$ (Baveye et al., 2018; Vogel et al., 2015). X-ray computed tomography has enabled the extraction of soil pore characteristics and pore network geometry from undisturbed soils (Munkholm et al. 2012). The application of near-edge X-ray spectromicroscopy, X-ray absorption spectroscopy or micro-flourescence spectroscopy to soil thin sections has shown sharp heterogeneity of the chemical characteristics and new biological markers allow

to identify specific bacteria and their spatial distribution in soil thin sections. (Baveye et al., 2018)
Additionally soil zymography enables the nondestructive investigation of spatial distribution of extracellular enzyme activity. Heitkötter and Marschner (2018) were able to confirm the heterogeneous distribution of microbial activity in undisturbed soil samples via zymography. They showed that active microorganisms are not uniformly distributed in the soil matrix, but occupy a non-random, patchy distribution of microsites. There are spatially segregated hotspots, that are characterized by higher substrate availability compared to the surrounding bulk soil and highly active microbes, producing extracellular enzymes for degradation of organic material. The substrate in the areas outside of these hotspots has been depleted and microbes may only be present in dormant state in these areas. Great efforts have also been made in investigating the spatial patterns of further chemical and physical properties. Models for the prediction of air/water-interfaces in the pore space have been developed (Pot et al., 2015), which help to understand the uneven distribution of air and O_2 as an important reaction partner (Golparvar et al., 2021) and the distribution of water, that is crucial for diffusion processes.
Improvement of imaging techniques has lead to a huge amount of information about the distribution of voids and solids in soils in three dimensions. In order to make this information useful for computational models of organic matter decomposition the grey scale image from an X-ray scanning needs to be segmented and voxel-wise converted into a bimodal image that distinguishes between voids and solids first. Then the pore network can be extracted from these images by discretization of the 3D space. The pore space can be depicted in voxels or each pore is represented as ideal geometrical shape, which has the advantage that the computational effort is kept low and the model usually runs faster. In this step also statistical measures can be calculated, such as pore size distribution and length of the throats. (Ngom et al., 2011)

The 3D-structure of soil, the pore sizes and their distribution are a result of various factors like tillage method or diversity of crop plants and themselves are important for SOM decomposition. For instance, in a comparison of X-ray microtomography images from soil aggregates from a conventionally tilled soil and grassland the intra-aggregate porosity was higher in the former (15% in conventionally tilled soil) than in the latter (11% in grassland). Also the pore volumes and throat surface area were distinct in the aggregates from the two soil types. There were more small pores found in the conventionally tilled soil. (Peth et al., 2008)
A similar result gained Kravchenko et al. (2011) in a study of the impact of long-term differences in soil treatments. Conventional tillage resulted in higher overall porosity of the aggregates compared to no tillage treatment and native succession vegetation. Especially the porosity associated with small pores was the highest in the tilled soil. In contrast, very large pores originating from root channels were most abundant in the native succession vegetation soil. In addition, an effect of the fertilizer treatment on the soil structure could be found. A combination of inorganic fertilizer and organic manure decreased soil bulk density

compared to no fertilizer treatment, whereas application of inorganic fertilizer alone did not cause a change. (Zhou et al., 2016) As Kravchenko et al. (2019) showed by combining 2D zymography and 3D X-ray micro-CT-scanning the abundance of 6 extracellular enzymes related with microbial nutrient cycling depends on the pore sizes. The highest enzyme activities could be found in pores with radii ranging from $30\mu m - 150\mu m$. This effect was shown for different cropping systems. Further, it has been stated that diverse plant communities favor the formation of $30 - 150\mu m$ pores in contrast to monocultures.
It is worth noting, that results gained from CT images are always limited by the resolution of the scanning method and the simplifications introduced in the following processes, image processing and segmentation method (Menon et al., 2020; Pot et al., 2022).

All these studies contribute to the understanding of soil as a spatially structured habitat with high heterogeneity. For various biological systems it was shown that the heterogeneity of the habitat can either enhance or undermine the invasion (Pérez-Reche et al., 2012). Also in models of the spread of a disease in a population the dynamics change extensively when heterogeneity is introduced by environmental stochasticity (Neri et al. 2010, Miller 2007). It therefore is of high interest how the spatial structure of the soil pore network affects the microbial decomposition of organic matter.
Pot et al. (2022) reviewed models of microbial soil processes with regard to their representativeness of real soil architecture. They classified the models according to two criteria: The way they describe attributes of the grid nodes (explicit or implicit) and the precision with which the architecture of the soil is included. The representation of soil architecture ranges from idealized porous media to simplified architectures to the extraction of the real soil pore network from soil samples. Grid node attributes may be described implicitly as averaged bulk soil values or explicitly as local characteristics of the soil phases. Many implicit models do not take into account the soil architecture at all and model the microbial processes on a 2D-grid. An explicit description of node attributes is a precondition for including more detailed information about the soil structure. Algorithms or imaging techniques can be used to describe the pore architecture and pore size distribution of columns filled with glass beads. This resembles an idealized soil architecture. Another approach to imitate idealized soil pore structure is to assign pore and solid nodes randomly on a grid. (Pot et al., 2022)

Ngom et al. (2011) used a very simple model of organic matter decomposition in combination with network information extracted from CT images. In their model pore space was represented by connected ball chains that were extracted from CT images from two soil samples in the above described manner. The microbial metabolism was reduced to one single form of substrate that can be directly taken up by microbes. In addition to the microbial biomass and the decrease of substrate the emitted CO_2 was tracked. Similar to the results of experimental studies they observed differing efficiency in the decomposition of organic matter for the two soil types (agriculturally treated and forest soil). For the network structure of an agriculturally treated soil sample they found that only 45% of the initial substrate was used up compared to 90% in the network extracted from a grassland sample.

In a similar way Pérez-Reche et al. (2012) implemented a model of a soil pore network to explore the effect of the network structure and preferential spread of microbes on the invasion efficiency. From six soil samples (3 of untreated soil and 3 of ploughed soil) the pore network was extracted and represented as nodes, the branching points of pores, and links, the pore channels between branching points. Microbial growth and degradation of organic matter is left out in this approach. Microbes are assumed to invade pores through the links of the network with a certain transmissibility. The dependence of the transmissibility on structural characteristics of pores and links was modified in four different models from no dependence on the pore structure to a dependence on channel length and diameter. The invasion efficiency with four different definitions for the transmissibility and differing microbial preferences was studied. These models showed that an increased heterogeneity in the transmissibility by dependence on the heterogeneous pore characteristics can lead to a reduced invasion of the pore network. But this effect is reversed by stronger microbial preference for longer channels. Because of a "bridging effect" of long channels the invasion is then increased. The uptake of substrate and microbial production of extracellular enzymes was not part of this model.

So today, as described above, there are models of soil processes with different focus and approaches. On the one hand there are very sophisticated models that take into account the microbial metabolism and the substrate degradation in detail but by modelling the processes on a grid, they neglect the spatial complexity of the soil habitats (Kaiser et al., 2014, 2015). On the other hand there are very simple models of soil microbes considering only the invasion of the pore space which take into account the architecture of the soil pores (Pérez-Reche et al., 2012). There were also attempts to bridge the gap between the two approaches. The MOSAIC model proposed by Monga et al. (2014) combines a realistic representation of the pore network extracted from CT scans with a model of some aspects of biological activity. In the model organic matter is decomposed by microbes at constant rates, provided it can reach microbes via diffusion. Microbes themselves are fixed in space.

In the following manuscript, to contribute to a deeper understanding of microbial processes in a heterogeneous pore space, we connect crucial aspects of the spatial heterogeneity of the soil pore space with a detailed model of microbial decomposition and the invasion of the pore space. With a bottom-up modelling approach the impact of the spatial structure of the soil pores and the heterogeneous distribution of environmental factors on the efficiency of microbial soil organic matter decomposition will be explored.

Part II

Manuscript

Chapter 1

Introduction

Microbial soil organic matter (SOM) decomposition as one of the major drivers of terrestrial carbon cycling is of great importance for some of today's most urgent societal issues. Carbon, that is taken up by plants via photosynthesis from the atmosphere is subsequently added to the soil as dead plant material or remnants from other living organisms. The efficiency of microbial decomposition determines how much of the carbon is stored in the soils of the earth and how much CO_2 and other greenhouse gases are emitted to the atmosphere again. Changes in temperature, precipitation and atmospheric CO_2 will affect net primary production, carbon inputs to soil and soil carbon decomposition rates and therefore potentially change terrestrial carbon storage (Falloon et al., 2011). However, the mechanisms underlying these interrelations are not precisely understood and large uncertainties remain. The global mean temperature is predicted to increase by 2-7°C and precipitation to change globally by the end of the century (Wu et al., 2011). When considering the fact, that globally there is more carbon stored in soils than in living plants or in the atmosphere (Ciais et al., 2013), the importance of soils and the allocated microbial processes in climate change becomes clear. Soils offer significant potential to serve as buffer against atmospheric CO_2 increase and as potential sink for additional C depending on the balance between photosynthesis, respiration of decomposer microbes and C stabilization in soils (Dungait et al., 2012).

Soil is built up hierarchically from soil aggregates (Menon et al., 2020) and provides a heterogeneous 3-dimensional pore system, that serves as habitat for an enormous diversity of microorganisms (Nannipieri et al., 2017). The soil habitat is spatially structured and highly heterogeneous in its biological, chemical and physical properties (Pot et al., 2022). In between solid soil particles expands pore space that consists of more or less connected microhabitats with varying environmental conditions. Organic matter that serves as substrate for microbial growth is not evenly distributed but rather very patchy. There are various disconnected microhabitats that allow for microbial growth and other areas where microbes won't find substrate. Where water is present parts of the substrate will be distributed by diffusion (Baveye et al., 2018). The distribution of water and air within the pore space depends on water saturation and is formed by inter-facial and capillary forces (Pot et al., 2022). Nunan et al. (2003) were able to show how the heterogeneous distribution of microbes in the pore space depends on architecture by analyzing soil thin sections. Microbes occur spatially isol-

ated in microhabitats from which some are connected through pores. In addition to many other important functions, active microbes in the soil pores produce extracellular enzymes that break down the organic material available to them into smaller units for uptake (Nannipieri et al., 2003).
Soil microbes are able to rapidly decompose organic matter independent of its chemical composition (Kleber et al., 2007). Nevertheless, organic matter persists in soils and chemical recalcitrance of organic matter alone is an insufficient explanation for carbon storage. Dungait et al. (2012) give an overview on further mechanisms that lead to preservation of carbon. In addition to physical protection within aggregates or adsorption onto minerals they describe another C stabilization mechanism in soil: regulation of microbial activity by local availability of substrate and other necessary factors like water and oxygen.

Computational models are widely used in soil system science on various scales. In the past decades bulk soil parameters that were commonly used to describe soils failed to predict microbial efficiency and the emission of greenhouse gases in numerous cases (Baveye et al., 2018). Individual-based models have enabled insight in interconnected soil processes and contributed to a deeper understanding at the micro-scale in the past (Kaiser et al., 2014, 2015; Allison, 2005). But integration of the heterogeneity and structure of soil microhabitats in computational models only became possible with technological progress made in the last decades (Baveye et al., 2018).
The description of actual soil architecture relies on imaging techniques, such as X-ray computed tomography. Up to date systems provide reliable information about soil architecture, the distribution of pores and solids, at a resolution that is high enough for assessing the structure of microhabitats (Baveye et al., 2018). In addition, the development of new segmentation algorithms to quantify the 3D geometry of the pore space from the stack of 2D grey-scale images resulting from CT scans has brought significant progress. These algorithms assign to each voxel in the CT scan one of the phases solid or pore space based on certain thresholds (Pot et al., 2022; Ebrahimi et al., 2013).
The degree of representativeness of soil architecture in computational models varies from idealized porous media to simplified architecture (pore network representation) and even voxel-wise representation of soil pore space extracted from actual soils (Pot et al., 2022). Including the actual soil architecture voxel-wise in the model has the advantage that it allows for realistic representation of the soil voids, the water/air-distibution, diffusion pathways and the localization of organic matter and microbes. Nevertheless, such models are only used in a minority of all studies. Their major disadvantage is that they only allow small-scale simulations due to the large computational effort involved and the high volume of input data needed (Pot et al., 2022). Here simplified representations of soil architecture are of advantage. In pore network models the void space is represented by a network of pores connected by throats (Ebrahimi et al., 2013) which reduces the computational effort and at the same time preserves important spatial information. In this way, sufficiently large areas can be simulated in a reasonable amount of time.
Besides the progress made in characterizing the physical structure of soil, advanced spectro-

scopic methods like NanoSIMS provide spatial information regarding chemical pore properties (Baveye et al., 2018). Heitkötter and Marschner (2018) have used in-situ zymography on undisturbed soil samples to gain spatial information on the activity of extracellular enzymes and detect microbial hotspots that included 2.4% of the total area on average. This nondestructive method, that allows for repeated measures, is also suitable for assessing temporal changes.

Since integration of soil architecture in computational models of microbial activity on a microscale is a crucial step on the way to a macroscale integrated model of emergent processes (Baveye et al., 2018), a sizeable fraction of research has been devoted to this area. There are early models that investigate the invasion of soil pore space by microbes through a pore network without taking into account decomposition processes (Pérez-Reche et al., 2012; Ebrahimi and Or, 2014). Then more advanced models were developed, where microbial processes were represented more accurately. Monga et al. (2008) provide a model that simulates decomposition of soil organic matter in the 3D pore space. The pore network is obtained from CT images with Delaunay Triangulation. The model, called MOSAIC, models microbial growth using Monod kinetics. Organic matter is decomposed linearly, independent of the amount of microbial biomass in a pore, extracellular enzymes and their production by microbes are neglected. Microorganisms do not move, only substrate can diffuse to them. They showed that a reduced connectivity due to reduced water content caused a decrease of decomposition efficiency. Mbé et al. (2022) attempted to link microscopic soil pore organization to measurable macroscopic descriptors by introducing an accessibility coefficient (based on the geodesic distance between microorganisms and organic matter). In their slightly adapted MOSAIC model the CO_2 emissions strongly correlated with the accessibility coefficient.

The studies described above, which are limited to simulations on sampled networks are not capable of giving answers on what elements of network structure are crucial determinants of the system dynamics or determine the sensitivity of the results to the network structure. In other research areas like epidemic modelling and opinion dynamics in social networks artificial idealized network types have been successfully used to fulfill these tasks and contributed to a more systematical understanding of the impact of network structure (Keeling and Eames, 2005; Sen and Sen, 2010). The aim of the model we introduce here is to combine an artificial pore network model with a detailed description of microbial processes related to organic matter decomposition and microbial invasion of the pore space. With this we aim to fill the gap between existing soil microbial models with different focus and approaches. On the one hand there are very sophisticated models that take into account the microbial metabolism and the substrate degradation in detail but by modelling the processes on a grid, they neglect the spatial complexity of the soil habitats (Kaiser et al., 2014, 2015; Allison, 2005). On the other hand there are very simple models of soil microbes considering only the invasion of the pore space which take into account the architecture of the soil pores (Pérez-Reche et al., 2012). There were also other attempts to bridge the gap between the two approaches. The MOSAIC model proposed by Monga et al. (2008) combines a realistic representation of the pore network extracted from CT scans with a model of some aspects

of biological activity. In the model organic matter is decomposed by microbes at constant rates, provided it can reach microbes via diffusion. Microbes themselves are fixed in space. Our novel approach connects crucial aspects of the spatial heterogeneity of the soil pore space in form of artificial pore networks with a detailed model of microbial decomposition and the invasion of the pore space. We improve the degree of detail in the description of microbial processes compared to previous models. Decomposition of organic matter at constant rates is a rough approximation as it neglects enzyme production by microbes, which itself depends on microbial biomass and available C for uptake. Therefore, we model the production of extracellular enzymes proportional to microbial C-uptake and include enzymatic breakdown of primary substrate according to Michaelis-Menten-kinetics. We also contribute to the understanding of microbial invasion of the pore space by incorporating microbial motility in the model. Pérez-Reche et al. (2012) and Ebrahimi and Or (2014) already modeled invasion processes, but their models on the other hand lack of a detailed representation of microbial physiological processes. By drawing on the mathematical concept of SIR models, that has been successfully used to study virus spreading or the diffusion of knowledge in social systems, we describe the passage of microbes from one node of the network to a neighbor through a connecting link. In that way we want to tackle the questions how the pore network architecture affects the efficiency of microbial organic matter decomposition in soils.

- How do network properties like average node degree, shortest path length and clustering coefficient affect the efficiency of C-turnover?
- How is the propagation of microorganisms trough the pore network influenced by microbial growth dynamics?

In many systems the network geometry has great impact on the dynamics of the system (Sen and Sen, 2010). Especially, the research effort in determining effects of network properties on epidemic spreading has been enormous in the last years. Epidemic outbreaks have been shown to be a decreasing function of the clustering coefficient in small world networks. And in contrast to networks with no clustering even for transmissibility values just above the epidemic threshold in highly clustered networks epidemics reach most of the people who are reachable (Pastor-Satorras et al., 2015). We hypothesize, that due to fundamental similarities in the description of epidemic spreading in a social network and microbial spreading in a soil pore network, these network properties will also have a significant impact here.
In contrast to previous pore network models, we combine a model of microbial invasion of the pore space with detailed modelling of biological processes, including enzyme production and enzymatic breakdown of organic matter according to Michaelis-Menten-kinetics. We simulate decomposition on various network types with certain properties to investigate the effect of the network structure parameters.
Along structural network characteristics in many biological systems additional heterogeneity of nodes and/or links is known to have great impact on the behavior of the system. Soil is, as described above, a highly heterogeneous habitat in which the co-occurrence of microbial enzymes and substrate leads to the decomposition of the latter. Also, already

Monga et al. (2014) reported much higher decomposition rates in their model when microbes were distributed evenly, than when they were distributed in a patchy way. The effect also depended on the network structure. Our model incorporates additional details regarding microbial physiology and mobility and the possibility to investigate the effect of heterogeneous substrate distribution and pore sizes. The second research question we aim to answer is:

- How does additional heterogeneity in pore properties like pore sizes or substrate concentration affect microbial efficiency?

We built a pore network model that supports 5 different idealized network types and an explicit description of the nature of the attributes of the microhabitats. In various simulation experiments we assess the impact of network structure and heterogeneity on microbial efficiency.

Chapter 2

The Model

The diffusion of pathogens in a population and the spread of knowledge, innovations or beliefs in a social network are well-studied processes. They rely on very similar models that can as well be used to describe more generalized invasion processes (Pastor-Satorras et al., 2015). To model the microbial invasion of the pore network, we used a mathematical formulation that is very similar to that of the systems mentioned above.
We built the model in netlogo (Wilensky, 1999) in discrete time steps of 1 hour. Our combined approach of agent-based-modelling and equation-based modelling is well-suited to take into account the vast heterogeneity in soil properties but at the same time moderate computational effort.
Standard values for all parameters described in the following section can be found in table 2.1. As long as not stated other, these values were used in the simulations.

2.1 Structure

2.1.1 Network Types

Networks can be characterized by their structural properties. In that way distinct network types can be outlined. In the supplement, we provide a description and definitions of some measures and metrics that enable the quantification of structural network properties. Average node degree, clustering coefficient and shortest path length will be calculated for the artificial pore networks used in the simulations and shall be investigated due to their effect on the microbial efficiency. We have studied the spread of microorganisms in different network architectures. The intensive effort in theoretical research regarding network measures and characteristics has helped to develop algorithms that generate networks with controlled topological properties (Pastor-Satorras et al., 2015). These synthetic networks can help answering questions about the impact of network structure on the behavior of the modelled system (Newman, 2018). We included algorithms for generation of four different network types: random network, spatially clustered network, scale-free network and small world network. Also, we compared to the same model run on a regular grid. All pore network architectures used in the simulations are shown in figure 2.1. The random network is characterized by a binomial degree distribution and the absence of structural or hierarchical

Figure 2.1: Network types

Different network architectures included in the model. Adapted from Needham and Hodler (2019).

patterns. In the small world network most nodes can be reached from every other node through a relatively small number of links, which means it has short average path lengths, and in addition, it is highly clustered, i.e. neighbors of a node are likely to be connected with a link by themselves. Networks with a high power law degree distribution are referred to as scale-free networks and consist of few highly connected nodes (hubs) and a large number of nodes with only very few connections (Newman, 2018). The spatially clustered architecture is typical for networks in which the nodes are geometrical elements embedded in space (Barthélemy, 2011).[1] A grid can also be described as connected nodes, where nodes are arranged regularly and each node has exactly 4 neighbors.

2.2 Dynamics

The description of the microbial invasion dynamics is related to the description of contagion processes in epidemics. One simplified mathematical representation of an epidemic is the so-called SIR-model (**S**usceptible-**I**nfected-**R**ecovered). In SIR-models individuals that are embedded in a social network can take 3 distinct epidemiological states:

- Susceptible: The individual does not have the disease but can catch it if it comes in contact with someone who has the disease.
- Infected: The individual is infected and can pass the disease potentially to a susceptible individual if they come in contact.
- Recovered: After some time, individuals usually recover from a disease because their immune system fights the disease off. Often, they also gain immunity and cannot catch the disease again.

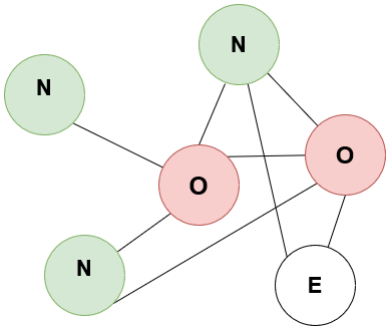

Figure 2.2: Schematic Pore Network

A schematic view of a soil pore network. Soil pores are depicted as circles and colored according to their state. N: nutritious (green), O: occupied (red), E: empty (white)

[1] A detailed description of the algorithms used for the network built up and the and the resulting characteristic properties is provided in the supplement.

While in a traditional approach in SIR-models the population is assumed to be well-mixed, more realistic models take into account the patterns of social interactions. Individuals are embedded in a social network of interactions which may lead to a transmission of the disease. The individuals are represented as the nodes of a social network and the links represent their regular interactions that potentially lead to a transmission of the disease. The transmissibility describes the probability that an infection will be transmitted from an infected individual to a susceptible individual that is connected by a link in one time step (Newman, 2018).
The invasion of the soil pore space by microorganisms can be modelled in analogy to the spread of a virus in a social network. Comparable to the individuals in an SIR-model the nodes in the microbial model can take 3 distinct states:

- Nutritious: The pore holds SOM that can be degraded by microbes. Microbes can potentially live here but there are no microbes at the moment.
- Occupied: The pore is occupied by microbes.
- Empty: The pore does hold neither SOM nor microbes. Microbes find no substrate here and therefore cannot invade this pore.

In a nutritious pore SOM is available for degradation by microbes that occupy this pore. Microbes produce extracellular enzymes that break down the primary substrate. They take up the degraded substrate and grow. If the biomass in a pore reaches the threshold B_{max} they invade a new pore, if there is a neighboring pore that is not occupied yet. For this, half of the microbial biomass is transferred to the new pore. Also, a fraction of extracellular enzymes that corresponds to the share of biomass is transferred to the new pore. If there is no neighboring pore that is not already occupied by microbes, biomass continues to grow according to the density dependent Contois-growth-function. The invasion mechanisms described here are based on the assumption, that microbes are mobile with a relatively small exploration radius. Within a given time period, they are able to pass to the neighboring pore but would not move over large distances. This applies most to various species of bacteria and less to other soil microbes like fungi. A schematic picture of a soil pore network with pores in different states can be seen in 2.2.

2.3 Dynamics within a Pore (Node)

The soil pores are characterized by variables, that catch some of the most important biotic and abiotic environmental properties. By combining in situ zymography of six extracellular enzymes with μ CT scanning it was suggested that pores in a size range from $30\mu m$ to $150\mu m$ radii contain the most active microorganisms (Kravchenko et al., 2019). To represent typical soil pore size distributions (Weller et al., 2022) we draw the radius of the pore from a normal distribution with mean pore radius $60\mu m$ and a standard deviation α. For answering the first two questions the standard deviation is kept at 0 for all simulations, which means all pores had the same radius ($60\mu m$). For the purpose of assessing the impact of heterogeneity in pore properties we then carried out simulations with altered α values. How heterogeneity is

introduced is described in detail in section 2.3.5.
In addition to size, pores are assigned chemical and biological characteristics. Every pore holds two pools of substrate, the complex primary substrate C_{Sp} and degraded substrate C_S, a pool of extracellular enzymes C_{Enz}, and a biomass pool C_B. The size of the pools is given in $fmolC_{Sp}/\mu m^3$, $fmolC_S/\mu m^3$, $fmolC_{Enz}/\mu m^3$ and $fmolC_B/\mu m^3$, respectively. They interact in a nonlinear way that is described in the following sections. Kravchenko et al. (2019) found that the soil volume within $180\mu m$ distance to the occupied pores was potentially affected by processes taking place in the pores. To account for this fact, we approximate the volume of a sphere including the soil volume in close proximity to the pores ($< 180\mu m$) as the volume where substrate can potentially be degraded by enzymes and degraded substrate (C_S) can be taken up.

2.3.1 Microbes

In real soils an enormous variety of microbes can be found, which fulfill many life-supporting tasks. There are numerous species of bacteria, archaea and fungi. In recent estimates it is considered that in one gram of soil over 10 000 different bacterial species can be found (Nesme et al., 2016; Fierer, 2017), that are interrelated in a complex network of dependencies. Next to other soil functions they are responsible for the production of many different extracellular enzymes involved in the degradation of organic material (Schloter et al., 2018).
But in soil systems microbial functions are highly redundant. Therefore, it is an efficient approach to think of the processes in terms of distinct pools and fluxes between these pools (Nannipieri et al., 2003). In this respect, microbial diversity is summarized in one type of microbes that produce one type of enzymes in this model.

Microbial growth

In addition to substrate limitation, density dependent factors can regulate microbial growth. Competition for substrate, space constraints, or production of toxins dampen microbial growth. Therefore, we chose a growth function that includes microbial density as a regulation factor. Coche et al. (2020) highlighted the importance of including density regulation in degradation models especially for heterogeneous distribution of microbes and substrate. Further, they presented the Contois growth function as a valuable alternative to the Monod growth function for modelling decomposition processes.

In our model, microbial uptake is determined by their maximum growth rate v_{max}, concentration of the limiting substrate C_S and population density C_B in the pore, based on the formula for microbial growth described by Contois (1959).

$$C_S^{uptake}(t) = \frac{v_{max} \cdot C_S(t)}{K_c \cdot C_B(t) + C_S(t)} \tag{2.1}$$

$$C_B(t + \Delta t) = C_B(t) + (1 - e_{fr}) \cdot C_S^{uptake} - r \cdot C_B(t) \tag{2.2}$$

The growth parameter K_c is a constant regulating the density dependence of growth.

v_{max}, the maximum growth rate, is also constant under defined conditions.
Maintenance respiration is considered as a constant fraction r of biomass that is calculated every time step. If the C taken up is sufficient for maintenance and is not used up, the remaining C is used for enzyme production and growth. A fraction e_{fr} of the remaining C is used for enzyme production, the rest is added to the biomass. Standard values used for the parameters in the simulations can be found in table 2.1.
Under starvation, if the C-uptake is not sufficient for meeting maintenance respiration the lack of C is compensated with C from the biomass.

Death

A loss of microbial biomass can take place either by starvation or by stochastic catastrophic death. Catastrophic death is represented in the model as a small fraction of randomized size of the microbial biomass that is lost every time step. The actual size of the fraction that is lost by catastrophic death is calculated as a random number in the range of d for each pore every time step. Starvation means that the microbial C uptake does not meet the needs for maintenance respiration. In that case the C needed for respiration is taken from the microbial biomass minus C uptake in that time step. Biomass cannot get negative. If biomass reaches 0 in a pore, the pore is considered no longer occupied. Biomass is not recycled in the model.

2.3.2 Substrate

Pores hold two pools of substrate, the complex primary substrate C_{Sp} and degraded substrate C_S accessible for microbial uptake. A fraction *diff-fr* of the degraded substrate diffuses to the neighboring pores in equal parts in every time step.[2] There is no regrowth of substrate in the model.

Enzymatic breakdown

The enzymatic reactions involving various enzymes that are responsible for degradation of organic matter originating from plant material through multiple steps are simplified to one degradation step. We do not differentiate different types of enzymes, but there is a single pool of enzymes and a single form of complex substrate. Microbes produce extracellular enzymes proportionately to their biomass in each pore. The enzymes are exuded to the pore space and added to the pool C_{Enz}, they act in the entire space of the pore where they are located, but not further. The enzymes contained in the pool C_{Enz} of a pore break down the polymers of the complex primary substrate contained in the pool C_{Sp} in one step to monomers that can be taken up by microbes. The enzymatic reaction is carried out according to Michaelis-Menten-kinetics(Wang et al., 2012):

$$C_S(t + \Delta t) = C_S(t) + k_{cat} \frac{C_{Enz}(t) \cdot C_{Sp}(t)}{k_{half} + C_{Sp}(t)} \tag{2.3}$$

[2]The standard value for diff-fr can be found in table 2.1

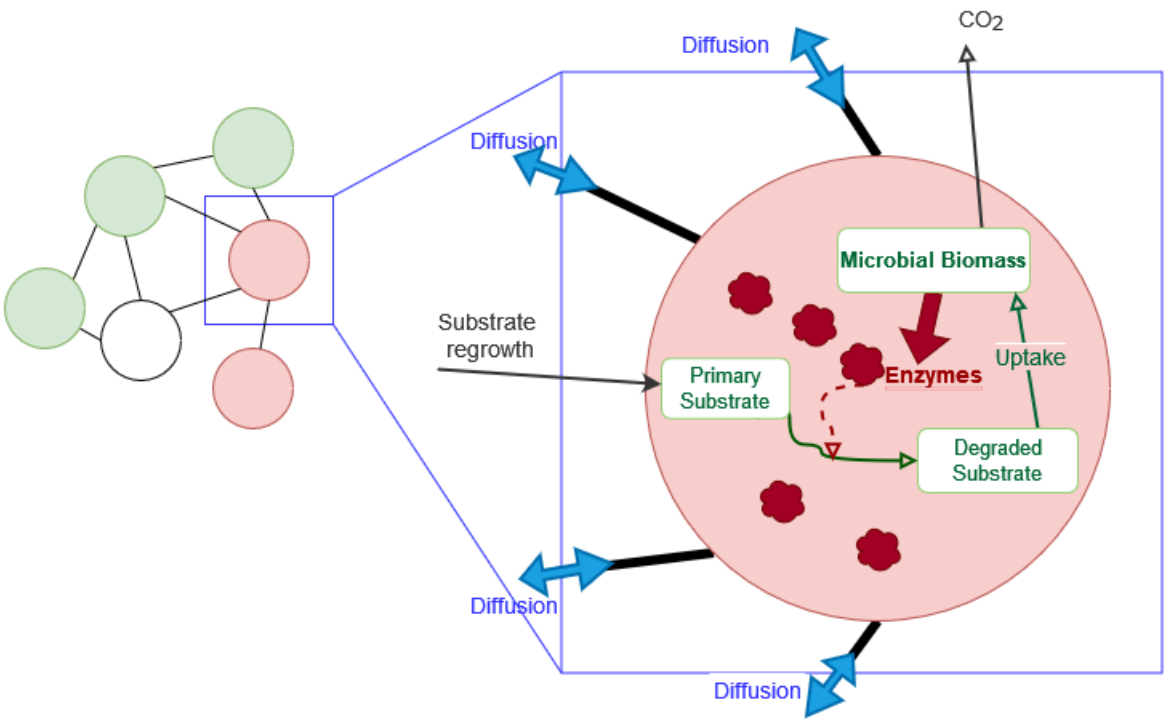

Figure 2.3: Conceptual Model of the processes in one pore
The biotic and abiotic processes as they occur in each occupied pore in every time step. Microbes produce enzymes and release them into the pore space, where with the help of the enzymes organic matter (primary substrate) is broken down. The degraded substrate is taken up by microbes according to the Contois-growth function. A given fraction of the degraded substrate diffuses to the neighboring pores.

In this formula k_{cat} is the maximum specific enzyme activity (maximum number of catalyzed reactions per mol C_{Enz} per time step) and k_{half} is the half saturation constant. The amount of C_S that results from the reaction in one time step is added to the C_S pool. Enzymes are not used up by these reactions, but rather are inactivated after a certain time. The amount of enzymes in a pore changes according to the formula:

$$C_{Enz}(t + \Delta t) = C_{Enz}(t) + e_{fr} \cdot C_S^{uptake}(t) - \frac{1}{k_{enz}} \cdot C_{Enz}(t) \tag{2.4}$$

Where $C_S^{uptake}(t)$ describes what microbes were able to take up in a certain time step. e_{fr} is the fraction of the uptake dedicated to enzyme production and $\frac{1}{k_{enz}}$ is the rate of enzyme inactivation. The values for the enzymatic parameters can be found in table 2.1.

2.3.3 Parameters

To determine parameter settings that represent the interrelated mechanisms taking place in the soil pore as authentic as possible, we first extracted measured values for all parameters from the literature to obtain a range of reasonable values. We then carried out a parameter sensitivity analysis within these ranges to find a setting that suits the real world as good

as possible. Parameters for which we could not find values in the literature, we calibrated such that the model outputs meets typical characteristics of similar systems. Additional information can be found in the supplement in section 6.3.

For the model calibration we focused on agriculturally used soils that were subjected to conventional tillage. Pérez-Reche et al. (2012) extracted the pore network of agricultural soil samples and gave the number of pores and number of links for the three samples. The average are 839 pores per cm^3 with an average node degree of 2.7 (Pérez-Reche et al., 2012). We assumed a bulk density of $1.43 g/cm^3$ and porosity[3] of 0.1679 which are average values for conventionally ploughed soils from samples from the Soil Structure library (Weller et al., 2022). Wang et al. (2012) collected values for many important enzyme parameters for model calibration, which we used as starting point for calibrating the enzyme parameters.

Standard Parameters used in the model simulation runs unless stated otherwise are summarized in table 2.1 and 2.2.

[3]fraction of volume of voids over the whole volume.

Table 2.1: Standard Parameter settings

Parameter	Description	Value	Unit	Source
diff-fr	fraction of C_S that diffuses to neighboring pores	0.1	h^{-1}	
v_{max}	maximum specific growth rate	0.29	h^{-1}	adapted from Zelenev et al. (2005)
K_c	density dependence constant of contois growth function	2*10^{-9}	$fmolC_B/\mu m^3$	achieved from parameter analysis
r	respiration coefficient	0.1	h^{-1}	Zelenev et al. (2005)
B_{max}	maximum biomass per pore	8.33	$fmolC_B/\mu m^3$	calculated from cell density and C content Kaiser et al. (2014)[3]
d	maximum catastrophic death rate	0.1	h^{-1}	
E-fr	fraction of uptake used for enzyme production	0.067	h^{-1}	Kaiser et al. (2015)
k-cat	maximum specific enzyme activity	1.98	fmol $C_S C_{Enz}^{-1} h^{-1}$	Wang et al. (2012)
k-half	half saturation constant	0.29*10^{-3}	$fmolC_S/\mu m^3$	adapted from Kaiser et al. (2015) [4]
k-enz	rate of enzyme inactivation	0.012	h^{-1}	Kaiser et al. (2015)

[3] assuming 80% water content of the cell fresh weight, a C content of 10% of the dry weight and a cell density of a microbial cell of $1000 fg/\mu m^3$ (**?**)

[4] value was adapted during model calibration according to the statement in (Wang et al., 2012), that the half saturation constant is thought to be comparable or greater than the average substrate concentration in the equilibrium state of the soil.

Table 2.2: Standard Network parameter settings

Parameter	Description	Value	Unit	Source
N	Number of nodes	839	pores	Pérez-Reche et al. (2012)
node-degree	average node degree	2.7		Pérez-Reche et al. (2012)

2.3.4 Initial conditions

This section describes the initial conditions used in the simulations, initial substrate concentrations S_0, distribution of microbial biomass C_B and enzymes C_{Enz} [4]. For a major part of the experiments primary substrate was distributed evenly over all pores at two levels, for which various comparisons are listed in the first two sections in chapter 3. For these experiments the substrate concentration in all pores was either $S_0 = 0.5$ fmol C_{Sp} / μm^3 or $S_0 = 5$ fmol C_{Sp} / μm^3. Note that substrate with a distance $< 180\mu m$ to the pore is assumed to be reachable, as described in section 2.3. The amount of substrate assigned to a pore therefore is proportional to the soil volume in close proximity and not only to the volume of the pore itself. In the section that is concerned with chemical pore properties a wider range of values for S_0 is used, but still the distribution is uniform over all pores. Only in the last section about the effect of additional heterogeneity one experiment investigates the effect of the distribution of primary substrate over the pores. How additional heterogeneity is introduced is described in the next section.
The initial microbial occupation by default is $B_0 = 0.1$ fmol C_B / μm^3 in 10% of all pores that are randomly chosen. The figures 6.9 and 6.8 in the supplement explore the effect of the number of initially occupied pores. In all initially occupied pores also an initial amount of enzymes, $E_0 = 0.02$ fmol C_{Enz} / μm^3, and degraded substrate, $D_0 = 0.01$ fmol C_S / μm^3, can be found.

2.3.5 Additional heterogeneity

Section 3.5 describes simulation results from experiments with varying heterogeneity in pore sizes, substrate concentration and B_{max}.

Heterogeneous pore sizes

For the experiments with heterogeneous pore sizes we intended to cover the range of radii from $30 - 150\mu m$ that Kravchenko et al. (2019) described as specifically important for microbial activity, but also expand the range to pores both smaller and larger than this range. Therefore, we choose as mean radius $80\mu m$ and draw the pore radii from a normal distribution with a standard deviation proportional to $alpha$, such that the maximum range, when $alpha = 1$, included radii from $10 - 170\mu m$. We kept the amount of initial substrate in each pore the same for this experiment. The size of the pores varied proportional to alpha, and the amount of substrate was the same as if all pores had the same size, therefore this resulted in large pores with low substrate concentration and small pores with high substrate

[4] Figures 6.5, 6.6 , 6.7, 6.8, 6.9 in the supplement display the impact of the initial conditions.

concentration. Since B_{max} depends on the pore size, it also changed in this experiment. In large pores a higher amount of biomass needs to be reached for invasion of a new pore.

Heterogeneous substrate distribution

In another experiment only the substrate concentration varied and the pore sizes were all equal. The same amount of initial primary substrate as in a system with equally distributed substrate is here distributed randomly over the pores corresponding to a normal distribution and ensuring that the values are within a given range ($0.01 - 8.6 fmolC_{Sp}/\mu m^3$ for the low mean initial substrate concentration of $0.5 fmolC_{Sp}/\mu m^3$ and $0.13 - 86 fmolC_{Sp}/\mu m^3$ for the high mean initial substrate concentration of $5 fmolC_{Sp}/\mu m^3$). The mean of the normal distribution was kept constant for all simulations and the standard deviation was varied in relation to alpha. The larger alpha, the larger the standard deviation of the normal distribution from which the values for the initial substrate concentration of a pore were drawn. This results in a very heterogeneous substrate distribution with larger alpha. When alpha is 0, the initial amount of substrate is the same in all pores. Pore sizes and other pore properties were kept constant and equal for all pores in this experiment.

Heterogeneous B_{max}

In the previous experiments the biomass concentration threshold for invasion of a new pore was always the same for all pores. In real soil pores this value might differ immensely for pores due to the spatial distance of the neighboring pore or chemical properties of the pores that enhance or undermine microbial active or passive mobility. To consider this, we studied the effect of heterogeneous B_{max} on the microbial efficiency. We draw the values from a normal distribution with mean $8\, fmolC_B/\mu m^3$ and a standard deviation proportional to alpha and constrained the range at the minimum at $0\, fmolC_B/\mu m^3$ and at maximum $16\, fmolC_B/\mu m^3$.

Chapter 3

Results

Efficiency of microbial soil organic matter decomposition can be described in terms of the proportion of initial substrate that was degraded, the time it takes to degrade the substrate, the carbon use efficiency of the microbes and the size of the occupied area in the pore network. In the sections below we investigate microbial growth parameters and various network properties with regard to their impact on microbial decomposition efficiency. In section 3.1 we show a comparison of the traditional grid model, where each node has exactly 4 neighbors, with the other network types. To achieve comparability between the grid architecture and the other network types, we constructed all networks in this section with an average node degree of 4.[1] Then, in section 3.2 we investigate in detail the influence of microbial growth parameters, substrate concentration and enzymatic parameters in the different network types. For a more accurate representation of soil pore networks sampled from soil CT scans, we construct all network types with an average node degree of 2.7 (Pérez-Reche et al., 2012) from this section on. Because this does not allow to compare to a grid model with 4 neighbors anymore, we use only the 4 network types in the simulations from this section on. Section 3.3 illustrates on which model parameters the probability of transmission to a neighboring node depends in our model and how it differs between the different network types. The last section (3.4) is about the influence of structural network properties on decomposition efficiency. Here we investigate the impact of the average node degree, clustering coefficient, shortest path length and number of nodes in a network on the decomposition efficiency.

3.1 Grid vs. Network

In this section we first give an overview of degradation dynamics in the grid model and in all network types. Then we compare the effect of microbial growth parameters on the decomposition efficiency on the grid and in all network types. To maintain comparability between the grid model and the model on the different network types, an average node degree of 4 was chosen for the construction of the networks in this simulation, despite being unrealistic for real soil pore networks. The number of nodes equals the number of grid-cells and is

[1] For a detailed analysis of the effect of the average node degree on the decomposition efficiency see section 3.4.2.

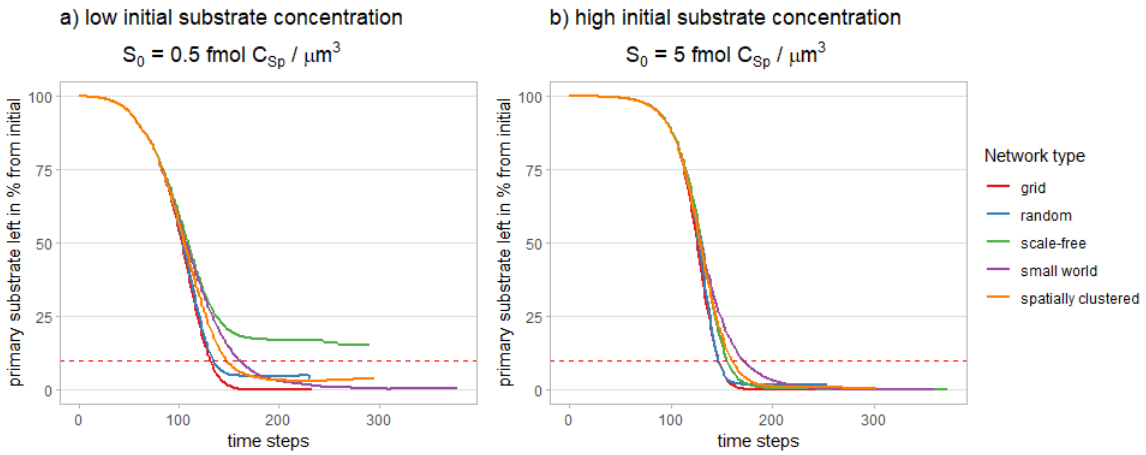

Figure 3.1: Temporal dynamics of primary substrate in different network types at two different initial substrate concentrations
The lines show the sum of primary substrate left in all pores, which is an indicator for decomposition efficiency. The colors represent the different network types and the grid model. The average node degree for all networks was 4, the number of nodes 841. The grid was also initialized with 841 grid cells. The dashed red line indicates 10% of the initial substrate. We find that the degradation of primary substrate is more complete at higher initial substrate concentrations, while at lower initial substrate concentrations the amount of primary substrate left over is strongly influenced by network type.

841 for all experiments in this section. This is a number of pores, relatable to as it may be found in $1cm^3$ of real soil (Pérez-Reche et al., 2012). The simulations in this section are initialized with a certain amount of primary substrate evenly distributed over all nodes. We simulated two scenarios: a high initial substrate concentration ($S_0 = 5$ fmol C_{Sp} / μm^3) and a low initial substrate concentration ($S_0 = 0.5$ fmol C_{Sp} / μm^3). There is no regrowth of substrate during the simulation.

3.1.1 Overview of degradation dynamics

Figure 3.1 gives an overview of the development of the primary substrate over time. The temporal development of the decomposition of the primary substrate shows some similarities and some differences between the different network types and on the grid. Since there was no regrowth of substrate in this simulation the initial primary substrate is broken down by enzymes, which can be seen by the decreasing amount of primary substrate in all network types. The time needed for degradation and the degree of completeness of degradation of the initial substrate were used as indicators for the degradation efficiency. The behavior of the small world network and the grid model is rather similar. They enable complete decomposition of the primary substrate in both initial substrate levels. The only difference is, that decomposition takes longer in the small world network. In all other network types at a lower initial substrate concentration (Figure 3.1, a) not all of the initial substrate could have been degraded. In the scale-free network about 17% of the initial substrate remained undegraded (Figure 3.4, a). What is somewhat counterintuitive is, that the decomposition is more efficient for higher initial substrate concentration in most network types. Although,

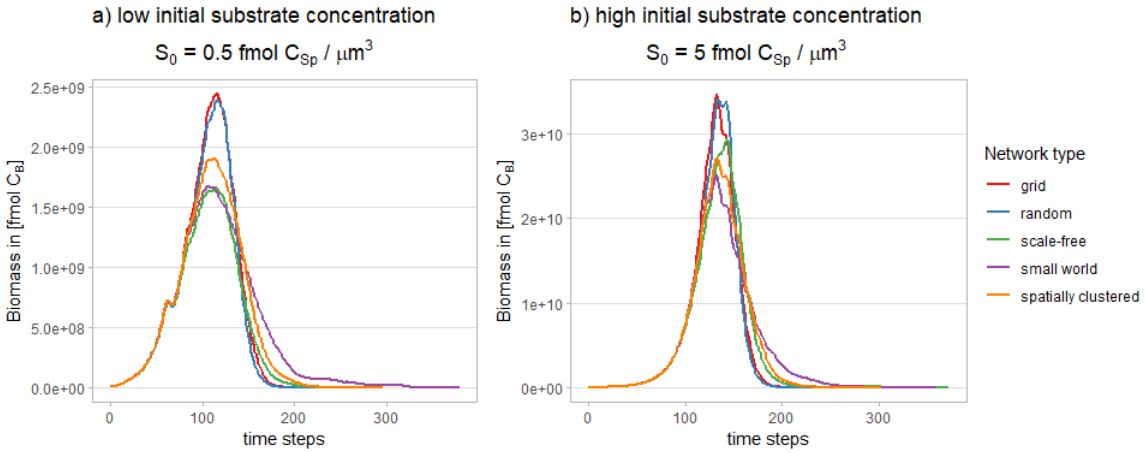

Figure 3.2: Temporal dynamics of microbial biomass in different network types at two different initial substrate concentrations

The lines show the sum of microbial biomass in all pores. The colors represent the different network types and the grid model. The average node degree for all networks was 4, the number of nodes 841. The grid was also initialized with 841 grid cells. We find that with a substrate concentration 10 times higher, the maximum microbial biomass is also more than 10 times higher. Further, the network structure impacts the dynamics of microbial biomass. The networks that have a lower maximum biomass allow the microorganisms to survive and spread through the network for a longer period of time.

in the beginning there is more primary substrate, the fraction that is left at the end is lower. This effect is illustrated in the figures 3.1, 3.4, 3.16 and also in figure 3.24. The intensity of this effect is different for different network types.

The enzymes that break down the primary substrate are produced by microbes which grow by taking up the degraded substrate. When the substrate is used up or no more substrate is reachable for the microbes to degrade, microbes die due to starvation. A comparison of the development of the microbial biomass in all network types and in the grid model is shown in figure 3.2 [2]. In the beginning microbes find enough substrate and biomass increases. When the available substrate is consumed biomass decreases again until all microbes die. How long this takes depends on the network type and the initial substrate concentration. For all network types we find more than 10 times higher maximum microbial biomass with an initial substrate concentration 10 times higher. Remarkable differences in the maximum biomass were observed among the different network types. In the random network and on the grid the biomass maximum was much higher compared to the other network types, especially with low initial substrate concentration. In these two network types microbial biomass first increased fast to a high value to afterwards also decrease fast. The stop condition of $C_B < 0.01 \cdot B_0$ was reached after a short time period. On the other hand, the networks that have a lower maximum biomass allow the microorganisms to survive and spread through the network for a longer period of time. It took the longest in the spatially clustered network until the stop condition was fulfilled, that only 1% of the initial biomass is left in all pores. Also, in the spatially clustered network which is one of the networks with lower maximum in biomass microbes were alive for a relatively long period. The scale-free network is special in the

[2] A more detailed depiction of the correlations between initial substrate concentration and biomass in all network types can be found in the supplementary material (figure 6.5).

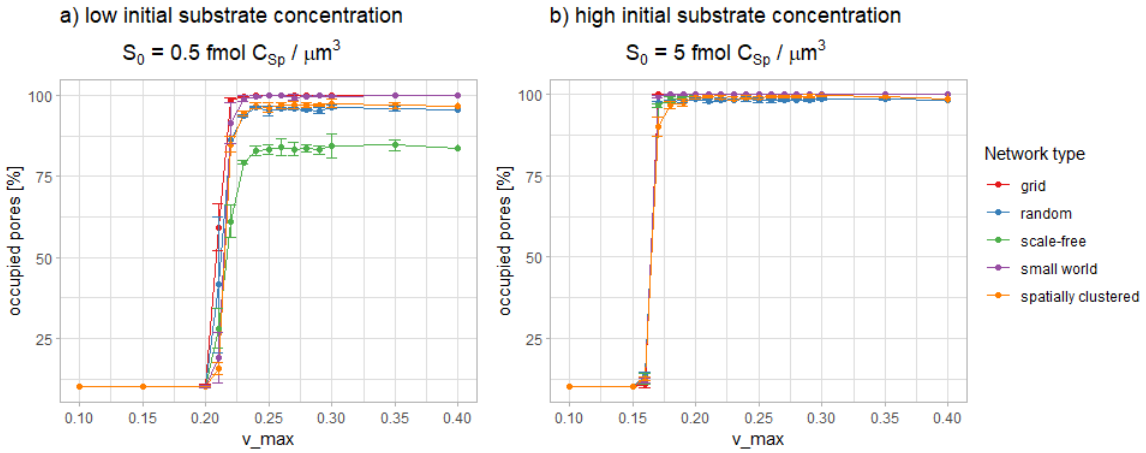

Figure 3.3: Number of occupied pores in dependence on maximum microbial growth rate v_{max} in all network types and the grid model

Efficiency of the microbial invasion in all network types and on the grid. The average node degree of all networks is 4 and the number of nodes 841. Each point depicts the accumulated number of pores invaded during one run. Each pore that was invaded by microbes was count once at its first time becoming occupied. The color of the point represents the network type. The system shows a threshold behavior: If a threshold value v^*_{max} for v_{max} is exceeded, even a small change will cause a large-scale invasion of the pore space. Below the threshold the number of occupied pores is 10% for all network types, as this was the fraction of pores that were initially occupied. The points overlay here.

sense that it has a low maximum but also the stop condition was reached relatively early. Similarly, the network structure affects the efficiency in terms of the proportion of primary substrate decomposed (figure 3.4).

3.1.2 Influence of microbial growth parameters

From the overview of degradation dynamics we will now turn to an investigation of the effect of an important factor determining microbial growth, the maximum microbial growth rate v_{max} (see equation 2.1). This section still investigates the differences in the network types and the grid model and therefore uses average node degree 4 for all network types. This is in contrast to the following section, where we provide a detailed analysis of the impact of further factors related with microbial growth, in more realistic networks with average node degree 2.7.

Our results show, that microbial growth rate is crucial for the invasion of the network. To obtain the fraction of pores that were invaded by microbes the accumulated number of pores invaded during one run was count. Each pore that was invaded by microbes was count once at its first time becoming occupied. Pores were not counted multiple times if they were invaded more than once.The system shows a threshold behavior with regard to a change in v_{max}. A smaller v_{max} slows down microbial growth. During this longer time period until the maximum is reached, microbes use up substrate for maintenance respiration in each time step (1 hour). The substrate left for growth then only allows for a lower maximum microbial biomass, which is too small to allow the passage to a new pore with v_{max} below the threshold v^*_{max}. So, in this case no new pores can be invaded and only the substrate in

Network type	v^*_{max} with low initial substrate	v^*_{max} with high initial substrate
grid	0.22	0.17
scale-free	0.23	0.17
random	0.22	0.17
small world	0.22	0.17
spatially clustered	0.22	0.17

Table 3.1: Threshold for the invasion of more than 75% of the pore space in the different network types and with low initial substrate concentration ($S_0 = 0.5$ fmol C_{Sp} / μm^3) and high initial substrate concentration ($S_0 = 5$ fmol C_{Sp} / μm^3). The scale-free network stands out in that it enables the invasion of 75% of the pore space only for higher v_{max} than all other network types in the lower initial substrate regime.

Network type	Proportion of occupied pores
grid	99.9%
scale-free	83.8%
random	95.9%
small world	99.9%
spatially clustered	97.0%

Table 3.2: Average invasion efficiency in terms of proportion of pores that could have been occupied. For all network types with average node degree 4 and $v_{max} >= 0.29$. The number of pores was 841 in all networks and the initial substrate concentration $S_0 = 0.5$ fmol C_{Sp} / μm^3.

the initially occupied pores is used up. Already a small change of v_{max} so that it lies above the threshold v^*_{max}, however, leads to a large-scale invasion. The transition from the state where no invasions occur to invasion of large parts of the network is smooth. We calculated threshold values v^*_{max} for an occupation of 75% of the pores. v^*_{max} is equal to 0.23 in the scale-free network and 0.22 for all other network types in the simulation with average node degree of 4 and initial substrate concentration $S_0 = 0.5$ fmol C_{Sp} / μm^3(Figure 3.3 and table 3.1). The difference in the invasion efficiency in the scale-free network is shown in figure 3.3. In the scale-free network not only a larger fraction of substrate is left undegraded, also the size of the invaded pore space is smaller. While in the scale-free network the average proportion of occupied pores for all $v_{max} > 0.24$ lies at 83.8%, in all other network types the invasion is significantly more efficient (over 95%, $p < 0.001$, see table 3.2). There are also highly significant differences between all other network types for the invasion efficiency in this experiment, but not between the grid and the small world network[3]. These two network types showed equal invasion efficiency. In both, the small world network and on the grid, the microbes invaded more than 99% of the pores on average (table 3.2).

Maximum microbial growth rate also determines the completeness of the decomposition of initial primary substrate. Data from figure 3.4, which shows a tipping point in the fraction of initial primary substrate that remained undegraded at the end of the run in dependence on v_{max}, can be compared with the data in figure 3.3 which shows a tipping point in invasion efficiency in dependence on v_{max}. Similarly, we also see a fast increase of the

[3]We used ANOVA and a Tukey post-hoc test to investigate significance of the differences.

decomposition efficiency in terms of the fraction of initial substrate that was degraded when v_{max} is high enough to enable microbes to pass to new pores. But beyond that threshold network structure becomes a limiting factor. Figure 3.6 provides a comparison of the impact of network structure on the decomposition efficiency and the impact of v_{max} in a parameter range above v^*_{max}. Above this threshold further increase in v_{max} does not affect the fraction of substrate that was degraded, but the determining factor is network structure. In the scale-free network 16% of the initial substrate remained undegraded averaged over v_{max} from 0.24 to 0.4. Whereas, in all other network types and on the grid the decomposition was much more efficient (Figure 3.4). Only in the random network a small fraction of the initial substrate (4% on average over v_{max} from 0.24 to 0.4) is left at the end of the run and an even smaller fraction (3% on average over v_{max} from 0.24 to 0.4) in the spatially clustered network. Surprisingly, the pattern looks very different with higher initial substrate concentration. For all v_{max} above the threshold the initial substrate was completely decomposed in the scale-free network with an initial substrate concentration $S_0 = 5$ fmol C_{Sp} / μm^3. In the other two network types where the degradation was not complete with a lower initial substrate concentration, the degradation was also more efficient but not complete with a higher initial substrate concentration, as can be seen in b) in figure 3.4. There were 1,6% of initial substrate left at the end in the random network averaged over all v_{max} above the threshold and 0.8% in the spatially clustered network. The network structure of the scale-free network featuring few highly connected hubs and a high number of nodes with very low degree leads to an increased amount of primary substrate left at the lower initial substrate concentration. When the substrate in the highly connected hubs is used up these pores become uninhabitable in this setting without substrate regrowth. Parts of the network, however, can only be accessed through these hubs. Therefore, these parts become effectively inaccessible for microbes and unconnected from the network. Primary substrate in the disconnected pores cannot be degraded. This effect diminishes with a very high primary substrate concentration. Then there is enough substrate to allow strong microbial growth. The microbes reach B_{max} more than once and pass through more links stemming from this hub and in that way also reach the network periphery.

In addition, figure 3.5 compares how long it takes to decompose 70% of the initial substrate in all network types for different v_{max} with two different initial substrate concentrations. In the lower initial substrate regime significant differences in the duration of the decomposition of 70% of the initial substrate for all network types compared to the model on the grid can be observed[5]. Averaged over all $v_{max} > 0.22$ (to guarantee that the 70% mark was reached in all network types) the decomposition was the fastest in the model on the grid (161 time steps) and in the random network (164 time steps). In the other three network types decomposition was much slower: it took 185 time steps in the spatially clustered network, 197 in the small world network and 178 time steps in the scale-free network to decompose 70% of the initial substrate on average. All of these network types showed highly significant differences in the decomposition time compared to the model on the grid ($p < 0.001$) and also between the network types there can highly significant differ-

[5]We used ANOVA and a Tukey post-hoc test to investigate significance of the differences.

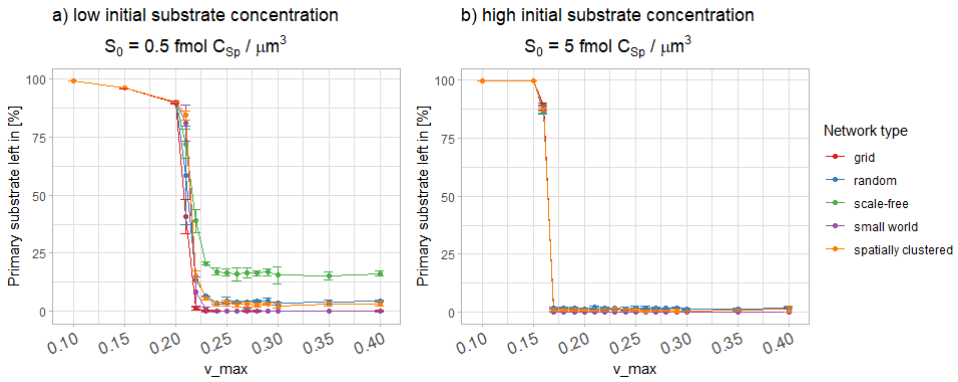

Figure 3.4: Remaining primary substrate for different maximum microbial growth rates v_{max} in all network types and the grid model.
Fraction of initial primary substrate that remained undegraded at the end of the run in all network types and on the grid. All networks were constructed with average node degree 4 and 841 pores. The colors depict the network types. Maximum microbial growth rates v_{max} on the x-axis. Values are averaged over 5 runs, error bars indicate standard devaition. Below a threshold v^*_{max} no invasions occur and only the subsrate reachable from the initially occupied pores can be degraded. Above the threshold we found a dependence of the decomposition efficiency on the network type. At lower initial substrate concentration there was significantly more substrate left undegraded in the scale-free network ($p < 0.001$) compared to the other network types for $v_{max} > 0.24$[4]. This difference even remains for higher maximum growth rates of the microbes and is not compensated for by faster growth.

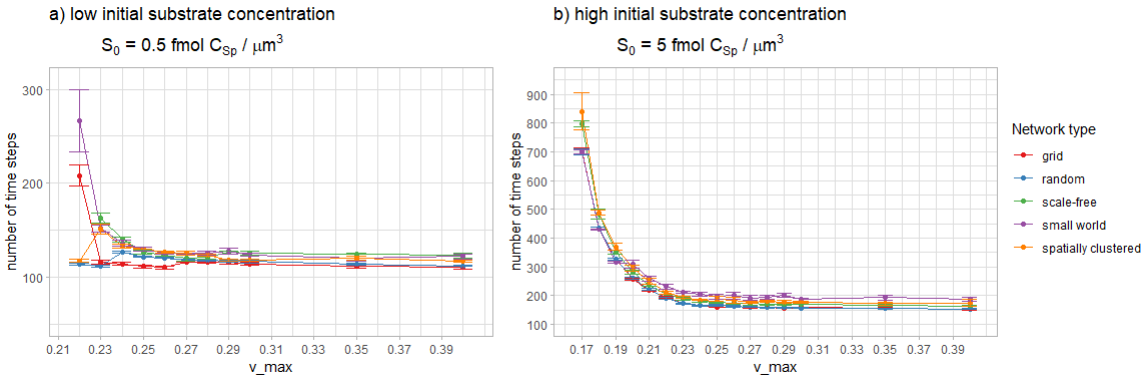

Figure 3.5: Time until 70% of initial substrate were degraded in all network types and the grid model.
Duration of the decomposition of 70% of the initial substrate in all network types and on the grid. The average node degree of all networks is 4. Only simulation runs are shown where at least 70% of the initial substrate were degraded. Averaged over 5 runs, error bars indicate standard deviation.

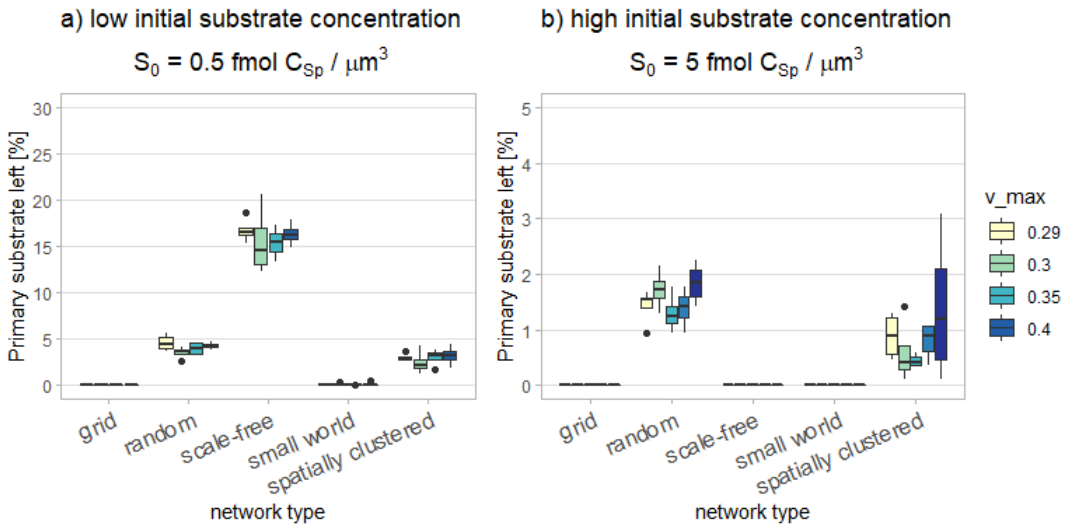

Figure 3.6: Remaining primary substrate for different maximum microbial growth rates v_{max} above v^*_{max} in all network types and the grid model

Fraction of initial primary substrate that remained undegraded at the end of the run in all network types and on the grid for v_{max} above v^*_{max}. All networks were constructed with average node degree 4 and 841 pores. All values for v_{max} lie above the threshold v^*_{max}. In this range of values, no further increase in decomposition efficiency can be achieved by an increase of the maximum microbial growth rate. The amount of substrate left at the end of the run strongly depends on the network type.

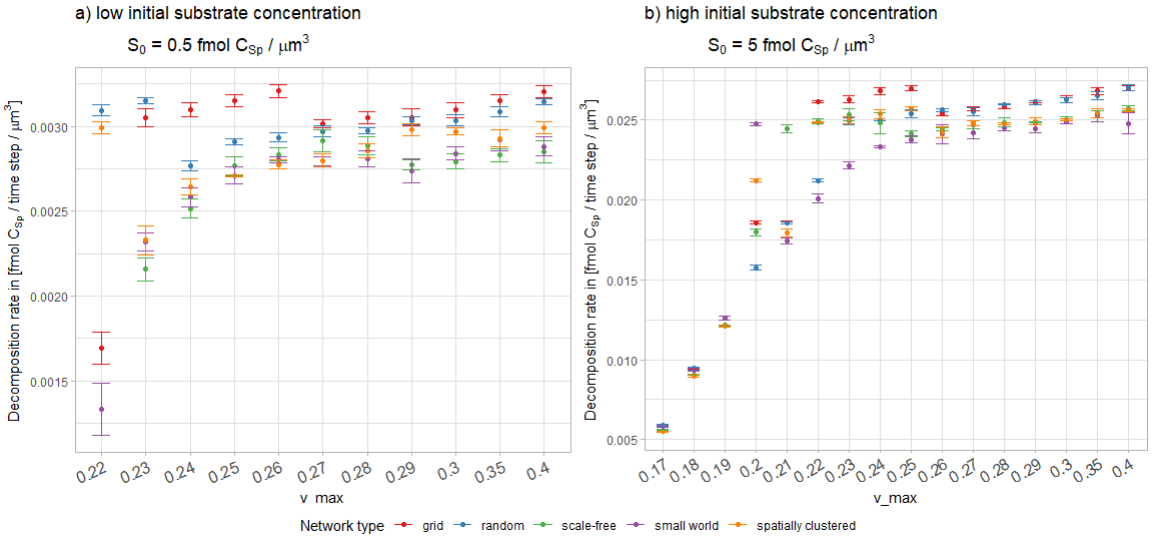

Figure 3.7: Decomposition rate for the first 70% of initial substrate

Substrate decomposed per time step for the first 70% of the initial substrate in all network types and on the grid for different v_{max}. The average node degree of all networks is 4. Averaged over 5 runs, error bars indicate standard deviation. The overall rate of decomposition is smaller with the smaller v_{max}, and especially close to the threshold v^*_{max} the decomposition rate is very low.

ences be found between most pairs[6]. The lower initial substrate concentration only enabled to reach the 70% mark with a $v_{max} >= 0.23$ in the scale-free network and $v_{max} >= 0.22$ in all other network types. Decomposition was very slow with v_{max} close to the threshold for large-scale invasion v^*_{max} (compare with table 3.1).
From b) in figure 3.5 it can be seen, that in the high initial substrate regime in all network types it was possible to reach the 70% mark already with a lower v_{max}. $v_{max} = 0.17$ enabled to decompose 70% of the initial substrate, but it took significantly longer to achieve this in all network types ($p < 0.001$). A significant difference between the two initial substrate concentrations could be found when only taking $v_{max} > 0.22$ into account. Although the amount of substrate is 10 times higher in the high initial substrate concentration regime, it did not make a large difference in the time needed to decompose 70% of this. With the lower initial substrate concentration, decomposition of 70% of the initial substrate took 135 time steps averaged over all network types. With high initial substrate concentration, it took 145 time steps. Higher initial substrate concentration enables more complete decomposition already for smaller v_{max}.
We defined the decomposition rate as $d = \frac{\sum_{t=0}^{t^*} C_{deg}(t)}{t^*}$, where t^* is the time necessary to degrade 70% of the initial substrate and C_{deg} is the amount of C_{Sp} degraded in each time step. The decomposition rate is not constant but changes over time, we compute an average decomposition rate over the time interval that is needed to decompose 70% of the initial substrate. How the degradation changes over time is set out in figure 3.1. The rate of decomposition in all network types and on the grid for the first 70% of the initial substrate is compared in figure 3.7. The overall rate is smaller with the high substrate concentration, and especially close to the v_{max} threshold the decomposition rate is very low.

3.2 Comparison of the network types

The previous section has compared the model behaviors on different network types and on a regular grid. However, in real soil pore networks the average node degree is usually lower than it is used in the previous section to guarantee for comparability of the network types with the grid. In the following an average node degree of 2.7 is used, to approximate pore networks extracted from actual soils more correctly (Pérez-Reche et al., 2012). We first illustrate the impact of maximum microbial growth rate, the initial substrate concentration and the interplay between these factors on the decomposition efficiency in all network types. Then, we analyse enzymatic parameters with regard to their impact on microbial efficiency in all network types.

3.2.1 Interplay between maximum microbial growth rate and initial substrate concentration

Figure 3.8 shows the connection between initial substrate concentration and microbial invasion efficiency. There is a threshold S^*_0 between 0.4 and 0.5 fmol C_{Sp} / μm^3 over which invasion of large network parts is possible. Below this threshold only in the initially occupied

[6]We used ANOVA and a Tukey post-hoc test to investigate significance of the differences.

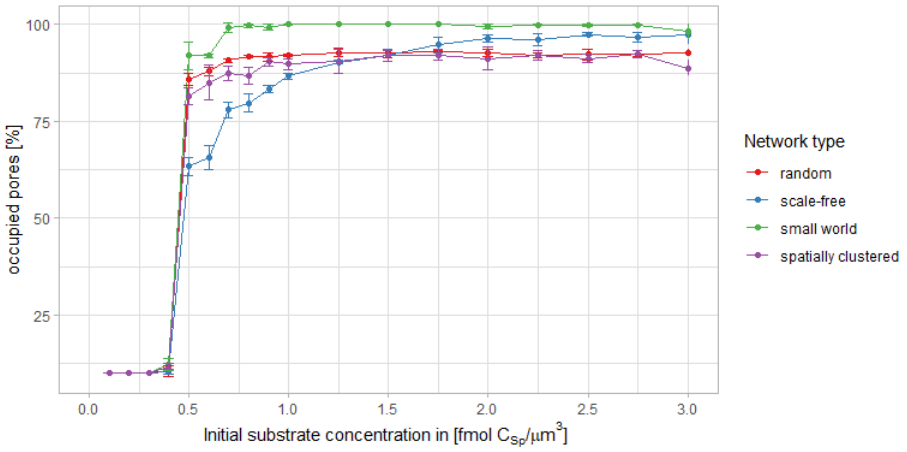

Figure 3.8: Number of occupied pores for different initial substrate concentrations

Number of occupied pores for different initial substrate concentrations in fmol C_{Sp} / μm^3. Each point depicts the accumulated number of pores invaded during one run. Error bars show the standard deviation. Each pore that was invaded by microbes was count once at its first time becoming occupied. The color of the point represents the network type. The average node degree of all networks in this experiment was 2.7. Therefore we leave out the grid model from now on, due to insufficient comparability. Values from 5 runs. We observed a threshold behavior in the initial substrate concentration for large-scale invasion of the pore space. Below the threshold S_0^* it is not possible for microbes to invade new pores. Whereas a small increase in S_0 above the threshold leads to an invasion of large parts of the network.

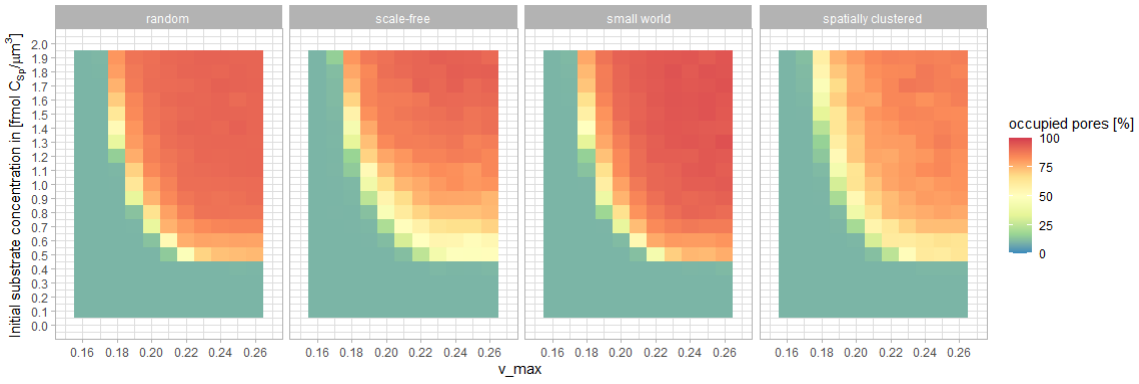

Figure 3.9: Proportion of occupied pores for different initial substrate concentrations and different v_{max}

The colors depict from green to red increasing proportions of pores that were invaded by microbes in dependence on initial substrate concentration and microbial growth parameter v_{max}. Each network type is shown in one plot. The average node degree was 2.7 for all networks (therefore without the grid model). Averaged values from 5 runs.
There is a minimum initial substrate concentration (0.5 fmol C_{Sp} / μm^3) and a minimum microbial growth rate v_{max} (0.17) to allow microbes to invade pores at all, that were similar for all network types. Above these minima, v_{max} and initial substrate concentration interplay with the network type in enabling invasions. Invasion was the least efficient in the spatially clustered network, whereas in the small world network a relatively high number of nodes was occupied for wide parameter ranges.

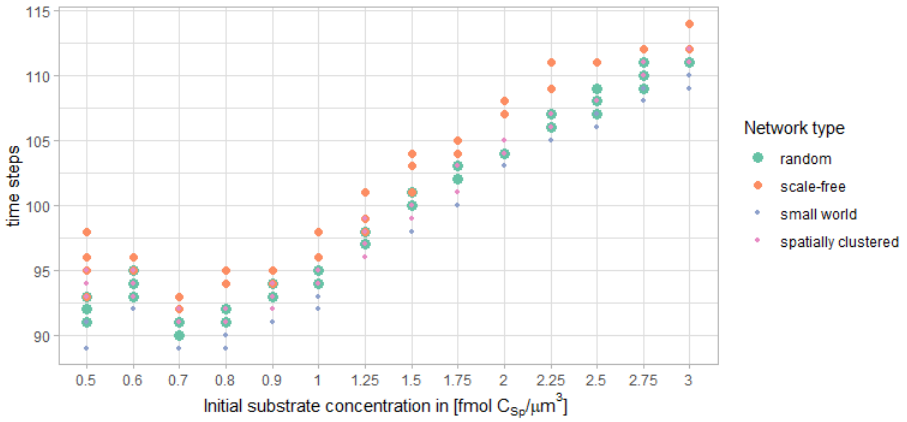

Figure 3.10: Time needed for decomposition of 70% of initial substrate for different initial substrate concentrations.

Number of time steps until 70% of the initial substrate is degraded for different initial substrate concentrations in fmol C_{Sp} / μm^3. For each setting 5 runs were simulated, but only runs where at least 70% of the initial substrate were degraded are shown.
With initial substrate concentrations higher than 1 we see a linear correlation between initial substrate concentration and time needed for decomposition. These are values of initial substrate concentration, where in all network types the maximum number of invadable pores is reached by microbes (Figure 3.8). Below an initial substrate concentration of 1 C_{Sp} / μm^3 decomposition is remarkably slower. We observed slower degradation close to the threshold (S_0^*).

pores microbes can be found. Between 0.5 and 1 fmol C_{Sp} / μm^3 there can be seen high variability in the number of occupied pores within and between the different network types. Furthermore, it depends on the network type whether microbes are able to invade all pores ore not. The construction algorithms of the random network and the spatially clustered network produce disconnected networks that consist of many smaller components for an average node degree of 2.7 (figure 3.21). There may exist unconnected areas of the network from which no node was occupied initially. Due to lack of connections an invasion of these areas is not possible from other network parts.
The impact of the initial substrate concentration on the duration of the decomposition is shown in figure 3.10. With initial substrate concentrations higher than 1 we see a linear correlation between initial substrate concentration and time needed for decomposition of 70%. These are values of initial substrate concentration, where in all network types the maximum number of invadable pores is reached by microbes (Figure 3.8). Below an initial substrate concentration of 1 C_{Sp} / μm^3 decomposition is remarkably slower. We observed slower degradation close to the threshold (S_0^*), which is similar to what we observed earlier for v_{max} values close to the threshold v_{max}^* in figure 3.5. The interrelations between S_0 and v_{max} and their impact on the occupied pores are summarized in figure 3.9.

3.2.2 Impact of enzymatic parameters

Enzymatic reactions also strongly impact microbial activity and decomposition efficiency (see equation 2.3). This section is concerned with the impact of k_{cat}, the maximum kinetic

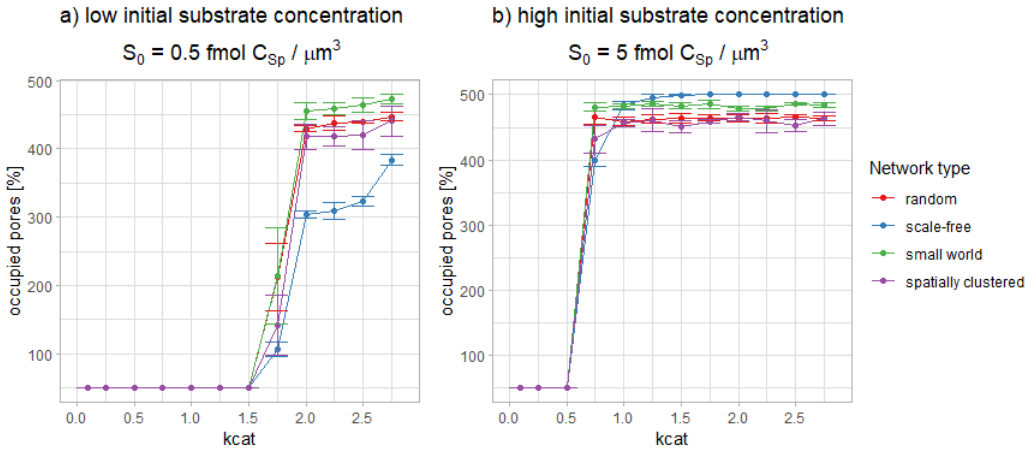

Figure 3.11: Impact of k-cat on the number of occupied pores.

Pores that were occupied by microbes for different maximum enzyme activity parameter k-cat. Colors indicate network types. The average node degree was 2.7 for all networks. Values from 5 runs. Enzymatic activity is fundamental for microbial uptake and growth. We observed, that for too low k-cat microbial growth stays below the threshold B^*_{max} and invasion of pores is not possible. Is k-cat high enough to enable invasion in principle, the invasion efficiency strongly depends on the network type.

enzyme activity. Figure 3.11 summarizes the impact of k_{cat} on the fraction of pores that were occupied. Aside from v_{max} and S_0, high enough enzyme activity is fundamental for an efficient invasion of the pore space. With too low k_{cat} microbes only stay in the initially occupied pores, because they never reach B_{max}. These results are also reflected in figure 3.12.

3.3 Transmission

To compare the system of microbes decomposing substrate in a pore network with classic SIR-models it is also useful to assess what impacts the rate of transmission of microbes from one pore to another. In SIR-models the transmission rate is fundamentally influenced by the transmission probability. We define transmission probability as the mean fraction of neighboring pores that was invaded from a pore. In our model the transmission probability depends on the network type, microbial growth factors and available substrate. 3.13 presents the average transmission rate of a pore in all network types with different initial substrate concentrations. If the substrate concentration is very low, microbes don't reach B_{max} and no invasions happen. Is the substrate concentration high enough, microbes reach the neighboring pores which also provide substrate and enable microbial growth. But the figure also shows, that over a minimum initial substrate concentration that is needed to reach B_{max} no further increase of transmission probability was observed with higher substrate concentration. The network type also influences the transmission probability. In the scale-free network the transmission probability was lower than in the other network types for all substrate concentrations. Also a dependence of the maximum microbial growth rate on the transmission probability was observed. Figure 3.14 presents the transmission probabil-

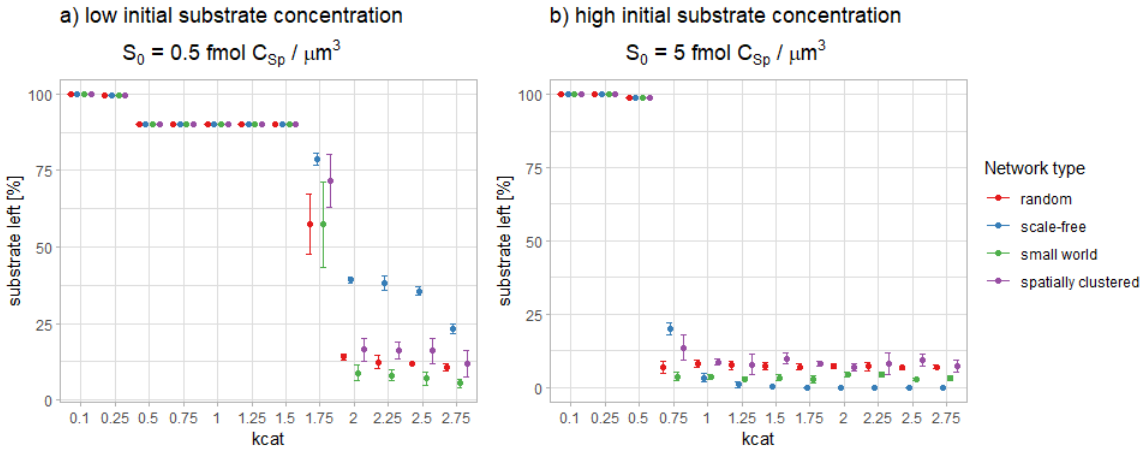

Figure 3.12: Impact of k-cat on the amount of primary substrate left at the end.

Proportion of primary substrate that was left at the end for different enzymatic enzyme activity parameter k-cat in al network types. Error bars indicate standard deviation. The average node degree was 2.7 for all networks. Values from 5 runs.
In the decomposition efficiency there is a step from no decomposition to decomposition of the available substrate in the initially occupied pores with an increase in k-cat from 0.25 to 0.5 (in the low substrate concentration scenario). With further increase in k-cat, we observed an interplay with the network structure and different decomposition efficiency depending on the network type.

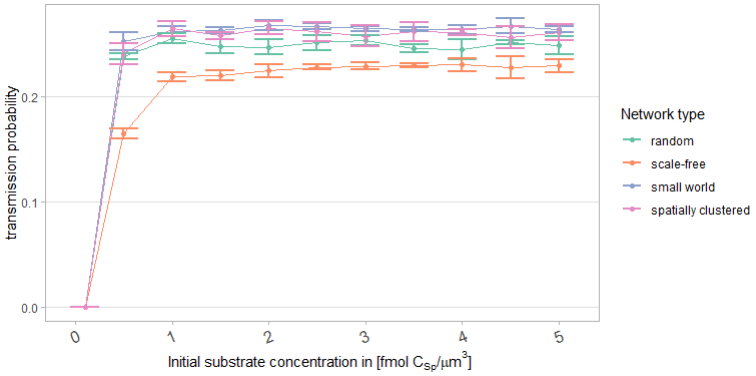

Figure 3.13: Transmission probability for different initial substrate concentrations in all network types
Transmission probability as the mean fraction of neighbors of a pore that was invaded from a pore per time step in all network types. Initial substrate concentrations from 0.1 to $5 fmol\, C_{Sp}/\mu m^3$. v_{max} was 0.29. Averaged over 5 runs. Error bars indicate standard deviation.
If the substrate concentration is very low, microbes don't reach B_{max} and no invasions happen. Is the substrate concentration high enough, microbes reach the neighboring pores which also provide substrate and enable microbial growth. But over a minimum initial substrate concentration that is needed to reach B_{max} no further increase of transmission probability was observed with higher substrate concentration. With high substrate concentrations the network type shows strong influences on the transmission probability.

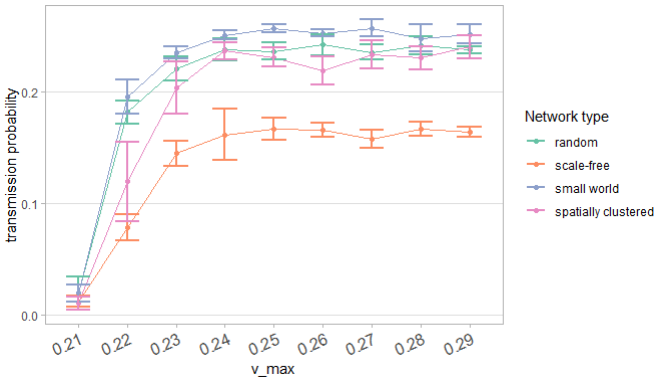

Figure 3.14: Transmission probability for different v_{max} in all network types.
Transmission probability as the mean fraction of neighbors of a pore that was invaded from a pore per time step in all network types. v_{max} from 0.21 to 0.29. Initial substrate concentration was $0.5\,fmol\,C_{Sp}/\mu m^3$. Averaged over 5 runs. Error bars indicate standard deviation.
With increasing v_{max} the transmission probability increases up to a certain value where then further increase in v_{max} does not impact transmission probability anymore. Network structure plays a crucial role for the transmission probability.

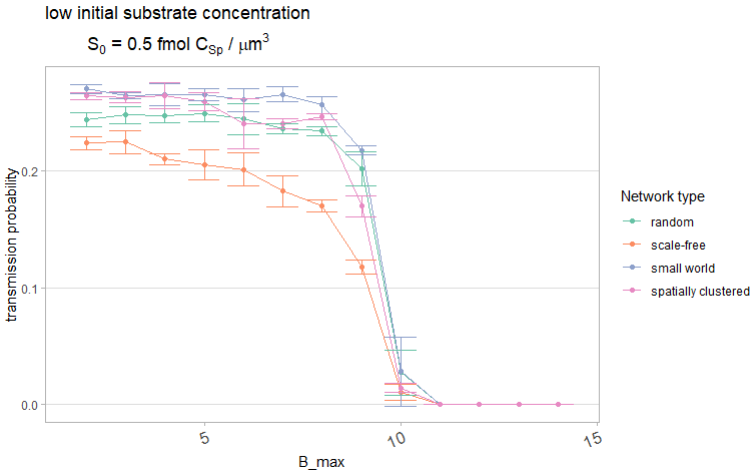

Figure 3.15: Transmission probability for different B_{max} in all network types
Transmission probability as the mean fraction of neighbors of a pore that was invaded from a pore per time step in all network types. B_{max} from 2 to 14 on the x-axis. Initial substrate concentration was $0.5\,fmol\,C_{Sp}/\mu m^3$. $v_{max} = 0.29$. Averaged over 5 runs. Error bars indicate standard deviation. Is B_{max} too high, so that microbes can not reach this value, no invasions occur and the transmission probability is 0. In the lower range of B_{max} again the network type governs transmission probability.

ity for different v_{max} values with an initial substrate concentration of $0.5\,fmol\,C_{Sp}/\mu m^3$. Similar dependence of the transmission probability on the microbial growth parameter as on the substrate concentration is shown. With increasing v_{max} the transmission probability is increasing up to a certain value where then further increase in v_{max} does not impact transmission probability anymore. This value was approximately the same for all network types (for $v_{max} > 0.24$ no further increase in the transmission probability was observed). However, the transmission probability differed between the network types. It was the lowest again in the scale-free network.[7] Figure 3.15 displays the interrelation of the transmission probability with B_{max}. In a range where B_{max} is reachable for microbes with the specific parameter settings ($S_0 = 0.5\,fmol\,C_{Sp}/\mu m^3$, $v_{max} = 0.29$) network structure has strong impact on the transmission probability. If B_{max} is too high, microbia biomass never reaches this value in a pore and no invasions occur at all.

3.4 Network properties

The second research question aims to determine the effect of network properties like number of nodes, average node degree, shortest path length and clustering coefficient on the efficiency of organic matter decomposition. A strong indicator for the impact of the connectivity pattern of the different network types is figure 3.16. It compares the fraction of substrate that was left at the end of the run in all network types with different network sizes. The effect of the network size on the decomposition efficiency was only marginal. But the effect of the interplay of initial substrate concentration and the network structure on the decomposition efficiency is very clear. The scale-free network which is the network type where the largest fraction of initial substrate remained undegraded with low initial substrate concentration is also the network type where decomposition was very efficient when the substrate concentration was high enough. With a substrate concentration of $5\,fmol\,C_{Sp}/\mu m^3$ nearly all of the initial substrate was degraded. This effect can also be seen for the other network types but it is outstandingly strong in the scale-free network. The following section is concerned with a detailed analysis of the impact of network properties on decomposition efficiency.

3.4.1 Clustering coefficient and average shortest path lengths

The clustering coefficient and average shortest path lengths of a small world network depend on the rewiring probability (figure 3.17). Because in this network type the parameters clustering coefficient and shortest path length can be changed while the other network properties are conserved, this type is very well suited to experimentally investigate the effects of these parameters. To analyze the effect of these network properties on the decomposition efficiency, we used the small world network type with varying rewiring probability. The rewiring probability p is defined as the probability with which each link is randomly rewired after all nodes are connected to their close neighbors in the setup of the small world network.

[7] Details on the distribution of the transmissions over the pores in the different network types can be found in the supplementary material.

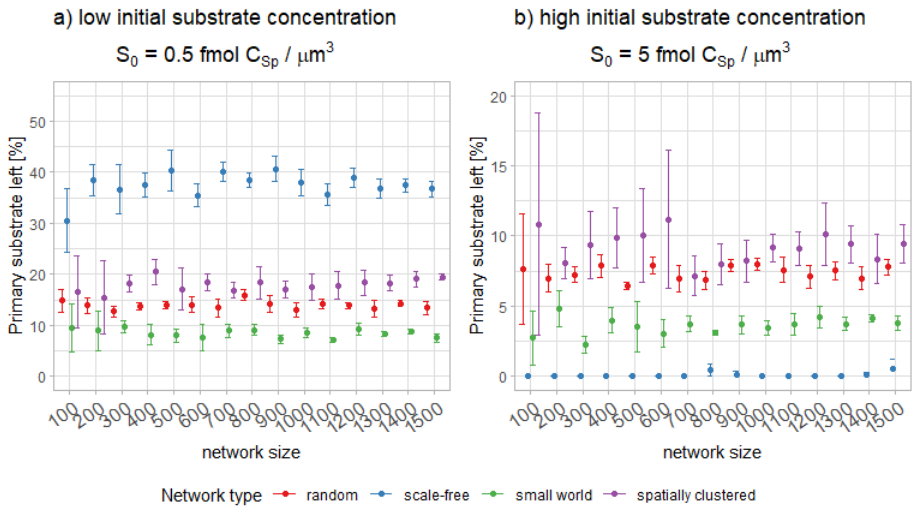

Figure 3.16: Primary substrate left for different network sizes

Fraction of primary substrate that was left at the end of the run for different network sizes in all network types. The average node degree was 2.7 for all networks. Averaged over 5 runs. Error bars indicate standard deviation. Note the different scales of the y-axes.
We found that the number of nodes does not influence the decomposition efficiency. The overall proportion of substrate left was similar for all network sizes in both substrate level scenarios. A dominant factor is the network type and the initial substrate concentration.

This rewiring process introduces shortcut connections over long distances in the network. The rewiring probability is decisive for the clustering and the path lengths in the network. The more links are rewired in the construction of the small world network, the lower the local clustering and the shorter the average path lengths. The connectivity structure of a small world network without rewiring ($p = 0\%$) is equivalent to a regular grid. Whereas with $p = 100\%$ all links are randomly rewired, what results in a random network. Between these extremes, more or less strongly clustered networks can be identified. Furthermore, the larger the network, the longer the average shortest path length. Figures 3.17 and 3.18 illustrate the connection of the rewiring probability with the shortest path length and clustering coefficient in small world networks. The higher the rewiring probability, meaning that more links are reconnected during the set-up process, the lower is the clustering in the network. Small world networks with a rewiring probability of 5% can reach clustering coefficient values that are similarly high as in the spatially clustered network. This is true at least for an average node degree of about 4 (3.18, a).

The comparison in figure 3.19 shows high similarity between the two initial substrate concentration regimes, which is in accordance with previous observations in the small world network, where also only small changes in the decomposition efficiency were shown for higher initial substrate concentration in small world networks[8]. In both plots we see shorter runs with higher rewiring probability and longer runs with lower rewiring. In the more clustered networks it took longer to decompose 70% of the initial primary substrate.

Not only the duration of the decomposition in small world networks depends on the

[8] A detailed picture of the evolution of primary substrate over time (figure 6.15) can be found in the supplementary material

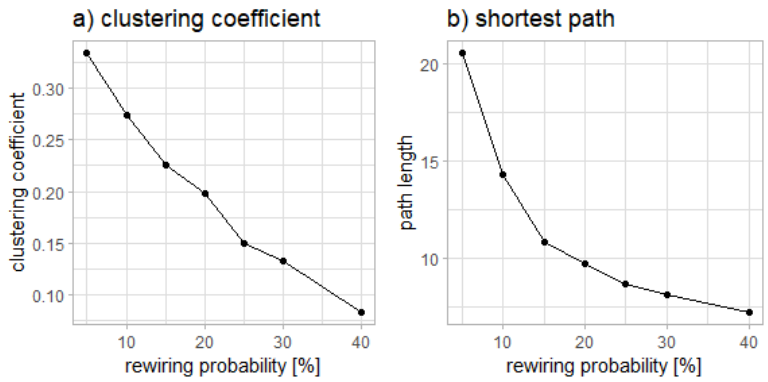

Figure 3.17: Clustering coefficient and average shortest path in the small world network in dependence on the rewiring probability.

a) clustering coefficient b) average shortest path
For small world networks with 400 nodes and average node degree 2.7. In networks that consisted of more than one component, the measures were calculated from the component containing the highest number of nodes. The clustering coefficient and the average shortest path length correlate with the rewiring probability. The rewiring process breaks up local clusters in the network structure and introduces short range connections, which reduce the path lengths.

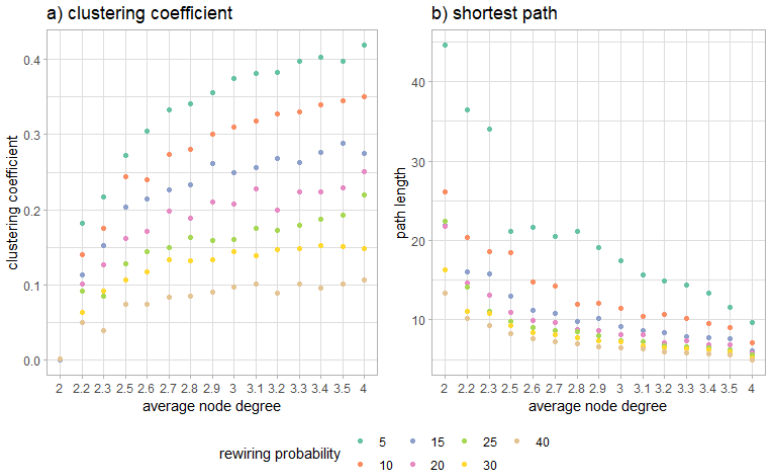

Figure 3.18: Clustering coefficient and average shortest path in the small world network.

a) clustering coefficient b) average shortest path
For small world networks with 400 nodes. In networks that consisted of more than one component, the measures were calculated from the component containing the highest number of nodes. In addition to the rewiring probability, the average node degree affects clustering coefficient and shortest path length.

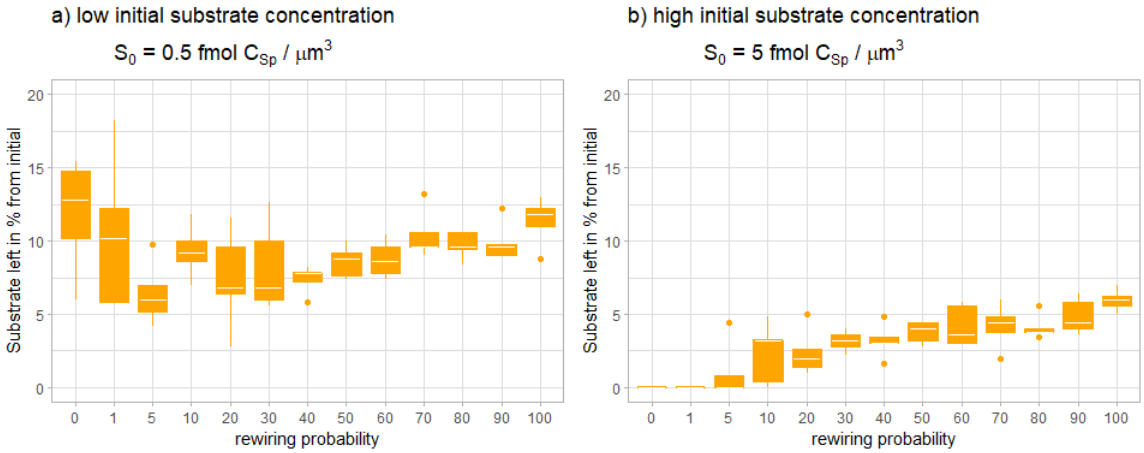

Figure 3.19: Primary substrate left in the small world network

Amount of primary substrate left at the end of the runs in % of the initial substrate in small world networks with 500 nodes and different rewiring probability. The rewiring probability p defines the probability with which each link of the network is randomly rewired to introduce shortcut connections in the setup of the network. The connection pattern of a small world network with $p = 0$ is equivalent to a regular grid, whereas a small world network with $p = 100$ is a random network. Results from 5 runs.
The figure shows only a small effect of the initial substrate concentration on the decomposition efficiency. The rewiring probability has a negative effect on the decomposition efficiency, at least in the high substrate regime and for the higher rewiring probabilities in the lower initial substrate regime.

rewiring probability, but also the efficiency in terms of the amount of substrate left at the end. More substrate was left at the end in % from the initial substrate in small world networks with higher rewiring probability (3.19). With higher initial substrate concentration more substrate remained undegraded for higher rewiring probability, with the most substrate left in the random network ($p = 100\%$). This indicates that strong clustering enables for more complete decomposition.
To compare networks with different average shortest path length, we constructed small world networks with different numbers of nodes, as the length of the shortest paths depends strongly on the network size (compare figure 3.23). As can be seen in figure 3.20, the decomposition rate depends on the rewiring probability and the number of nodes in the network. For all network sizes the decomposition rate was lower for low p. In highly clustered networks of all sizes the decomposition rate of the first 70% of the initial substrate was lower than in less clustered networks. Clustering enables for efficient decomposition in terms of completeness, but slows down the decomposition. Longer average shortest path lengths also slow down the decomposition rate. The rates were slightly smaller in networks with higher number of nodes. [9]

3.4.2 Average node degree

An average node degree of 4, as it is used in the experiments in the previous section, is unrealistic in real soils (Pérez-Reche et al., 2012) but the average node degree is an integral

[9] Frequency counts of invasions per pore can be found in the supplementary material (figure 6.13).

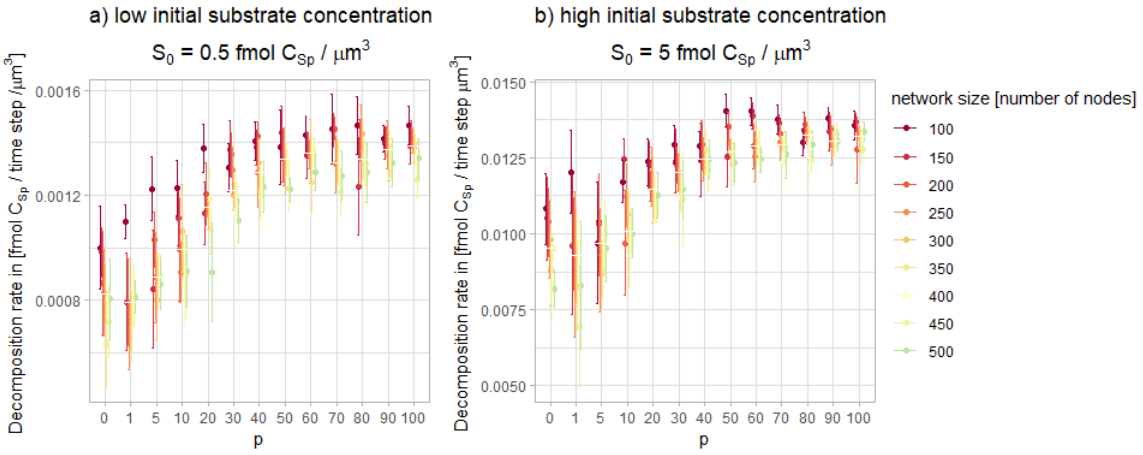

Figure 3.20: Rate of decomposition in the small world network

Decomposition rate in the small world network with different numbers of nodes and different rewiring probabilities. Rewiring probability p on the x-axis. Colors indicate number of nodes in the network. Averaged over 5 runs. Error bars indicate standard deviation.

factor defining properties of a network. Therefore, this section is concerned with the effect of average node degree of the network.[10]

In figure 3.21 the average number of components, connected subgraphs of the network (Pastor-Satorras et al., 2015) as a function of average node degree are presented. The number of components of a network is important, as it determines the fraction of nodes microbes starting from one randomly selected node in the network are in principle able to invade. Does the network only consist of one large component, the possibility exists that microbes can reach all nodes in the network, given the right conditions. In a network that consists of one large component every node in the network is connected by a path of links with every other node. Each network type exhibits a certain connectivity pattern, which determines the probability of occurrence of disconnected components. In contrast to the other network types, all constructed scale-free networks are composed of one large component. In the small world networks the rewiring of links can disconnect parts of the networks especially for small average node degrees. During the rewiring process some connections from a fully connected network are deleted and reestablished between a random pair of nodes (see also section 3.4.1). The spatially clustered and the random network are more likely to consist of more than one component. The average number of components steeply increases for lower average node degrees.

Also, the clustering and shortest path length of a network depend on the average node degree and are supposed to impact the behavior of the dynamics on the network. The clustering coefficient is a measure for how connected neighbors of a nodes are themselves.[11] This is why we also compared the network types with regard to their clustering coefficient and shortest path lengths in figure 3.22 and 3.23 and had a look at the effect of the rewiring

[10] Since the average node degree of a grid is always 4 it is left out of discussion in the following section.

[11] A definition of clustering coeffiecent and average shortest path are given in the supplement in section 6.1.

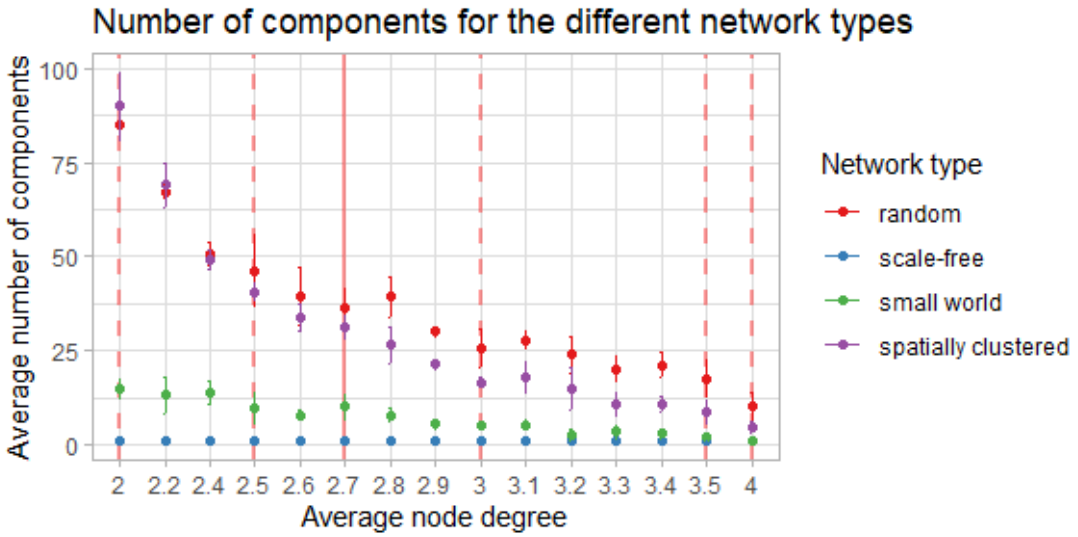

Figure 3.21: Average number of unconnected components in all network types.

Average number of unconnected components for all network types as a function of average node degree. The scale-free network always consists of only one large connected component. The random network has the highest number of components for almost all average node degrees. And the number of components in the spatially clustered network is also high. The red lines are drawn at values of average node degree, that are used in the following sections to analyse the system behaviour. The values at the dashed red lines are used to explore the effect of the average node degree of the system. The solid line is drawn at an average node degree of 2.7, which is the standard value for all other experiments.

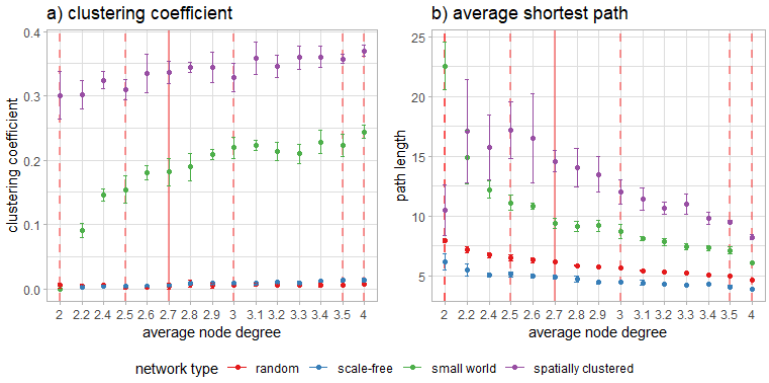

Figure 3.22: Clustering coefficient and average shortest path of the networks.

a) clustering coefficient b) average shortest path
For networks of all types, consisting of 300 nodes with different average node degrees. The rewiring probability for the small world network was $p = 20\%$. In networks that consisted of more than one component, the measures were calculated from the component containing the highest number of nodes. The values at the dashed red lines are used to explore the effect of the average node degree of the system. The solid line is drawn at an average node degree of 2.7, which is the standard value for all other experiments.

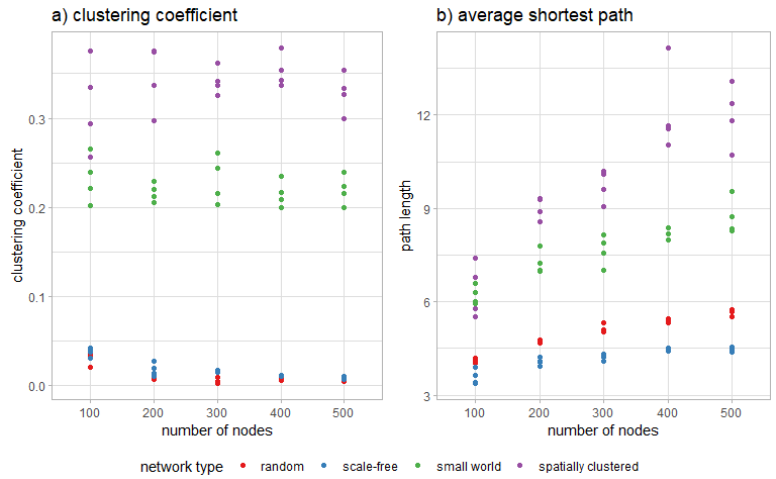

Figure 3.23: Clustering coefficient and average shortest path of the networks for different network size.

a) clustering coefficient b) average shortest path
For networks of all types, with increasing number of nodes. Average node degree was 3 in all networks. The rewiring probability for the small world network was $p = 20\%$. In networks that consisted of more than one component, the measures were calculated from the component containing the highest number of nodes. The clustering coefficient in independent of the number of nodes, whereas we found a positive correlation between the shortest path lengths and number of nodes in a network.

probability in small world networks on the clustering coefficient and shortest path lengths in figure 3.18. Clustering is the highest in the spatially clustered network overall and also high in the small world network, that was set up with a rewiring probability $p = 20\%$.

The network types with the lowest clustering were the scale-free network and the random network. In these two network types also the increase of the clustering coefficient with higher average node degree was not as strong as in the spatially clustered and small world network. In the opposite direction the average node degree affects the shortest path length of a network. For all network types the shortest path lengths decrease for increasing average node degree in b) in figure 3.22. The longest average shortest path lengths have the spatially clustered networks, this difference is the greatest with small average node degree. The second largest path lengths can be found in the small world network with $p = 20\%$. It needs to be kept in mind that the average shortest path strongly depends on the rewiring probability in small world networks as b) in figure 3.18 depicts. The network geometry of the scale-free networks, that consist of few highly connected hubs, provides very short paths between all pairs of nodes on average. Most nodes are close to one highly connected hub and the hubs are connected to other hubs with high probability. In that way short paths to nearly all nodes in a network are provided.

Clustering coefficient and average shortest path of a network also depend on the number of nodes in the network. This is compared in figure 3.23. In a) in 3.23 an overview of the clustering coefficient for different network sizes in all network types is given. In the scale-free and random network the clustering coefficient is higher when the network is relatively small. In the highly clustered networks no relation between the network size and the clustering coefficient can be seen in this figure. Probably, if the range of network sizes would be

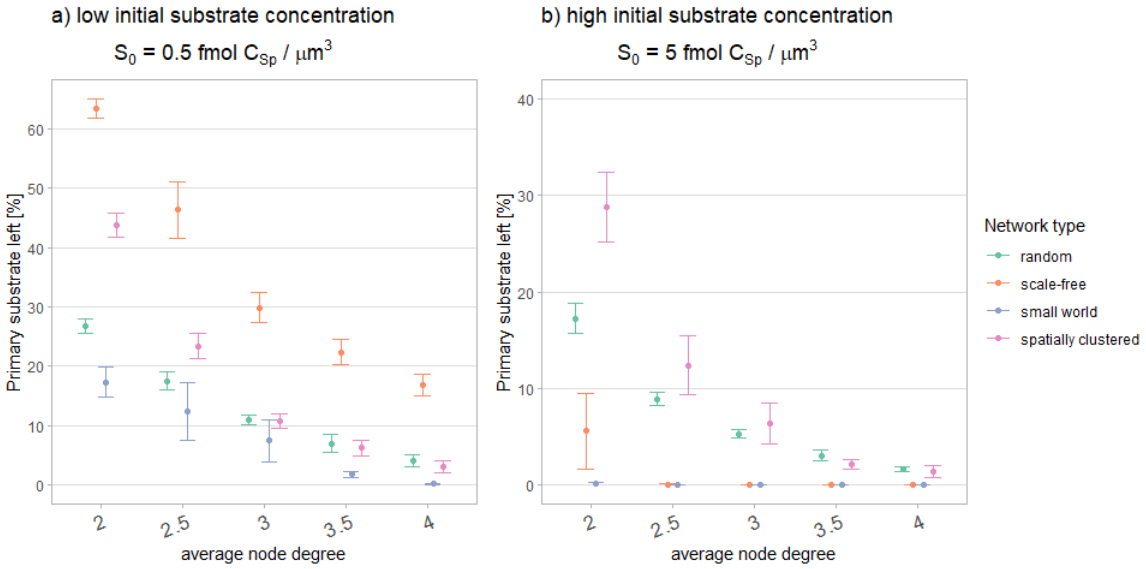

Figure 3.24: Primary substrate left undegraded

Percentage of initial substrate remaining undegraded at the end of a run. Simulations ended if the stop condition was fulfilled ($B < 0.01B_0$ in all pores). Averaged over 5 runs. Error bars indicate standard deviation. Data points are grouped along the x-axis. Note that the scale of the y-axes is different in the two plots. Overall, in the plots we see an increase in decomposition efficiency with an increase in average node degree.

increased also here a relation will become visible. The average shortest path length increases sharply in dependence on the network size in all network types (figure 3.23, b).

Figure 6.10 in the supplementary material gives an overview of the development of the primary substrate over time in all network types with average node degrees of 2, 3 and 4. Closer investigation of the rate of decomposition can be seen in figure 3.26.

There can be found similarities also in the decomposition of the substrate in the networks with very low average node degree for both initial substrate concentrations. The plots from networks with average node degree 2 both show much flatter curves of substrate decomposition for all network types. And the time it took to reach the 1% mark of biomass in all pores increased remarkably in all network types. Although, this increase in the duration was the smallest in the random network.

Also differences in the completeness of substrate decomposition can be seen. Especially in networks with average node degree 2 there seems to remain more substrate undegraded at the end of the run. Since we look at lines here, which are averaged over multiple runs that all end at different times, the endpoints may be misleading. More meaningful results on the fraction of primary substrate that is left at the end of the runs is presented in figure 3.24.

In all network types and both initial substrate levels the decomposition of the initial primary substrate was the more complete the higher the connectivity of the pores was. When there was substrate left at the end of the runs, the fraction of the initial substrate was higher for lower average node degree. The most incomplete was the decomposition of initial substrate in the scale-free network with lower initial substrate concentration. Averaged over all average node degrees in the scale-free network 36% of the initial substrate remained undegraded with low initial substrate concentration. Then comes the spatially clustered

network where 17% of the initial substrate remained, then the random network with 13% overall and in the small world network only 8% of the initial substrate remained. There are also large differences for different average node degrees. Overall, in can be said, that the decomposition was more incomplete for lower average node degrees. Averaged over all network types with average node degree 2 38% of the initial substrate was left, with average node degree 3 there were only 15% left overall and with average node degree 4 the substrate largely was degraded and only 6% were left. There were also considerable differences within the network types. In the scale-free network the fraction of undegraded substrate ranged from 63% to 17% for average node degree 2 and 4 respectively. A wide range could also be found in the spatially clustered network (from 44% with average node degree 2 to only 3% with average node degree 4). Smaller were the ranges in the random network (27% left with average node degree 2 and 4% left with average node degree 4) and the small world network (17% with average node degree 2 to 0% with average node degree 4). The small world network with average node degree 4 was the only one that enabled a complete decomposition of the initial substrate with an initial substrate concentration $S_0 = 0.5$ fmol C_{Sp} / μm^3.
The picture looks very different in various terms for a higher initial substrate concentration $S_0 = 5$ fmol C_{Sp} / μm^3 (figure 3.24, b). The network type that enables the most efficient decomposition overall is still the small world network, where no substrate was left at the end of the run for all average node degrees. But also, in the scale-free network, that was the least efficient structure with low initial substrate concentration now also only 1% of the initial substrate remained. In the spatially clustered and the random network also more substrate was degraded with higher initial substrate concentration (10% and 7% remained undegraded respectively). Overall, although more substrate was there in the beginning, even larger parts of it could have been decomposed in all network types. This change was the most prominent in the scale-free network.

A dependence of the transmission probability on the average node degree can be observed with low and high initial substrate concentration (Figure 6.20). In the scale-free network, the transmission probability is lower for smaller average node degree with low initial substrate concentration and higher for smaller average node degree with high initial substrate concentration. This effect of a decrease in the transmission probability for higher average node degree with the higher substrate concentration was also found in the other network types. Whereas, with low substrate concentration an increase of the average node degree only from 2 to 2.5 induced a slight increase in the transmission probability in the small world, spatially clustered and random network. For further increase of the average node degree the transmission probability decreased again in these network types.

The average node degree can also impact the time needed for decomposition of 70% of the initial substrate and the rate of decomposition in some network types. The decomposition rate was lower in networks with lower average node degree for all network types and both initial substrate levels (figure 3.26). What stands out is the effect in the spatially clustered network and the scale-free network, where the decomposition rate was particularly lower with low average node degree. Overall, the decomposition rate is larger with

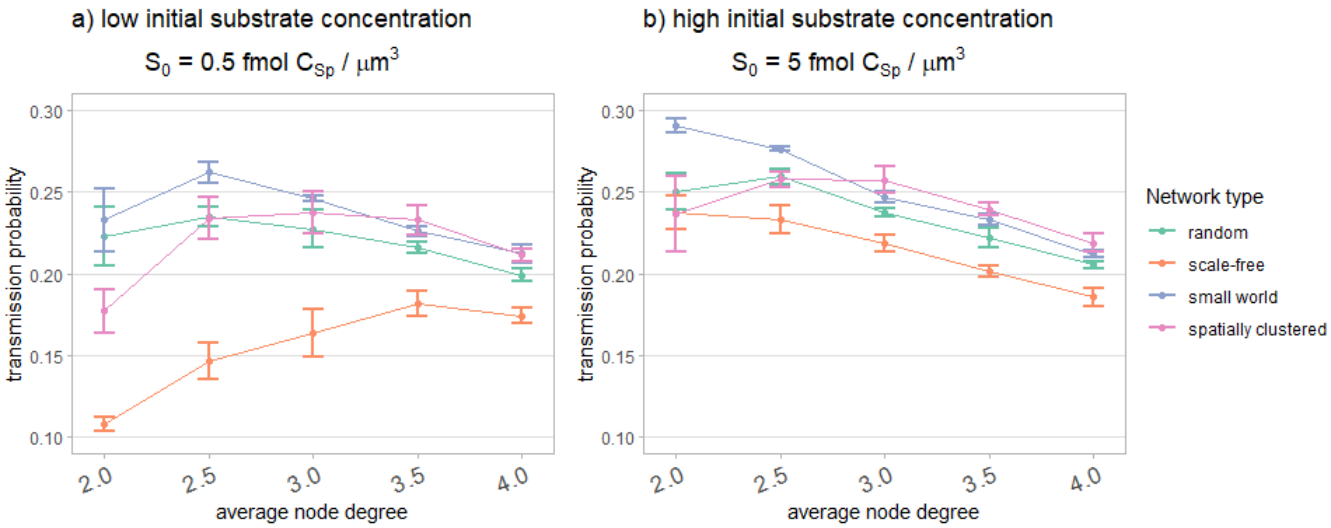

Figure 3.25: Transmission probability for different average node degree in all network types Transmission probability as the mean fraction of neighbors of a pore that was invaded from a pore per time step in all network types. Averaged over 5 runs. Error bars indicate standard deviation. We found a dependence of the transmission probability on the average node degree with low and high initial substrate concentration. The transmission probability in addition differs between network types.

higher initial substrate concentration and larger average node degree. The impact of the average node degree on the decomposition rate is very strong in the spatially clustered network.

3.4.3 Carbon use efficiency

Carbon use efficiency (CUE) can be defined as $CUE = \frac{\text{uptake} - \text{respiration}}{\text{uptake}}$, the fraction of C uptake which is used for the build-up of microbial biomass (Sinsabaugh et al., 2013; Manzoni et al., 2012). Figure 3.27 summarizes the impact of the average node degree on the carbon use efficiency of microbes in all network types. In all network types and both initial substrate levels the carbon use efficiency was higher with higher average node degrees. This means, that a larger fraction of the carbon that was taken up could be used for the built up of microbial biomass in more connected networks. Aside from that, network type could be identified as an important determinant for CUE. In the spatially clustered network CUE was significantly lower than in other network types with lower initial substrate concentration. Whereas, the random network showed a relatively high CUE. The substrate concentration did not heavily affect the CUE, but a higher initial substrate concentration lead to small shift towards higher CUE in all network types but the scale-free network. With high initial substrate concentration the CUE overall was lower in the scale-free network compared to the other network types.

3.5 Additional Heterogeneity

To explore the impact of heterogeneity in some network properties on the efficiency of decomposition in this section first networks with heterogeneous pore sizes will be investigated.

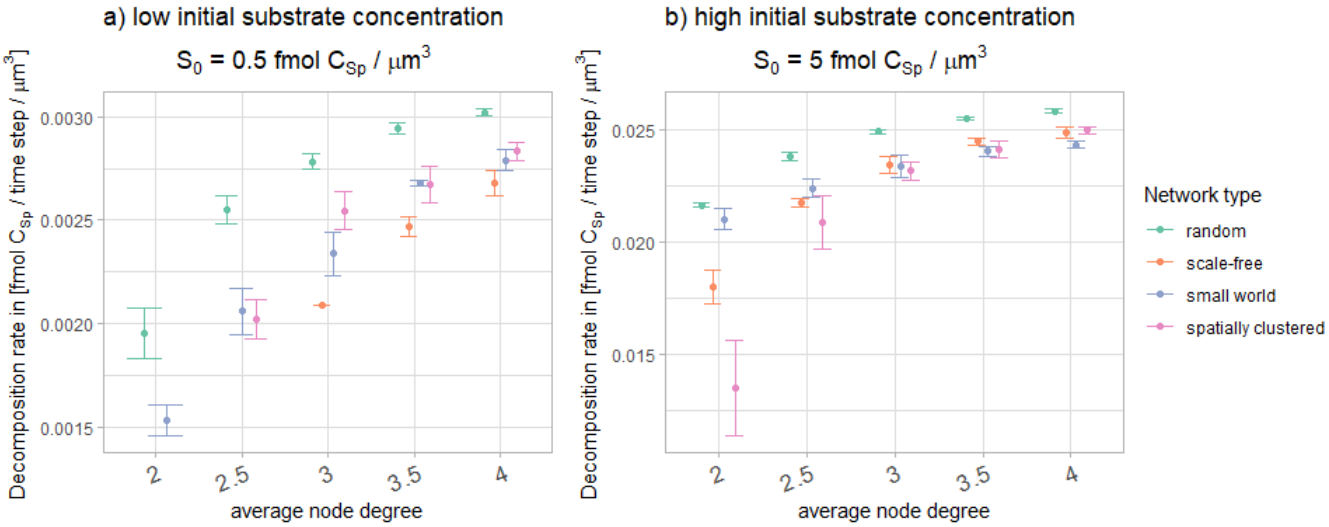

Figure 3.26: Decomposition rate for different average node degree in all network types
Substrate decomposed per time step on average until 70% of the initial substrate are degraded in all network types with different average node degrees. Averaged over 5 runs. Error bars indicate standard deviation. Data points are grouped along the x-axis. Note that the scale of the y-axes is different in the two plots. The decomposition rate was lower in networks with lower average node degree for all network types and both initial substrate levels. The decomposition rate was particularly lower with low average node degree in the scale-free network and in the spatially clustered network.

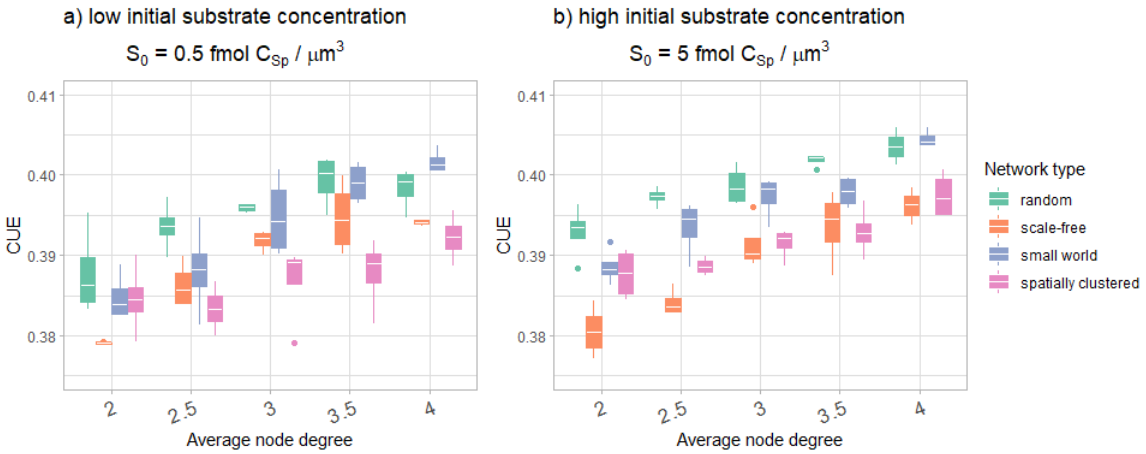

Figure 3.27: Carbon use efficiency for different average node degree in all network types
Carbon use efficiency in all network types with different average node degrees. The carbon use efficiency was calculated of the fraction of C from the uptake that is allocated in microbial biomass: $CUE = \frac{\text{uptake} - \text{respiration}}{\text{uptake}}$ Results from 5 runs.
For both of initial substrate concentrations a two-way Anova test states significant differences in the carbon use efficiency between the network types and between the average node degree ($p < 0.001$) and also shows that the relationship between average node degree and CUE depends on the network type ($p < 0.05$).

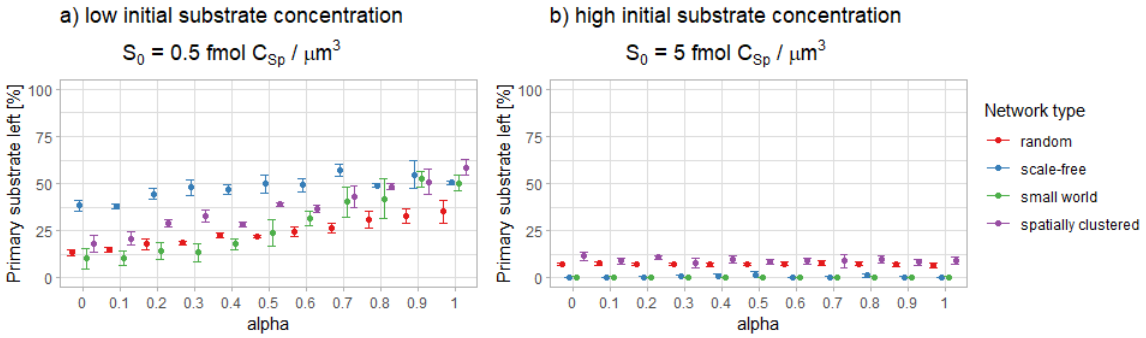

Figure 3.28: Primary substrate left for different heterogeneity in pore sizes

Each point shows the average fraction of primary substrate that was left at the end of the run in all network types. On the x-axis alpha indicates different levels of heterogeneity in the pore sizes. The average node degree was 2.7 for all networks. Averaged over 5 runs. a) The initial substrate concentration was $S_0 = 0.5$ fmol C_{Sp} / μm^3. b) The initial substrate concentration was $S_0 = 5$ fmol C_{Sp} / μm^3.
We found, that the efficiency of the decomposition strongly depends on the heterogeneity of the pore sizes in the lower substrate concentration regime in all network types. Whereas the amount of substrate left at the end of the run differs for the network types in the higher substrate concentration scenario, but is similar for all heterogeneity levels.

Then heterogeneity in chemical pore properties is generated in terms of the initial substrate concentration S_0 and B_{max}, the threshold for invasion of a new pore. B_{max} is a measure for how easily microbes can pass to a neighboring node. Lower B_{max} indicates that microbes find good conditions for movement and are able to invade new nodes already at low microbial biomass concentration in the current node. In contrast, higher B_{max} represents conditions of decreased flagellated velocity and dispersal ranges, and as a result microbes invade new pores only under high density pressure (Tecon and Or, 2016).
Alpha is the measure for the heterogeneity. The higher alpha, the more widespread are the values. How heterogeneity was introduced in the model is described in detail in section 2.3.5.

3.5.1 Heterogeneous pore sizes

In real soils pores are not only spatially distributed heterogeneously but can also strongly differ in their sizes. Therefore, this section reports results from simulations with heterogeneity in the sizes of the pores.

It can be seen in figure 3.28 a) that the efficiency of the decomposition strongly depends on the heterogeneity of the pore sizes in the lower substrate concentration regime. For all network types differences in the proportion of substrate that remains at the end of the run can be observed for different alpha values. In the random network with no heterogeneity in pore sizes on average 14% of the initial substrate remained undegraded. This value increases for increasing alpha up to 22% for $alpha = 1$. In the scale-free network the range is even wider. With all equal pore sizes 38% remain and with the most heterogeneous pore sizes there are 51% left at the end. In the small world network the values range from 14% ($alpha = 0$) to 25% ($alpha = 1$) and in the spatially clustered network from 19% ($alpha = 0$) to 25% ($alpha = 1$). We observed an interaction between pore size heterogeneity and network

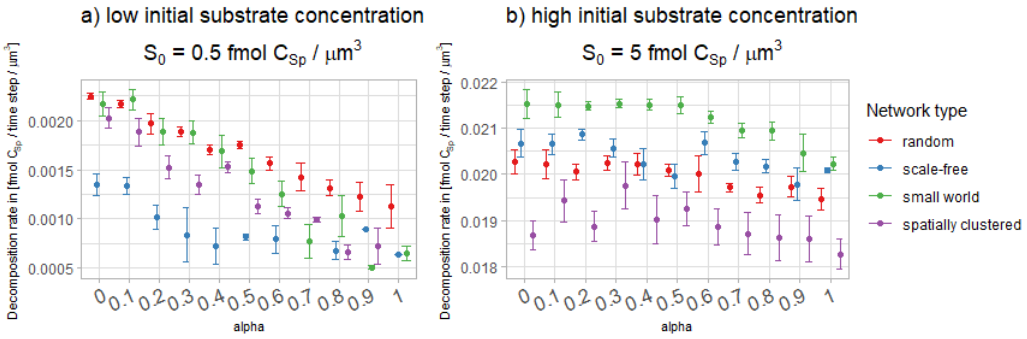

Figure 3.29: Decomposition rate for heterogeneous pore sizes

Each point shows the average decomposition rate of 70% of the initial substrate in different network types (colors). The average node degree was 2.7 for all networks. Values from 5 runs. On the x-axis alpha indicates different levels of heterogeneity in the pore sizes. a) The initial substrate concentration was $S_0 = 0.5$ fmol C_{Sp} / μm^3. b) The initial substrate concentration was $S_0 = 5$ fmol C_{Sp} / μm^3.
The figure illustrates, that in networks with high heterogeneity in the pore sizes the decomposition tends to be slower than in more homogeneous networks. For low substrate concentration there is a strong relationship between the decomposition rate and the heterogeneity of the pore sizes. This effect was smaller in the scale-free network than in the other network types. And it was also weakened by higher substrate concentration. The largest difference in decomposition rate for different alpha remains in the small world network in the high initial substrate concentration.

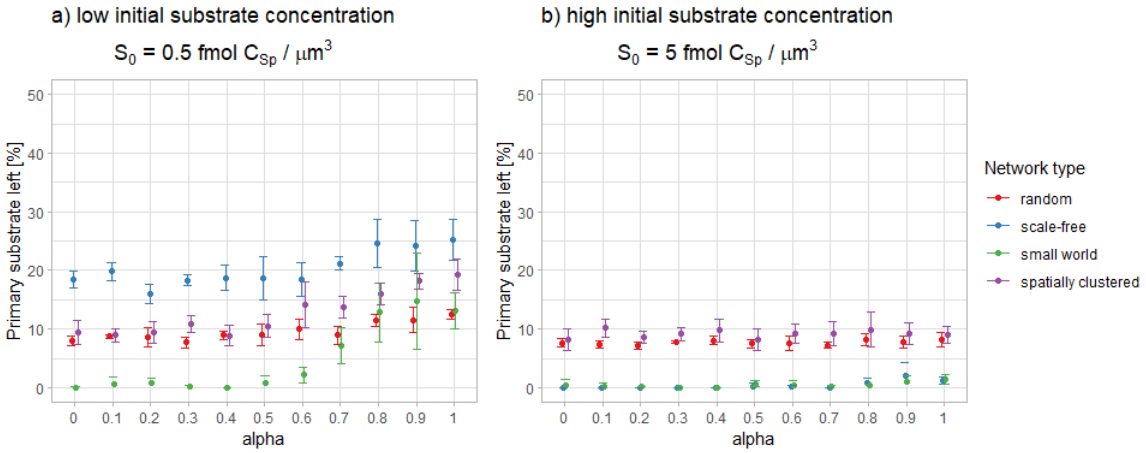

Figure 3.30: Primary substrate left for heterogeneous substrate distribution

Fraction of primary substrate that was left at the end of the run for different levels of heterogeneity in the primary substrate distribution in all network types (colors). On the x-axis alpha indicates different levels of heterogeneity in the distribution of initial substrate. The average node degree was 2.7 for all networks. Values from 5 runs. a) The mean initial substrate concentration was $S_0 = 0.5$ fmol C_{Sp} / μm^3. b) The mean initial substrate concentration was $S_0 = 5$ fmol C_{Sp} / μm^3.
In the simulations with a low mean substrate concentration in most network types an effect on the decomposition efficiency can be found. This effect was the strongest in the small world network. In the higher substrate scenario no differences in the heterogeneity levels were observed.

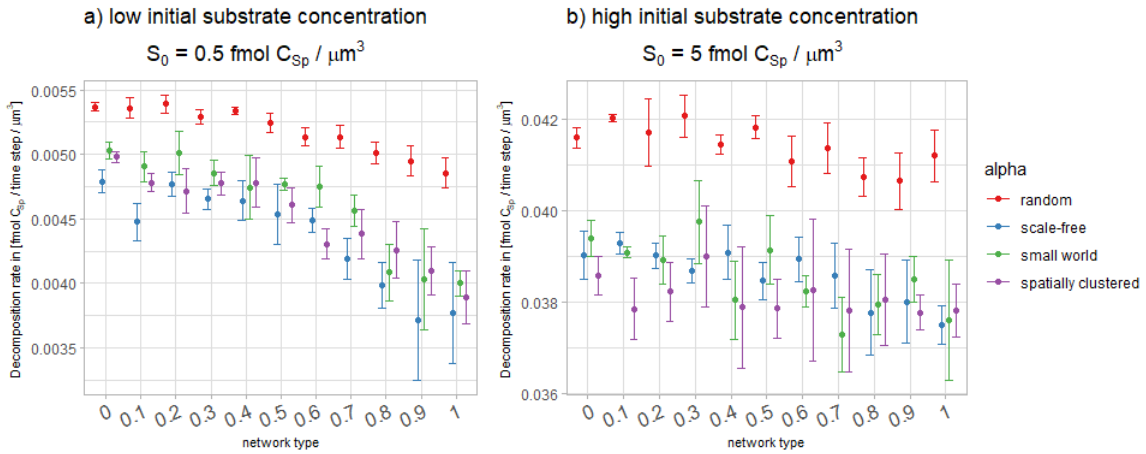

Figure 3.31: Decomposition rate for heterogeneous substrate distribution

Decomposition rate for the first 70% of primary substrate for different levels of heterogeneity in distribution of substrate in all network types(colors). On the x-axis alpha indicates different levels of heterogeneity in the distribution of initial substrate. The average node degree was 2.7 for all networks. Values from 5 runs. a) The mean initial substrate concentration was $S_0 = 0.5$ fmol C_{Sp} / μm^3. b) The mean initial substrate concentration was $S_0 = 5$ fmol C_{Sp} / μm^3.
We observed slower decomposition with more heterogeneously distributed initial substrate. Especially, with lower initial substrate concentration the decomposition rate was lower for all network types when the substrate was distributed more heterogeneously. Overall, the decomposition rate is higher with higher initial substrate concentration, but the effect of heterogeneity is not so strong.

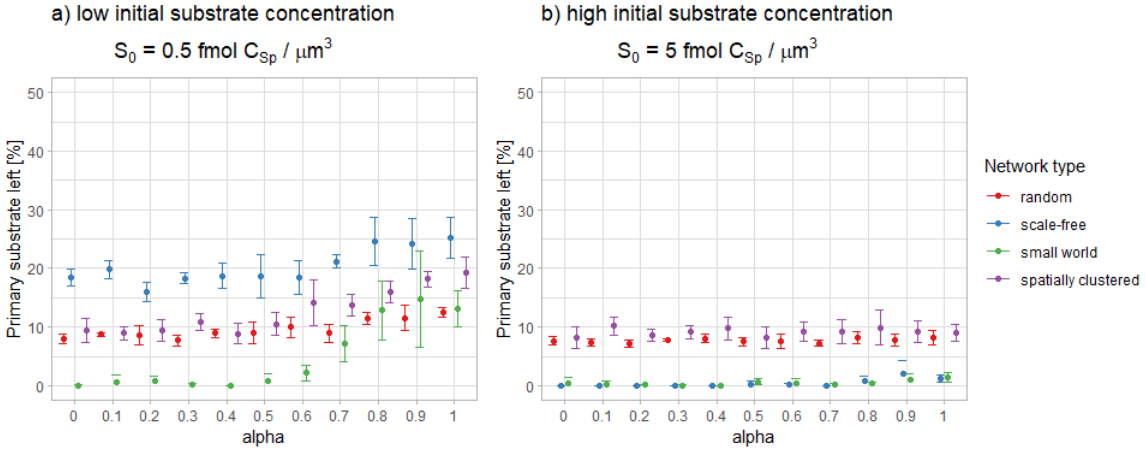

Figure 3.32: Primary substrate left for heterogeneous B_{max}

Each point shows the average fraction of primary substrate that was left at the end of the run in all network types (colors) for different heterogeneity in B_{max}. On the x-axis the heterogeneity level is shown. The average node degree was 2.7 for all networks. Values from 5 runs.
In a) a strong dependence of the decomposition efficiency on alpha can be found in all network types. In all network types more substrate was left undegraded with more heterogeneous B_{max}. This effect was not observed with higher substrate concentration.

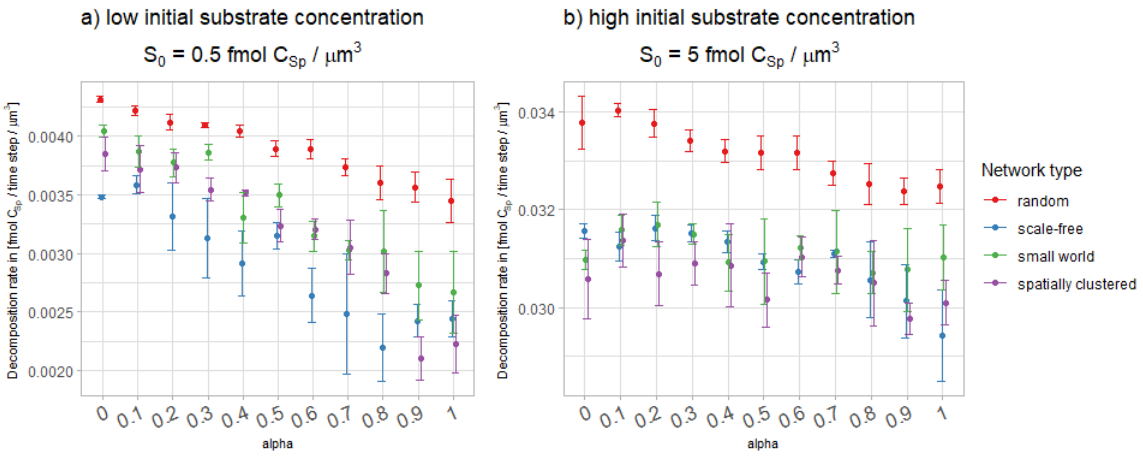

Figure 3.33: Decomposition rate for heterogeneous B_{max}

Decomposition rate of 70% of the initial subsrte for different levels of heterogeneity in B_{max} in all network types (colors). The average node degree was 2.7 for all networks. Values from 5 runs.
With lower substrate concentration decomposition rate was slower with higher heterogeneity. Again, this effect can only be observed at low substrate concentration.

type at least at low substrate concentration. While at a low pore size heterogeneity most primary substrate is left in the scale free network compared to all other network types, this changes at a high pore size heterogeneity, where small world and spatially clustered network have similar amount of substrate left compared to the scale-free network. In the higher substrate concentration scenario there was no remarkable effect of pore size heterogeneity on decomposition efficiency, as can be seen in figure 3.28, b).
The invasion efficiency in terms of the number of pores that could have been occupied in dependence on the heterogeneity of the pore sizes is shown in the supplement (figure 6.22). Only a modest effect of alpha on the number of occupied pores was detected with the lower initial substrate concentration. The dependence on alpha here also vanishes for higher substrate concentration (6.22, b).
The results shown in figure 3.29 indicate that additional heterogeneity can also impact the rate of decomposition. In simulations with high heterogeneity in the pore sizes the decomposition of the first 70% of the initial substrate tends to be slower than in more homogeneous networks. For all network types with low substrate concentration there is a strong relationship between the decomposition rate and the heterogeneity of the pore sizes. The rate is lower with more heterogeneous pore sizes. This effect was smaller in the scale-free network than in the other network types. And it was also weakened by higher substrate concentration. The largest difference in decomposition rate for different alpha remains in the small world network in the high initial substrate concentration.

3.5.2 Heterogeneous Chemical Pore properties

Heterogeneous Substrate concentration

In this section the impact of a heterogeneous distribution of the primary substrate over the soil pores is analyzed. Differences in the efficiency of the decomposition with respect to

different levels of heterogeneity in the distribution of the initial substrate were discovered in terms of varying proportions of the initial substrate remaining undegraded at the end of the runs. Figure 3.30 compares for two different levels of substrate concentration the efficiency of the decomposition. In the simulations with a low mean substrate concentration in most network types an effect on the decomposition efficiency can be found. In the random network for all $alpha$ between 8 and 13% of the initial substrate were left. In the scale-free network there were 17% of the initial substrate left undegraded with lower alpha values and for rather high heterogeneity ($alpha = 0.7$) it increased up to 22%. In the small world network, as already has been seen in previous experiments, with no heterogeneity in the substrate distribution merely all the initial substrate was degraded. Similar to the scale-free network then with increasing $alpha$ a slight increase in the undegraded substrate can be observed. Differences can also be observed in the spatially clustered network, where 9% of the initial substrate remained in the runs with no heterogeneity. Here the amount of substrate left slightly increases with increasing heterogeneity until the maximum of 13% at $alpha = 1$. In contrast, in figure 3.30 b) which shows the proportion of substrate left for higher mean initial substrate concentration no more differences could be found for all network types.
Figure 3.31 depicts results regarding an additional measure of efficiency, the decomposition rate. The heterogeneity of substrate distribution had remarkable impact on the decomposition rate. A trend can be observed, that shows slower decomposition with more heterogeneously distributed initial substrate. Especially, with lower initial substrate concentration the decomposition rate was lower for all network types when the substrate was distributed more heterogeneously. Overall, the decomposition rate is higher with higher initial substrate concentration, but the effect of heterogeneity is not so strong. In the supplement we provide further results on the impact of heterogeneity in substrate distribution on the number of occupied pores (Figure **??**).

Heterogeneous B$_{max}$

In this section the impact of heterogeneous B_{max} values on microbial efficiency is discussed. Presence and thickness of aqueous films in the pore network determine bacterial motility and dispersal in soil. Hydration levels in soil vary in space and time as a consequence of drainage, evaporation or plant root uptake (Tecon and Or, 2016). Therefore how easily microbes can move to neighboring nodes is highly heterogeneous between pores in unsaturated soils, what can be represented by heterogeneous B_{max}. Figure 3.32 compares the impact of heterogeneity in B_{max} in the lower and higher initial substrate concentration in all network types. In a) a strong dependence of the decomposition efficiency on alpha can be found in all network types. In the random network with no heterogeneity in B_{max} on average 8% of the initial substrate was left undegraded. This increases with increasing alpha up to 17%. In the scale-free network the proportion ranges from 22% to 26%. A strong dependence can also be seen in the small world network, where all the substrate was degraded with homogeneous B_{max} and 22% were left with $alpha = 1$ and in the spatially clustered network, where the values range from 11% to 30%. Figure 6.26 and 6.25 in the supplement in addition investigate the effect of heterogeneous B_{max} on the invasion efficiency.

A shift of the threshold in v_{max} can be observed with more heterogeneous B_{max}. In figure 6.25 the threshold values for more or less heterogeneous B_{max} are presented for all network types. All network types show a shift to higher threshold values for higher heterogeneity.

Figure 3.33 shows the differences in the time used for decomposition of 70% of the initial substrate at different heterogeneity levels in B_{max}. In a) a strong dependence of the decomposition rate on the heterogeneity is apparent. The decomposition is substantially slower at high heterogeneity. Again, this effect can only be observed at low substrate concentration.

Chapter 4

Discussion

In this work we propose a new model of microbial soil organic matter decomposition which combines the microbial growth dynamics with the spread of microbes in a pore network. This approach offers a new perspective on the decomposition of complex substrate in soils, by taking into account the soil heterogeneity and pore structure. Using this model we were able to analyze how biological parameters and soil architecture influence decomposition, and to identify potential interactions between these two factors. First, we compared the simulation results of 4 different artificial network types to the results from a regular grid, as it is commonly used to investigate microbial processes at a micro-scale (Kaiser et al., 2014, 2015; Allison, 2005). Even with equal average number of neighbors the inclusion of spatial relationship between nodes changed the results regarding microbial efficiency (see figure 3.4). Certain network structures prevented a fraction of the primary substrate of being decomposed.

4.1 Parameters that influence local growth impact the decomposition efficiency and the invasion of the network

We found that parameters that influence local growth impact the invasion probability and the invasion of the network and thereby affect the efficiency. We observed a threshold behavior for growth parameters, v_{max} and S_0, and for the enzymatic parameter k_{cat} for the invasion efficiency and efficiency in terms of completeness of substrate decomposition. For too low microbial growth, either due to lack of substrate or due to low microbial growth rate, microbes live only in the initially occupied pores and are not able to invade new pores. When the substrate concentration or the growth rate reaches a threshold value, there is a jump to large-scale invasion of all reachable pores in the network. Close to the threshold v^*_{max} the substrates take considerably longer to decompose than for even higher values of v_{max} (see figure 3.5). This is a result of the sigmoid shape of the growth curve and the non-linear correlation between v_max and the time it takes to reach the maximum biomass. Over multiple invasions this time lag accumulates. Microbes start at a low biomass value in the new pore again and with lower v_{max} they slowly grow until B_{max} again.

Since v_{max} depends on temperature (Pietikäinen et al., 2005) the threshold value at higher temperature may be reached in soil regions where by then microbes were not able to invade neighboring pores or with changing temperature microbes will be prevented from invading areas of the pore space. Furthermore, an increase in temperature could lead to a strong acceleration of the degradation if the growth rate before was in a range where substrate is degraded only very slowly and is shifted into the range of fast degradation by the temperature increase. Similar effect of increasing temperature on k_{cat} can be expected. And also in a similar manner increased input of substrate may trigger invasion of large areas of the pore space and decomposition of previously unreachable substrate.
Once the invasion threshold is exceeded, further increase in growth parameters has no strong effects. Though, across this wide growth parameter range, network structure has a far higher effect than microbial physiological parameters. Values of microbial growth parameters in this range, however, are more realistic in soils than values below the threshold where there would be no microbial dispersal.
Overall, we found that the spatial structure of the pore network in addition to microbial physiological parameters, such as maximum microbial growth rates or extracellular enzyme kinetics had a pronounced effect on microbial decomposition efficiencies. These results further support the idea that physical protection and inaccessibility of organic matter limits the rate of decomposition as previously described by Schimel and Schaeffer (2012) and Dungait et al. (2012) among others. That for wide ranges of physiological parameters the outcome differs for the network types is another strong argument for the inclusion of pore network structural parameters in decomposition models. Only the consideration of pore network structure and pore connectivity allows for accurate prediction of decomposition efficiency on the basis of physiological growth parameters.

4.2 Impact of Network connectivity

Another important factor is the connectivity of the network. Does the network consist of multiple disconnected components or is there a path between each pair of nodes? There are network setup algorithms that tend to produce disconnected multiple component networks more likely than others. For instance, the spatially clustered, the small world or the random network often consist of multiple disconnected components, whereas in the scale-free network always only one large component connects all existing nodes. The disconnectedness of the other network types also depends on the average node degree, more components for lower node degree, and in the small world network on the rewiring probability. Our simulation results showed that the amount of substrate left is larger in networks with lower node degree (Figure 3.24). This indicates that more disconnected components lead to less efficient degradation. In a network that consists of numerous components, it is more likely that in some components no node is initially occupied, because microbes only occupy a small fraction of nodes in the beginning. When none of the nodes of a component is occupied in the beginning of the simulation, an invasion of this component is not possible during the simulation run, because there is no link over which microbes may invade this isolated area.

In networks with some highly connected nodes, another mechanism that leads to substrate remaining undegraded can be observed. That is, if the substrate in the highly connected nodes is used up and microbes cannot grow there anymore all nodes that can only be reached through these hubs are practically disconnected from the network. Therefore, these parts become effectively inaccessible for microbes and unconnected from the network. Primary substrate in the disconnected pores cannot be degraded. This effect is the strongest in a scale-free network with low substrate concentration but can also explain a proportion of the amount of primary substrate left in other networks at low substrate concentration. This mechanism is characterized by the fact that decomposition efficiency can strongly be facilitated by higher substrate concentration. If we look at the spatially clustered or the random network, which are two network types that can contain multiple components, higher substrate concentration does not facilitate much more efficient decomposition. A possible explanation is that here the actual disconnectedness of the network prevents microbes from spreading. In figure 3.24 the networks, that counted the largest number of components, i.e. the random and spatially clustered networks, in particular at low average node degrees (compare 3.21), show the least difference in primary substrate that is left undegraded for low and high initial substrate concentration. In contrast, in the scale-free network there is nearly no substrate left at the end of the run in the high-substrate scenario, although with low substrate concentration it was the one where decomposition was the least efficient. Because the scale-free network consists of only one large connected component, high substrate concentration enables very efficient invasion. Then, microbial biomass grows up to B_{max} repeatedly in highly connected nodes, enabling microbes to spread through each link stemming from it to the neighboring node. In that way, the whole network space can be invaded very efficiently.

The pore connectivity in real soils correlates with the bulk soil density. Mbé et al. (2022) found, that soil samples with lower bulk soil density showed more connected pores, whereas in samples with higher bulk soil density the overall porosity was smaller and there were more disconnected components found in pore networks extracted from these samples. These sample networks then were used for modelling decomposition with the MOSAIC model (Monga et al., 2008). Our results accord with the findings of Mbé et al. (2022): They reported lower mineralization of organic matter in the networks extracted from the samples with higher bulk density. Pérez-Reche et al. (2012) extracted pore networks from a total of 6 soil samples: 3 of them from ploughed soil and 3 from soils without tillage treatment. The networks from the ploughed soil samples showed typically larger pores and a slightly lower average node degree. Besides land use methods, climate factors can also alter pore connectivity. Rooney et al. (2022) analyzed the response of soil pore networks in aggregates from permafrost soils to laboratory incubation consisting of repeated freeze-thaw cycles. After 5 cycles pore connectivity was significantly reduced and the number of singly connected pores increased.

Water content plays an important role when describing the connectivity of soil pore networks. The invasion of new pores can only happen with enough humidity and substrate diffuses between water filled pores. Therefore, the actual connectivity of the network from a microbial perspective changes over time and is related to the water content.

We showed that pore connectivity may play a big role for decomposition efficiency. At the same time, pore connectivity is both, i) widely different between soils and ii) can be dynamic in the same soil (freeze-thaw, drying-rewetting). Further experimental investigation of what environmental and human factors impact pore connectivity in soil will be needed. Incorporation of these findings in soil decomposer models, then might be helpful to anticipate consequences of climate change on decomposition efficiency and suggest effective measures to decrease atmospheric CO_2.

4.3 Impact of the clustering coefficient

A goal of this manuscript was to identify network properties that have major effects on the efficiency of microbial decomposition. Two network properties were identified, that are crucial for microbial efficiency, clustering of the nodes on the one hand and the presence of a scale-free degree distribution on the other hand. Simulations on small world networks with differing rewiring probabilities showed that high clustering of nodes enables more complete decomposition of substrate, than in networks equal in all other properties but with lower clustering coefficient (Figure 3.19). The presence of highly connected nodes, as in scale-free networks, can decrease the efficiency of decomposition and lead to higher amount of substrate that remains undegraded (Figure 3.24).
Also, for epidemics it has been shown that the great number of redundant paths between individuals introduced by the clustering in the network enables the disease to reach nearly all people of a population that are reachable (Newman, 2003). Similarly, in the soil pore network high clustering causes existence of many redundant paths to most of the nodes, making it likely that most of the nodes that are reachable by microbes will be invaded by one route or another (Figure 3.19). The short term connections introduced by the rewiring process in small world networks reduce the path lengths, and at the same time lower the clustering coefficient. Therefore, small world networks with a very low rewiring probability also exhibit relatively long paths. As a result from the long path lengths, decomposition is slower in highly clustered networks, but introduction of few long-range rewiring connections in small-world networks can speed it up substantially (Figure 3.20). The situation is opposite in networks with a scale-free degree distribution. Networks of this type typically have a very low clustering coefficient and a connectivity pattern that has the following characteristics: there are few nodes with a much greater number of connections than most of the other nodes, what makes them disproportionately important for the microbial invasion of the pore space. Microbes must pass through these hubs to reach areas of the network where no other path leads to. If they do not find conditions that facilitate microbial growth there, this prevents microbes from spreading. This leads to large amounts of initial substrate remaining undegraded particularly in low substrate regimes. If the substrate is used up in a microhabitat that needs to be passed in order to reach nutritious areas of the pore space that are farther away the spread of microbes that have only limited mobility is blocked.
Pérez-Reche et al. (2012) stated that general properties of soil pore networks are high clustering and a restriction of links per pore due to the volume the links themselves occupy.

This implies that very large pores can have more connections than smaller ones, alone because of the larger space available. Therefore, a change in pore sizes also alters the connectivity pattern. If as a consequence of conventional tillage the number of very large pores ($< 100\mu m$) stemming from root channels reduces (Kravchenko et al., 2011), also the connectivity pattern changes.

4.4 Heterogeneity in pore sizes and substrate concentration

Heterogeneity in pore properties is another significant factor that affects the decomposition efficiency. Heterogeneity in the pore sizes affects the invasion efficiency, the decomposition rate and the amount of substrate that is left at the end. Is the pore size distribution more heterogeneous, meaning that there are more very small and more very large pores but less intermediate sized pores, the decomposition is less efficient. It has been shown that the pore size distribution of a soil can be altered by land use or vegetation (Kravchenko et al., 2011; Peth et al., 2008). Similar is the effect of heterogeneity in the distribution of the initial substrate. When substrate was distributed with higher heterogeneity, decomposition efficiency was lower. This reflects the findings of Mbé et al. (2022), who found that the amount of mineralized carbon was higher for a homogeneous distribution of microbes than for a patchy distribution. In their model microbes are immobile and substrate diffuses to them through the pore network. The strongest impact had heterogeneity in B_{max}, the threshold value of biomass that is needed to invade a new pore. Especially for low initial substrate concentration there was a much larger fraction of substrate left at the end in more heterogeneous networks compared to when all pores had the same B_{max}. And also, the decomposition rate was much lower with more heterogeneous B_{max}. B_{max} is a measure for how easily new pores can be invaded, where a low value could represent a higher humidity that enables more easy passage of the microbes. This accords with findings from epidemic studies, where a heterogeneous transmissibility can prevent a disease from spreading through a population (Miller, 2007). Pérez-Reche et al. (2012), who compared 4 models of microbial invasion of a soil pore network found, that heterogeneous transmissibility values that were randomly assigned to links had no significant impact on the invasion efficiency. But only in models where the transmissibility depends on heterogeneous network properties, like link length, microbial invasion efficiency was lower than in models with homogeneous transmissibility. Although, the transmissibility is not directly comparable with B_{max}, the result of the current study contrasts with this, as we found an effect on the invasion efficiency without linking B_{max} to actually heterogeneous structural parameters (see figure 6.26). These results should be considered when bulk soil properties are used as approximations for microbial environmental conditions at a microscale. Modelling results may fail to picture real dynamics, when the micro-scale heterogeneity of soil properties is ignored.

4.5 Limitations

In our model only one functional group of microbes is modelled, whereas in real soils a huge variety of bacteria, archaea and fungi can be found with many differing functional traits. It has been shown that interactions between functional groups have important influence on decay rates of organic matter and that for instance the presence of cheaters in a system downregulates the ratio of extracellular enzymes to total microbial biomass (Kaiser et al., 2015). Competitive and symbiotic relationship between and within functional groups are also strongly affected by spatial segregation (Carson et al., 2010) and therefore their interplay with pore network structure deserves attention.

Also, dynamical changes of the soil pore network are not considered in this model, but rather it is stable over the whole decomposition phase. In real soils, however, the pore space structure alters with time. Especially when also accounting for the presence of water transport mechanisms can change rapidly.

Chapter 5

Conclusion

The arguments for taking pore network architecture into account when modelling the response of soil microbial communities to climate change are compelling. Land-use changes, altered precipitation patterns and increased frequencies in freeze-thaw cycles in arctic permafrost alter pore network structure. Which in turn crucially influences microbial efficiency. Therefore, it is inevitable to include soil structural properties into earth system models. The impact of the architecture of the pore network was even shown to be stronger than the impact of microbial physiological parameters over wide ranges of these parameters (i.e. above their respective thresholds for microbial invasion of the pore space). In this study network properties were identified that need to be considered in integrated earth system models to be able to make reliable predictions. Also, the importance of considering the heterogeneous distribution of microbes and substrate has been confirmed once more.

Chapter 6

Supplementary Material

6.1 Network Properties

Shortest Path length

The shortest path length l_{ij} is a measure to characterize the distance among two nodes and is defined as the length of the shortest path connecting node i and j. The length of a path is the number of links that are passed throughout the way. The average shortest path is the average of all values of l_{ij} over all pairs of nodes. As network diameter, the maximum value of all pairwise shortest path lengths is defined. (Pastor-Satorras et al., 2015)

Degree and Degree Distribution

The number of links that connect a node with other nodes is called the degree k_i of node i. The degree distribution $P(k)$ in finite networks is the fraction of nodes in this network with a degree equal to k (Pastor-Satorras et al., 2015). A regular 2D-grid, as it is used in many studies on the decomposition of soil organic matter (Pot et al., 2022; Kaiser et al., 2014, 2015) can be seen as a regular network, where all nodes have exactly the same degree (Newman, 2018). Degree distribution for different average node degree for all network types are shown in figures 6.1 - 6.4.

Clustering coefficient

As a measure of clustering the average local clustering coefficient is used. Local clustering coefficient is defined as the ratio between the actual number of links among the neighbors of a node and the maximum number of possible links. Clustering of the network is the average local clustering coefficient from all nodes. (Pastor-Satorras et al., 2015) An overview of the clustering coefficients and shortest path length in different network types is provided in figure 3.22 and figure 3.23.

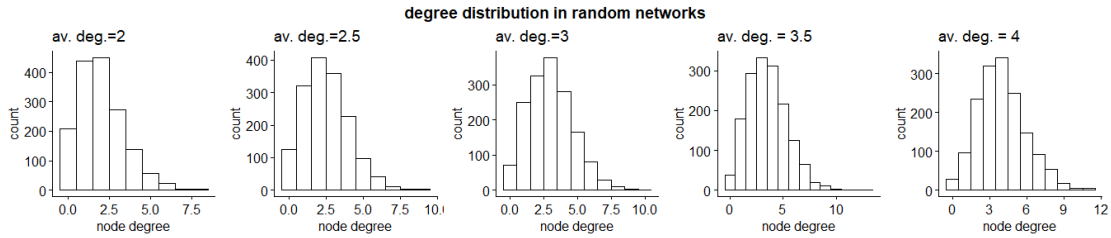

Figure 6.1: Degree distribution in random networks with different average node degree.

Each histogram is established from 4 networks with 400 nodes each. The number of nodes with a certain degree are shown for 5 different average node degrees. The distribution follows a binomial distribution in random networks. With the greatest frequency the average node degree occurs, in every case. Also, it can be seen in the histograms that the fraction of nodes with degree 0 is larger at lower average node degree.

6.2 Network types

Random Network

In the simplest random graph model first a given number of nodes is set up, then two randomly selected nodes are connected by a link at a time until the desired number of links is reached. The degree distribution in a random network corresponds to a binomial distribution. The clustering coefficient can be defined as the probability that two neighboring nodes of a node are also connected with a link. In a random graph the probability that two nodes are connected is the same for any pair of nodes (Newman, 2018). Figure 6.1 provides an overview of the degree distribution in the random network in this model.

Scale Free Network

The scale free network is generated by adding nodes and links with a preferential attachment rule. To initialize the algorithm 2 nodes are set up and connected with a link. Until the desired number of nodes is reached, one node is added after the other and every newly added node is connected with one end of a randomly chosen link. This way nodes with high node degree are more likely to be linked. Then until the desired number of links is reached additional links are added between one end of a randomly selected link and another randomly selected node. These mechanisms lead to a power-law degree distribution. Meaning that there is a small number of hubs, nodes with very high node degree, and many nodes with few connections. (Pastor-Satorras et al., 2015) The degree distribution for different average node degrees in scale-free networks is shown in figure 6.2. From this figure it can also already be seen, that in the scale-free network there are no nodes with degree 0. The network always consists of one large component, where a path from every node to every other node can be found. The highly connected hubs reach degrees far higher than the average node degree.

Small world Network

The small world network was proposed to capture the properties of a small network diameter and a large clustering coefficient. Nodes are arranged in a ring in the first place, then each node is connected to $\frac{average\,node\,degree}{2}$ neighbors on each side. Then a small fraction of links

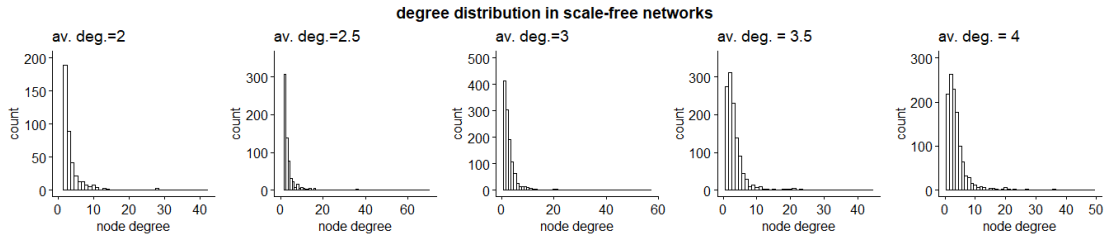

Figure 6.2: Degree distribution in scale-free networks with different average node degree.

Each histogram is established from 4 networks with 400 nodes each. The number of nodes with a certain degree are shown for 5 different average node degrees. There are few highly connected hubs and a large number of nodes with low degree.

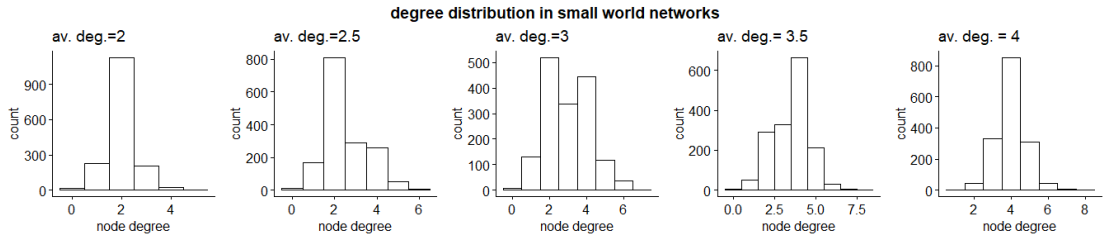

Figure 6.3: Degree distribution in small world networks with different average node degree.

Each histogram is established from 4 networks with 400 nodes each. The number of nodes with a certain degree are shown for 5 different average node degrees.

is rewired to connect two randomly chosen nodes. This rewiring introduces several long-range shortcuts that reduce the average shortest path and at the same time do not affect the high local clustering. Each link is drawn to rewire with a certain rewiring probability p. (Pastor-Satorras et al., 2015) The rewiring probability also impacts network properties of the small world networks, as can be seen in figure 3.18. The degree distribution resulting from this construction algorithm is presented in figure 6.3. Similar to the random network degrees close to the average node degree occur with the highest frequency in small world networks. And the highest occurring node degree is about 2 times the average node degree. In addition, from the histograms in the figure it already is apparent, that in the small world networks the fraction of single unconnected nodes is very low.

Spatially clustered Network

Soil pores are geometric objects allocated in a three-dimensional space. The spatial proximity is an essential factor determining the probability with which two nodes are connected. The generation of the spatially clustered network starts with randomly distributed nodes. One node is randomly selected at a time and connected to another node that is closest in space and not already connected to the current node, until the desired number of links is reached. From this a degree distribution of the nodes emerges, that is similar to the degree distribution of a random network (figure 6.4). The underlying spatial connectivity pattern, however, is distinct.

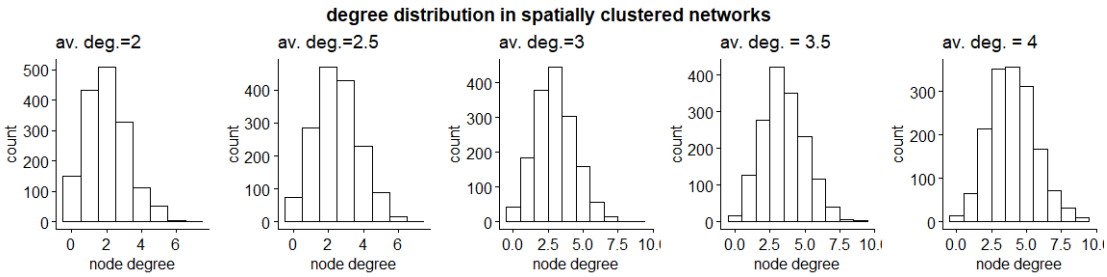

Figure 6.4: Degree distribution in spatially clustered networks with different average node degree.

Each histogram is established from 4 networks with 400 nodes each. The number of nodes with a certain degree are shown for 5 different average node degrees. Degrees around the average node degree occur most frequently and the highest occurring node degree in this network is not very much greater than the average. We can also see from the histograms that there is a remarkable number of single unconnected nodes for low average node degree.

6.3 Parameter sensitivity analysis

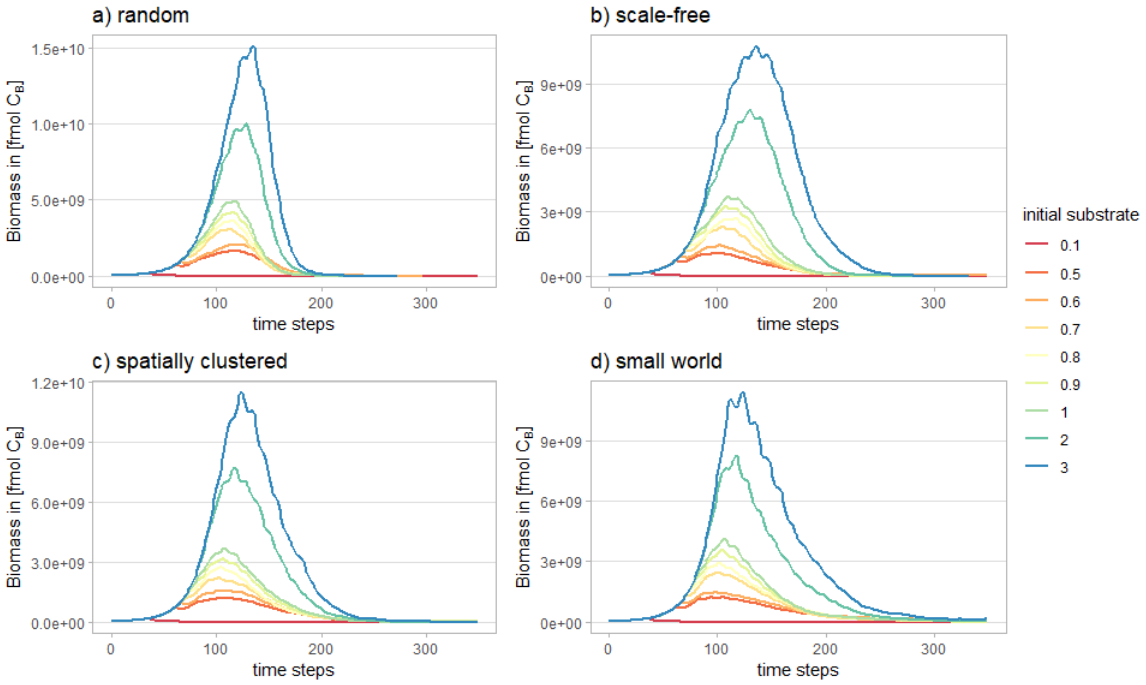

Figure 6.5: Biomass over time for different initial substrate concentration

Biomass over time in all network types for different initial substrate concentrations in [fmol C_{Sp} / μm^3]. The average node degree was 2.7 for all networks. Averaged over 5 runs. Each plot shows the development of biomass over time for one network type. The color of the lines represents the initial substrate concentration.

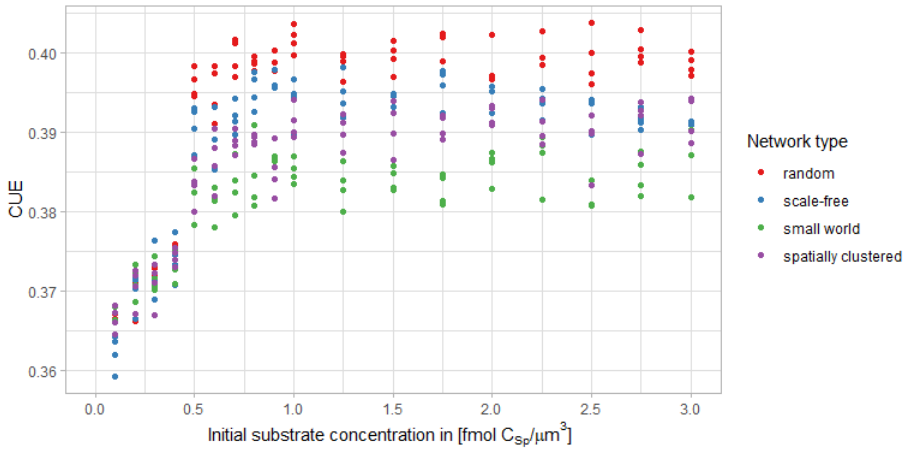

Figure 6.6: Impact of the initial substrate concentration on the carbon use efficiency

Carbon use efficiency for different initial substrate concentrations in fmol C_{Sp} / μm^3. The carbon use efficiency was calculated of the fraction of C from the uptake that is allocated in microbial biomass: $CUE = \frac{\text{uptake} - \text{respiration}}{\text{uptake}}$

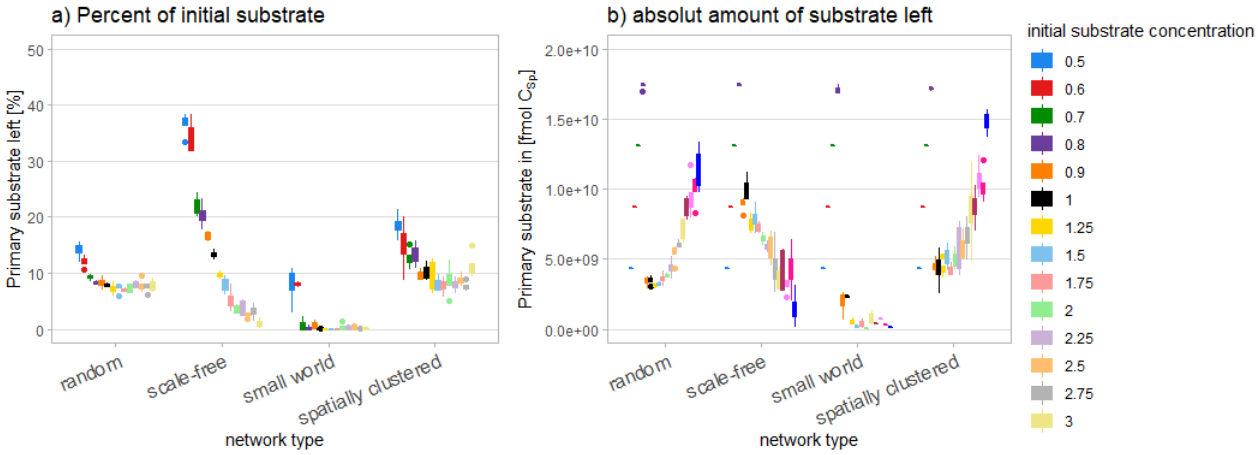

Figure 6.7: Impact of the initial substrate concentration on the amount of substrate left at the end

Primary substrate left at the end for different initial substrate concentrations. The average node degree was 2.7 for all networks. Values from 5 runs. a) Percentage of initial substrate. b) Absolut amount of primary substrate left at the end in fmol C_{Sp} / μm^3.

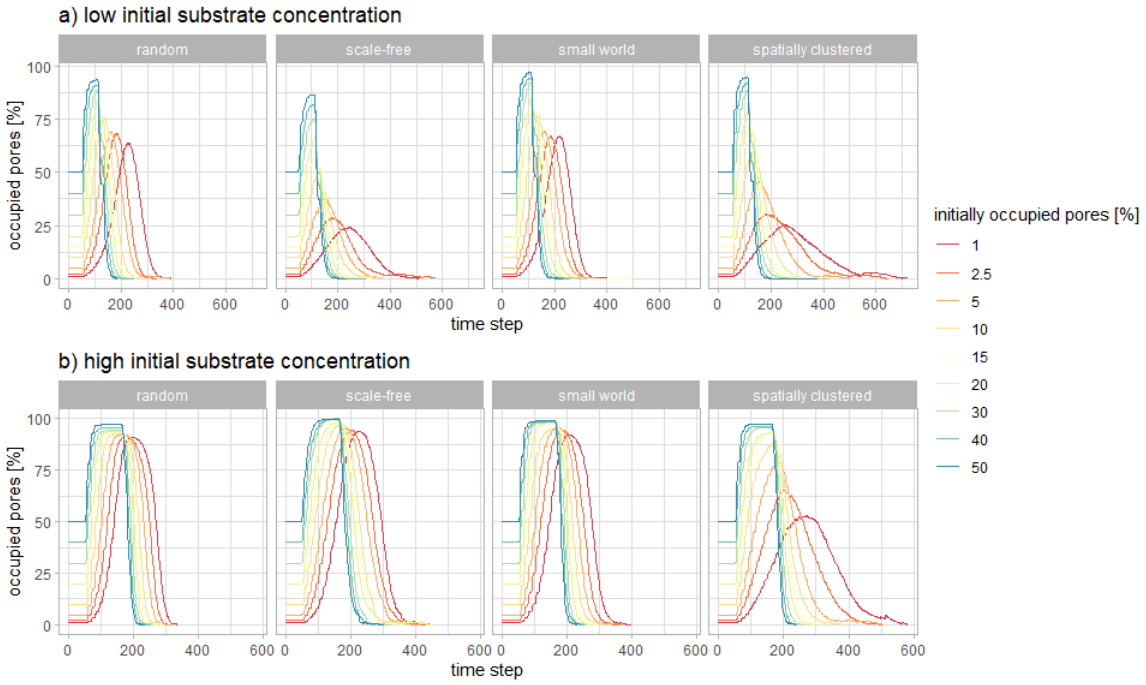

Figure 6.8: Number of occupied pores over time for different initial occupation

Number of occupied pores for different initial occupation over time. Average values from 5 runs. Each plot shows the dynamics of one network type. a) The initial substrate concentration was $S_0 = 0.5$ fmol C_{Sp} / μm^3. (upper row) b) The initial substrate concentration was $S_0 = 5$ fmol C_{Sp} / μm^3. (lower row)

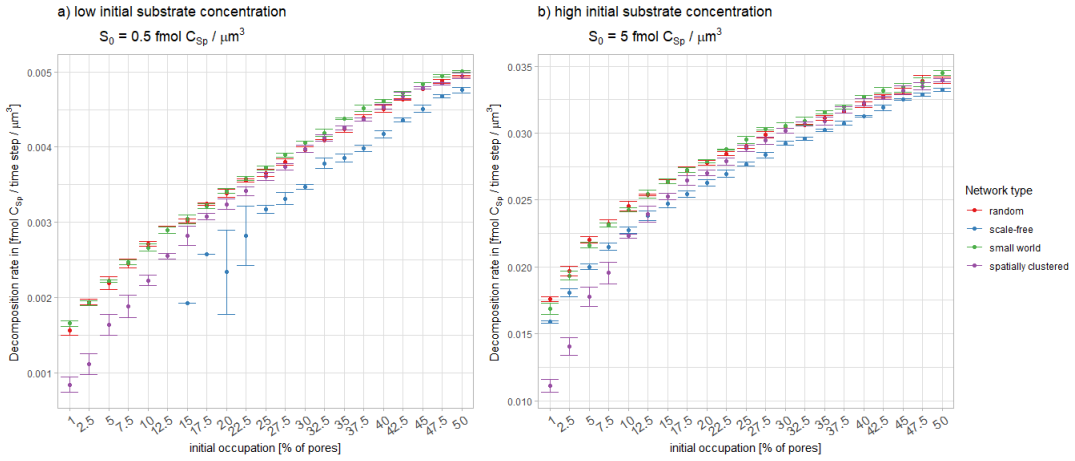

Figure 6.9: Decomposition rate for different initial occupation

Rate of decomposition of the first 70% of initial substrate for different fractions of the network that were initially occupied by microbes. On the x-axis the fraction of pores that was occupied in the beginning in % is shown. Values from 5 runs.

6.4 Supplementary Results

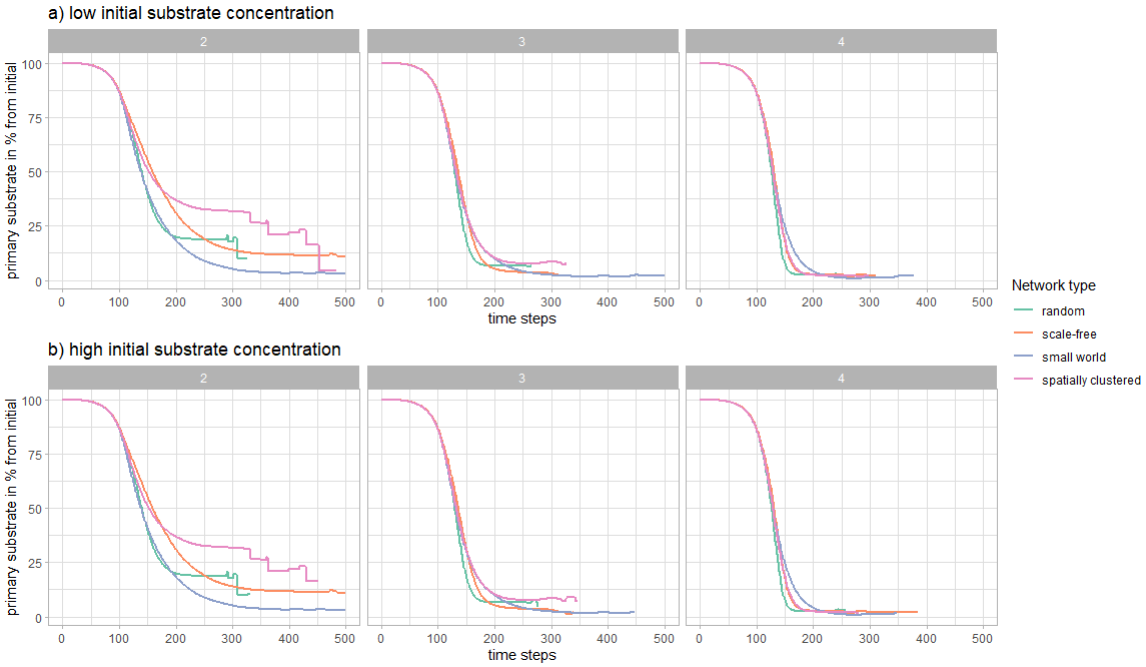

Figure 6.10: Primary substrate over time for different average node degrees

Comparison of the primary substrate over time for all network types with three different average node degrees. a) The initial substrate concentration was $S_0 = 0.5$ fmol C_{Sp} / μm^3. b) The initial substrate concentration was $S_0 = 5$ fmol C_{Sp} / μm^3. Each plot shows the decomposition of the initial substrate over time averaged over 4 simulations for a certain average node degree. In the upper row there are 3 low substrate concentration plots, each corresponds to one certain average node degree, as depicted in the frame (a). The lower row shows 3 plots with high initial substrate concentration and also certain average node degree in each plot (b). The colors of the lines represent the 4 network types. The plots overall show shorter degradation time for some network types with average node degree of 3 compared to networks with average node degree 2 with low initial substrate concentration and for all network types with average node degree 4. Also in the high initial substrate regime for all network types degradation was faster for higher average node degrees. Additionally, it can be seen that the degradation of the initial substrate was more complete in networks with higher average node degree. How much more efficient the decomposition was, also depends on the network type.

That there can be seen an increase of primary substrate in some groups, is due to the fact that these lines are average values from multiple runs. When runs that already only had a low amount of primary substrate left end early, they are not counted in this average anymore and the average of the remaining runs at this time jumps to a higher value.

The main characteristics that can be seen in figure 6.10 are the change in the rate of decomposition and the change in the efficiency of decomposition as a function of the average node degree. Overall, in networks with lower connectivity the decomposition is slowed down and the efficiency of the decomposition is reduced. In networks with an average node degree of 4 for all network types the decomposition was the fastest. The simulations run until only 1% of the initial biomass was left in all pores. This stop condition was fulfilled earlier in the more connected networks and the curve of the primary substrate decreased steeper in

these networks for all types. With average node degree 3 we see similarly steep degradation lines of the primary substrate and similar duration of the runs (stop condition: only 1% of initial biomass remain in all pores) for most network types. Only in the small world network it already took remarkably longer until the stop condition was fulfilled. These observations are true for both initial levels of primary substrate.

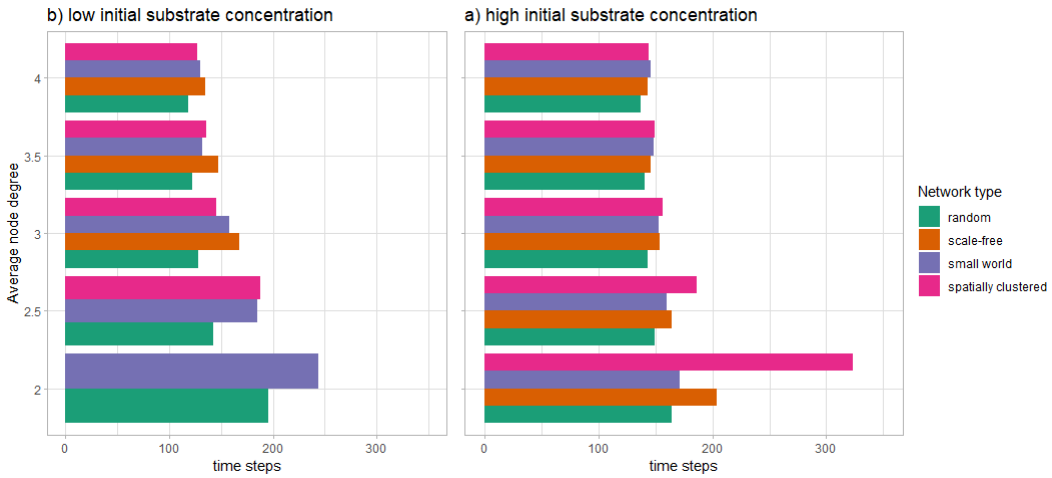

Figure 6.11: Time until 70% of initial substrate degraded

Duration of the decomposition of 70% of the initial substrate in all network types with different average node degree. a) The initial substrate concentration was $S_0 = 0.5$ fmol C_{Sp} / μm^3. b) The initial substrate concentration was $S_0 = 5$ fmol C_{Sp} / μm^3.
Only runs, where the 70% mark has been reached, are shown. In the scale-free network and the spatially clustered network with an average node degree of 2, at low substrate concentration less than 70% of the initial substrate were decomposed. That is why they are not shown at all in this group.

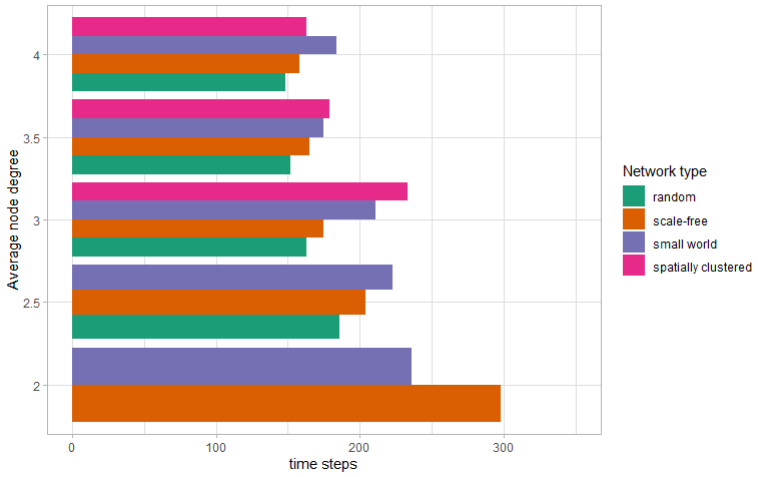

Figure 6.12: Time until 90% of initial substrate degraded

Duration of the decomposition of 90% of the initial substrate in all network types with different average node degree. The initial substrate concentration was $S_0 = 5$ fmol C_{Sp} / μm^3.
Only runs, where the 90% mark has been reached, are shown.

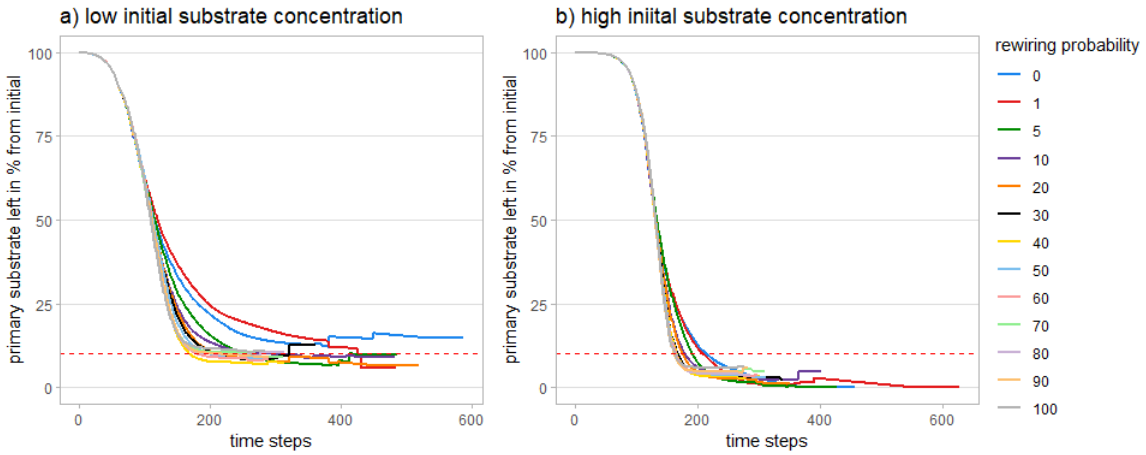

Figure 6.14: Primary substrate over time in the small world network

Primary substrate over time in the small world network with different rewiring probability. The rewiring probability p defines the probability with which each link of the network is randomly rewired to introduce shortcut connections in the setup of the network. The connection pattern of a small world network with $p = 0$ is equivalent to a regular grid, whereas a small world network with $p = 100$ is a random network. The dashed red line indicates 10% of the initial substrate. Averaged over 5 runs. a) The initial substrate concentration was $S_0 = 0.5$ fmol C_{Sp} / μm^3. b) The initial substrate concentration was $S_0 = 5$ fmol C_{Sp} / μm^3.

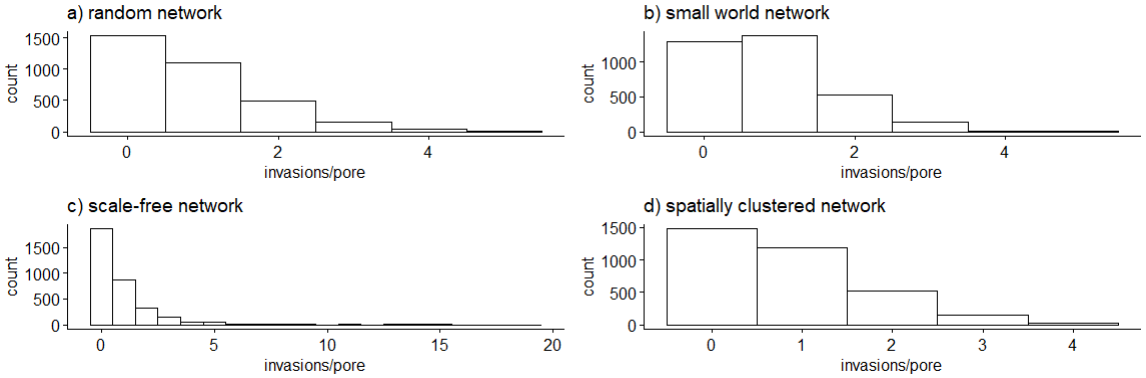

Figure 6.13: Invasions per pore for all network types

Frequencies of invasion counts per pore in all network types. The average node degree was 2.7 for all networks. Values from 5 runs. The initial substrate concentration was 3 fmol C_{Sp} / μm^3. As can be seen in a) in the random network from about 1500 pores no new pore was invaded. Next most frequent case is, that one new pore was invaded. And from only very few pores the maximum of 5 new pores were invaded. b) shows the small world network, where the most frequent case was that one pore was invaded. The maximum is equal to the random network, also maximum 5 pores were invaded from one pore. c) The distribution is very dissimilar in the scale-free network. From a higher number of pores no new pore was invaded here, but the maximum number of invaded pores from one pore is much higher than in all other network types. d) In the spatially clustered network the distribution is very similar to the random network.

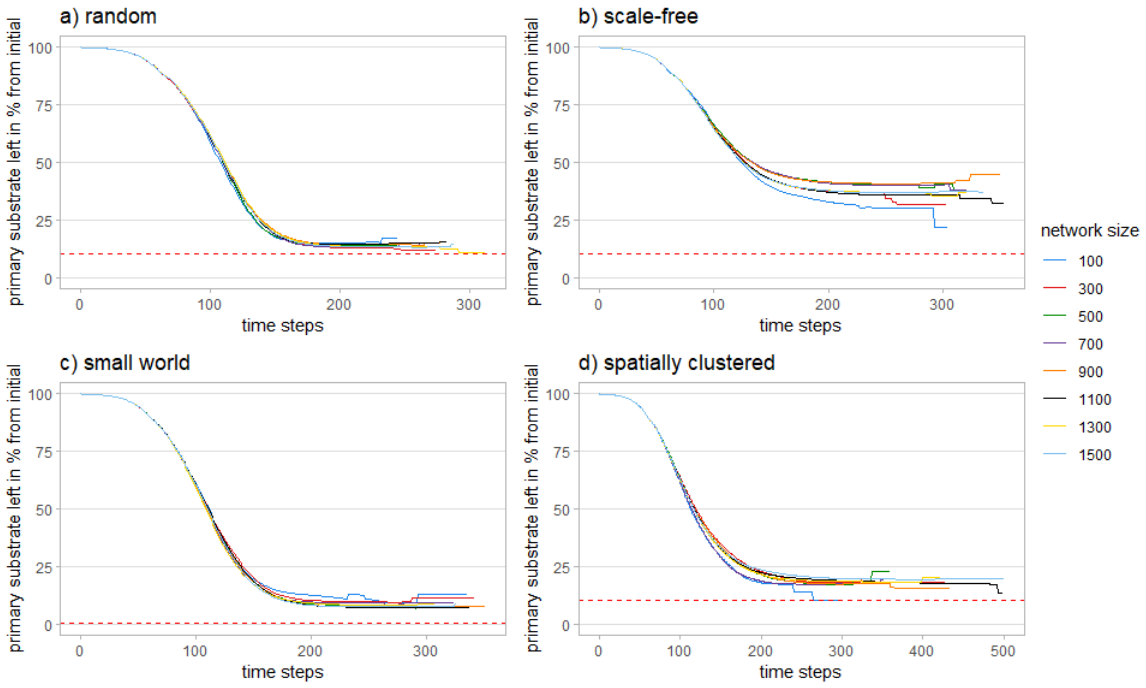

Figure 6.16: Primary substrate over time for different network sizes

Development of the primary substrate over time in all network types for different network sizes. The colors of the lines depict the size of the network, the number of nodes. The average node degree was 2.7 for all networks. Averaged over 5 runs. The initial substrate concentration was $S_0 = 0.5$ fmol C_{Sp} / μm^3. The dashed red line indicates 10% of the initial substrate.

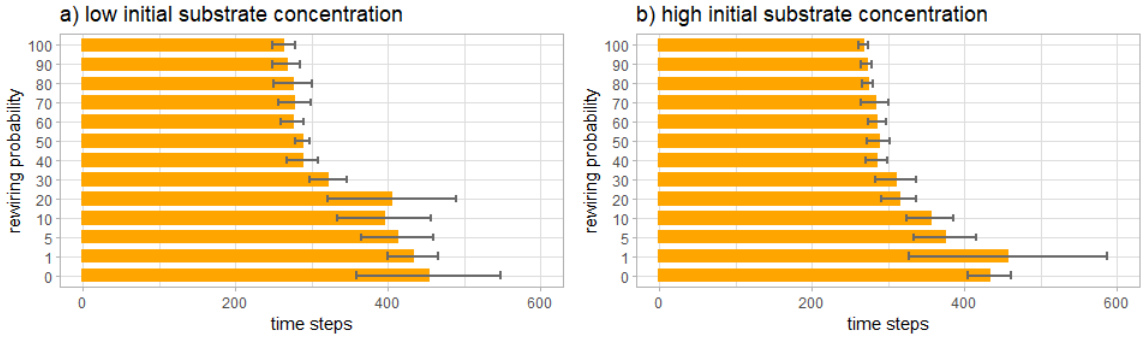

Figure 6.15: Duration of the runs in the small world network

Duration of the run until 70% of the initial substrate were degraded in small world networks with 500 nodes and different rewiring probability. The rewiring probability p defines the probability with which each link of the network is randomly rewired to introduce shortcut connections in the setup of the network. The connection pattern of a small world network with $p = 0$ is equivalent to a regular grid, whereas a small world network with $p = 100$ is a random network. a) The initial substrate concentration was $S_0 = 0.5$ fmol C_{Sp} / μm^3. b) The initial substrate concentration was $S_0 = 5$ fmol C_{Sp} / μm^3.

Figures 6.16 and 6.17 give information about the temporal characteristics of the decomposition in all network types in correlation with the size of the network. Figure 6.17 compares the decomposition rate for 70% of the initial primary substrate for different network sizes in

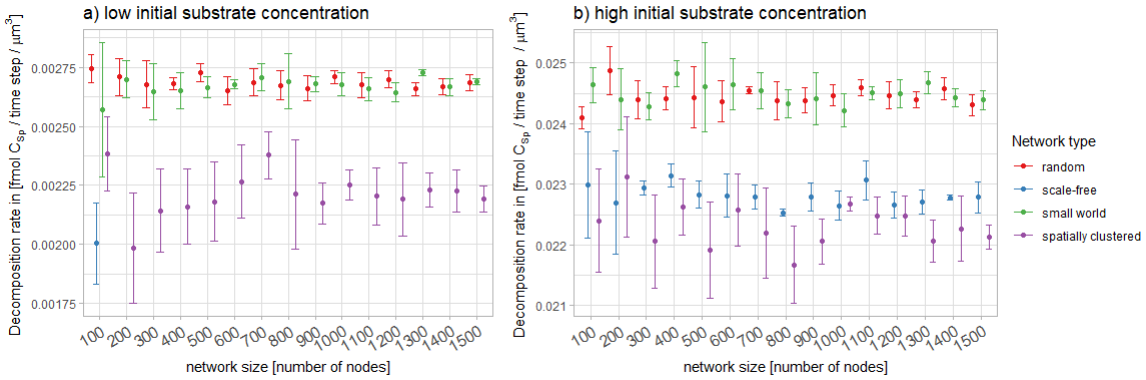

Figure 6.17: Decomposition rate of the first 70% of the initial substrate

Decomposition rate of the first 70% of the initial substrate for all network types for different network sizes. Boxplots are only shown for networks, where the 70% mark was reached in the runs. The colors of the bars depict the network types. The average node degree was 2.7 for all networks. Averaged over 5 runs. a) The initial substrate concentration was $S_0 = 0.5$ fmol C_{Sp} / μm^3. b) The initial substrate concentration was $S_0 = 5$ fmol C_{Sp} / μm^3.
A Two-way Anova test showed significant differences in the decomposition rate for different network types (p¡0.01), but no significance for the relationship between decomposition rate and network size.

all network types. Overall, we see shorter duration runs for larger networks and also more complete decomposition of the initial primary substrate for shorter runs.

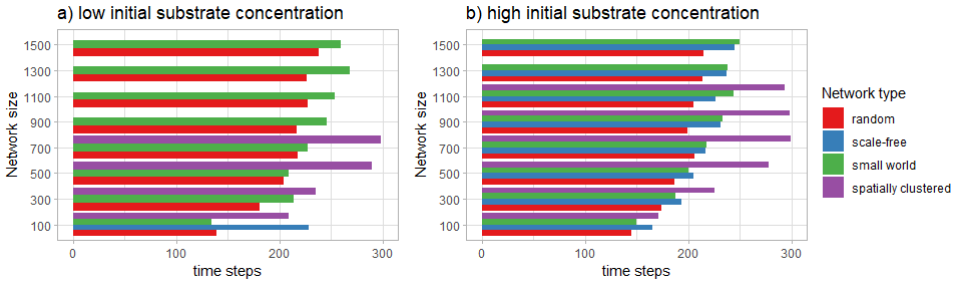

Figure 6.18: Time until 70% of the initial substrate were degraded

Time until 70% of the initial substrate were degraded in all network types for different network sizes. Bars are only shown for networks, where the 70% mark was reached in the runs. The colors of the bars depict the network types. The average node degree was 2.7 for all networks. Averaged over 5 runs. a) The initial substrate concentration was $S_0 = 0.5$ fmol C_{Sp} / μm^3. b) The initial substrate concentration was $S_0 = 5$ fmol C_{Sp} / μm^3.

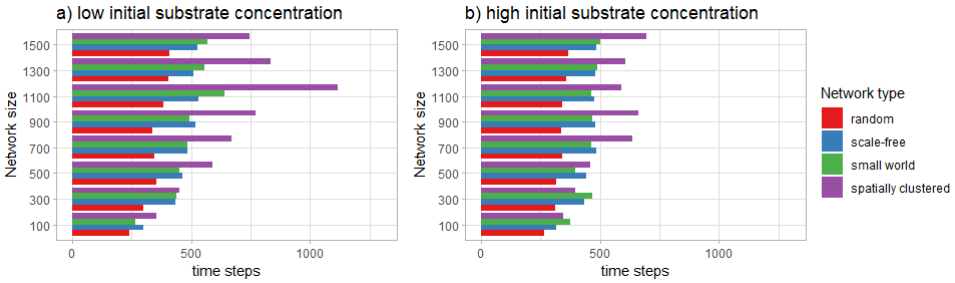

Figure 6.19: Duration of the runs

Time until all microbes died in all network types for different network sizes. The colors of the bars depict the network types. The average node degree was 2.7 for all networks. Averaged over 5 runs. a) The initial substrate concentration was $S_0 = 0.5$ fmol C_{Sp} / μm^3. b) The initial substrate concentration was $S_0 = 5$ fmol C_{Sp} / μm^3.

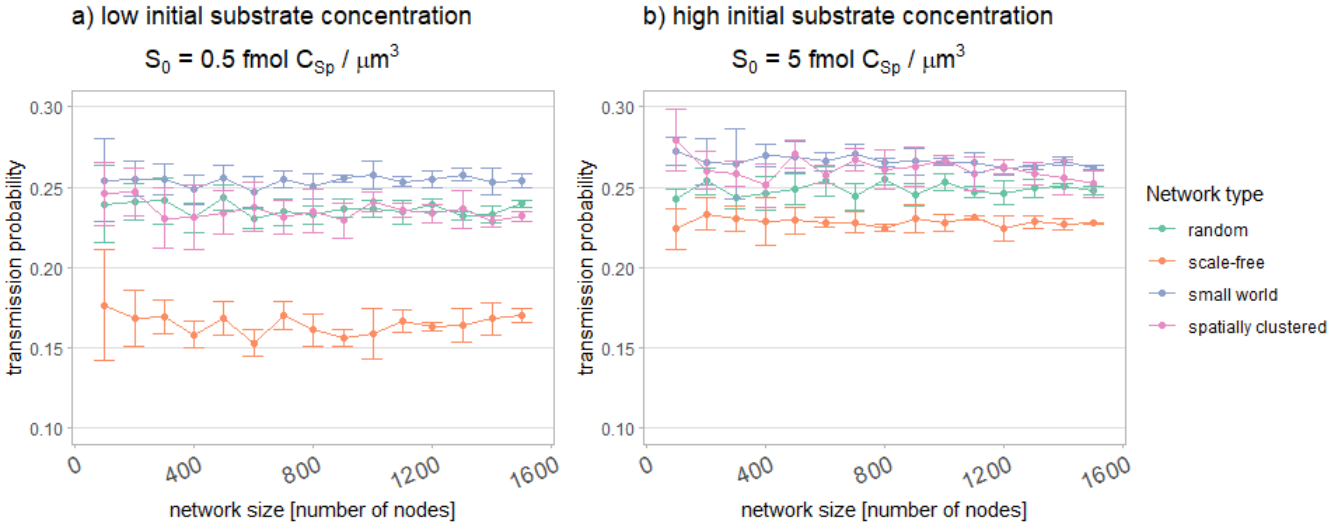

Figure 6.20: Transmission probability for different network sizes in all network types
Transmission probability as the mean fraction of neighbors of a pore that was invaded from a pore per time step in all network types. Network sizes differed from 100 to 1600 nodes. v_{max} was 0.29. Averaged over 5 runs. Error bars indicate standard deviation. No effect of the network size on the transmission probability can be observed, but the network type impacts the transmission probability. In the scale-free network the transmission probability was lower than in the other network types.

figures/plots/hetero/plot-sizehetero-oc.png

Figure 6.22: Invasion efficiency for different heterogeneity in pore sizes

Number of pores that could have been occupied by microbes for different levels of heterogeneity in the pore sizes in all network types. Each point depicts the accumulated number of pores invaded during one run. Each pore that was invaded by microbes was count once at its first time becoming occupied. The color depict the network type. In the random network for all values of alpha about 91% of the pores were occupied. In the scale-free network the values ranged from 83% ($alpha = 0$) to 78% ($alpha = 1$). In the small world network for all alpha values 99% of the pores could have been occupied and in the small world network a weak dependence can be observed. Here the values range from 91% ($alpha = 0$) to 87% ($alpha = 1$).The average node degree was 2.7 for all networks. Averaged over 5 runs. a) The initial substrate concentration was $S_0 = 0.5$ fmol C_{Sp} / μm^3. b) The initial substrate concentration was $S_0 = 5$ fmol C_{Sp} / μm^3.

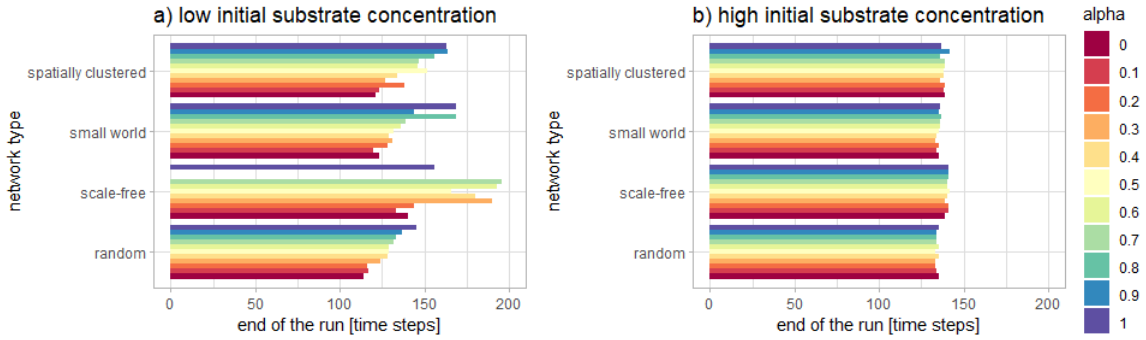

Figure 6.21: Duration of decomposition of 50% of initial substrate for different heterogeneity in pore sizes

Time until 50% of the initial substrate were degraded for different levels of heterogeneity in the pore sizes in all network types. The average node degree was 2.7 for all networks. Averaged over 5 runs. a) The initial substrate concentration was $S_0 = 0.5$ fmol C_{Sp} / μm^3. b) The initial substrate concentration was $S_0 = 5$ fmol C_{Sp} / μm^3.

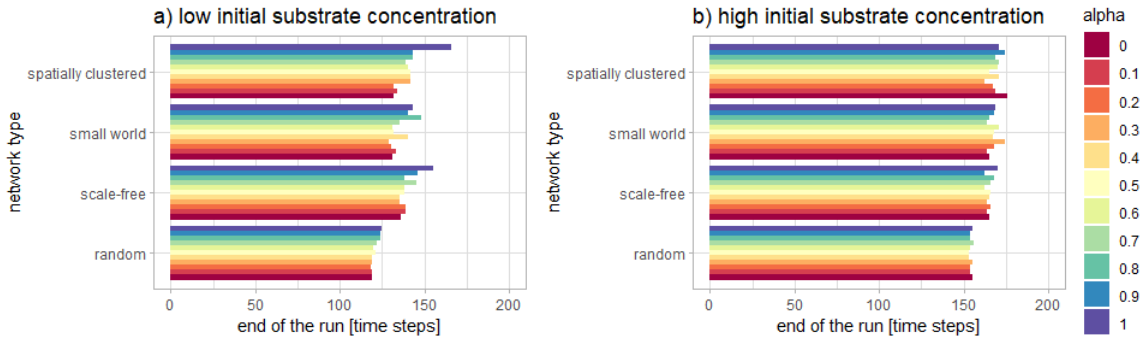

Figure 6.23: Time until 70% of the initial substrate were degraded for different alpha

Time until 70% of the initial substrate were degraded for different levels of heterogeneity in the primary substrate distribution in all network types. The average node degree was 2.7 for all networks. Averaged over 5 runs. a) The initial substrate concentration was $S_0 = 0.5$ fmol C_{Sp} / μm^3. b) The initial substrate concentration was $S_0 = 5$ fmol C_{Sp} / μm^3.

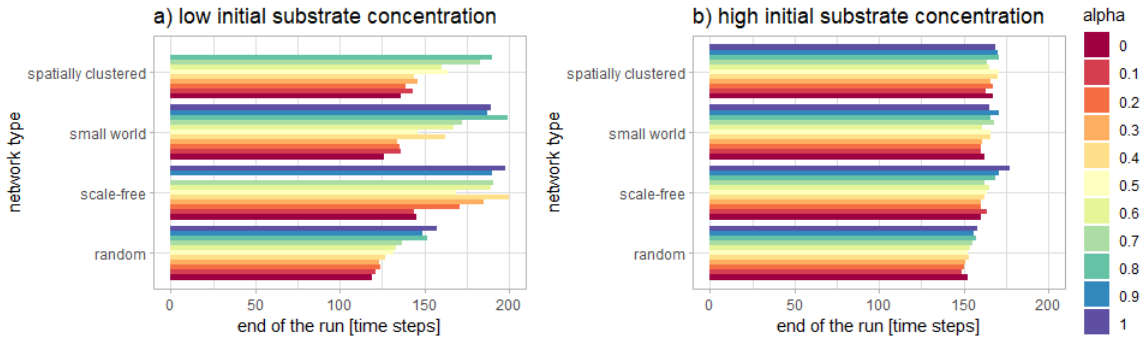

Figure 6.24: Time until 70% of the initial substrate were degraded for different alpha

Time until 70% of the initial substrate were degraded for different levels of heterogeneity in B_{max} in all network types. The average node degree was 2.7 for all networks. Averaged over 5 runs. a) The initial substrate concentration was $S_0 = 0.5$ fmol C_{Sp} / μm^3. b) The initial substrate concentration was $S_0 = 5$ fmol C_{Sp} / μm^3.

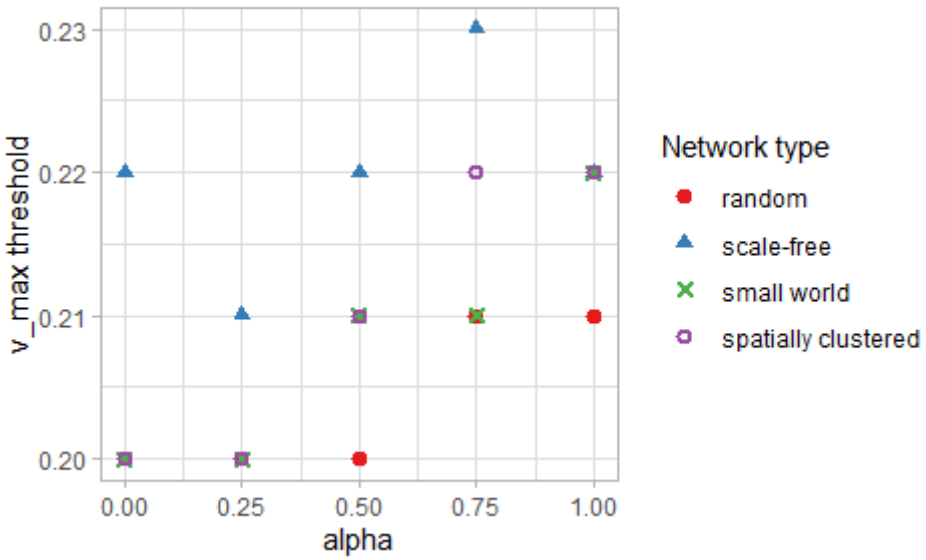

Figure 6.25: Threshold of v_{max} for invasion of more than 80% of the pores

Minimum v_{max} value that enables large-scale invasion of the pore network for different heterogeneity in B_{max} in all network types. The average node degree was 2.7 for all networks. Averaged over 5 runs. The initial substrate concentration was $S_0 = 0.5$ fmol C_{Sp} / μm^3.

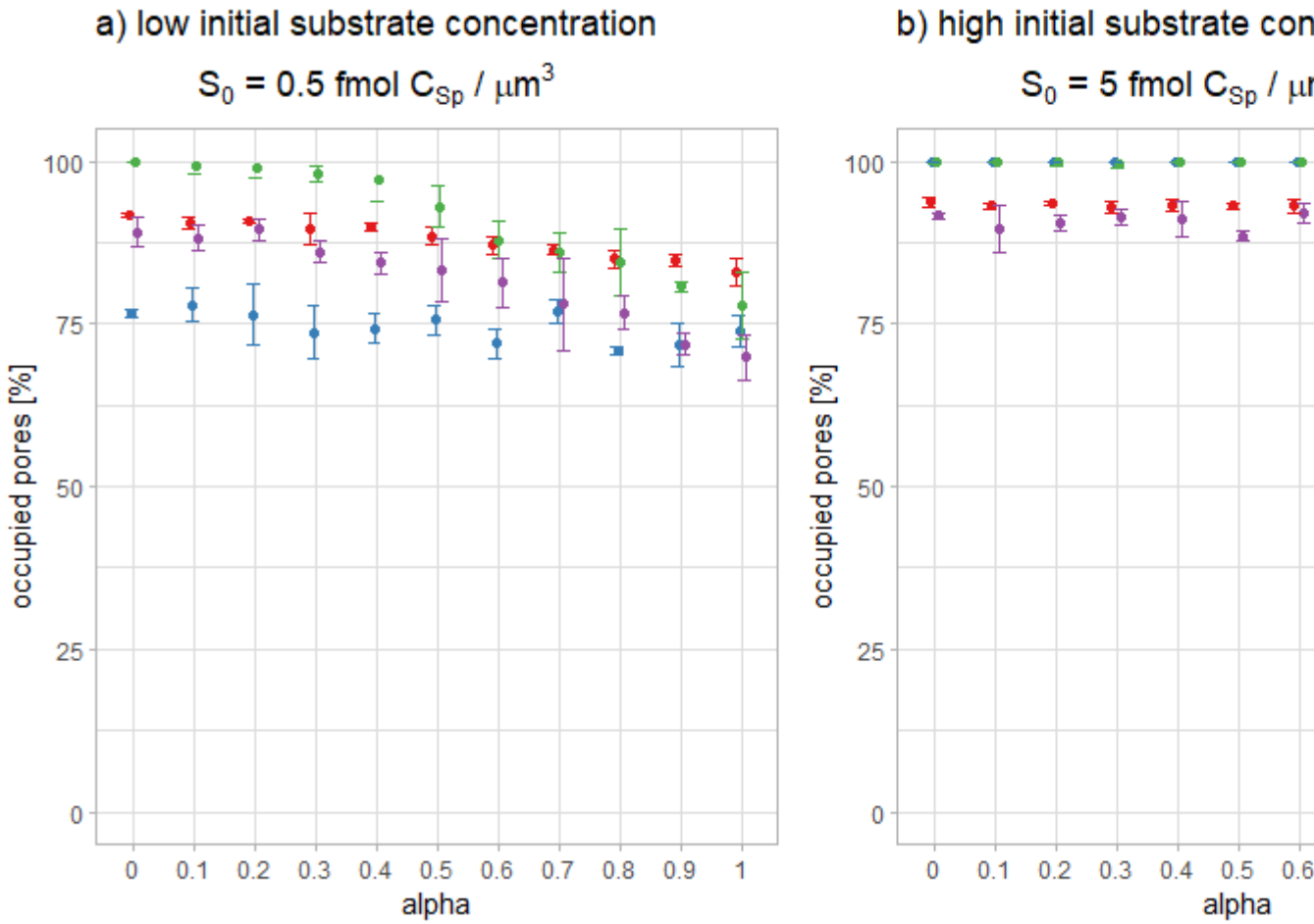

Figure 6.26: Number of occupied pores for different levels of heterogeneity in B_{max}

Number of occupied pores for different levels of heterogeneity in B_{max} in all network types. The average node degree was 2.7 for all networks. Averaged over 5 runs. a) The initial substrate concentration was $S_0 = 0.5$ fmol C_{Sp} / μm^3. b) The initial substrate concentration was $S_0 = 5$ fmol C_{Sp} / μm^3.

The results shown in this figure indicate that the invasion is less efficient a more heterogeneous pore space. With low substrate concentration the number of occupied pores in all network types is much smaller when B_{max} is very heterogeneous. With low heterogeneity, an average of about 90% of the pores can be reached by microbes in the random network, with this value being reduced to as low as 83% at high heterogeneity. In the scale-free network, on average 77% of the pores can be reached at low heterogeneity and only 72% at high heterogeneity. Also, in the small world network the invasion efficiency is reduced from 100% with no heterogeneity to a minimum of 78% with the highest heterogeneity. In the spatially clustered network with homogeneous B_{max} on average 89% of the pores were invaded, whereas at high heterogeneity only 70% were reached.

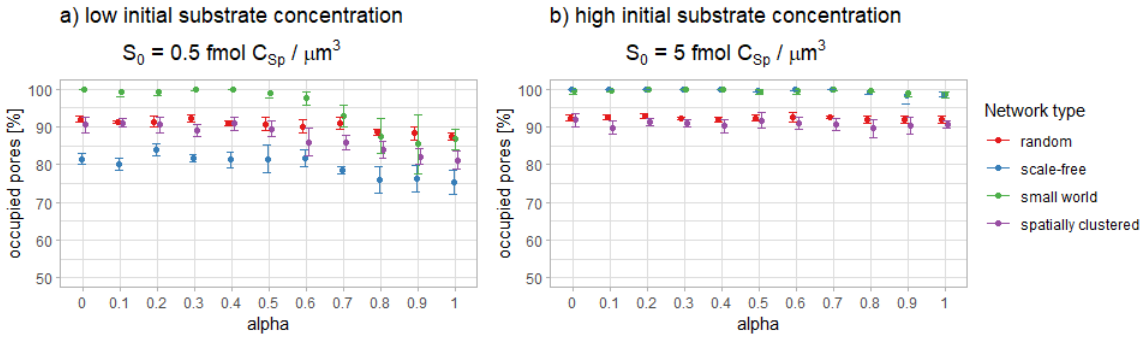

Figure 6.27: Number of occupied pores for different levels of heterogeneity in distribution of initial substrate

Number of occupied pores that were invaded in all network types. The average node degree was 2.7 for all networks. Averaged over 5 runs. a) The initial substrate concentration was $S_0 = 0.5$ fmol C_{Sp} / μm^3. b) The initial substrate concentration was $S_0 = 5$ fmol C_{Sp} / μm^3.

Chapter 7

Summary

Microbial decomposition of soil organic matter is the foundation of nutrient and carbon cycling in terrestrial ecosystems. A substantial body of research has been devoted to understanding the interconnected physical, chemical and biological processes related to soil microbial activity, that are crucial for some of the most urgent societal issues of today, like greenhouse gas emission or primary plant production. Soils are highly heterogeneous habitats built up hierarchically from soil aggregates that provide a complex pore system. An enormous diversity of microbes occupies the physically and chemically heterogeneous pore space. Although, in recent decades the consensus has largely been established, that microbial processes are strongly affected by the spatially heterogeneous architecture of the soil pore space and the patchy distribution of substrate, still, the integration of pore network characteristics in models of microbial activity is scarce.
We use an Agent-based modelling approach to address the question how the architecture of the soil pore network impacts the efficiency in soil microbial organic matter decomposition.

1. How does network structure affect the efficiency of organic matter decomposition?
2. How do network properties like average node degree, shortest path length, and clustering coefficient affect the efficiency of organic matter decomposition?
3. Can additional heterogeneity regarding pore properties affect microbial efficiency?

To acknowledge the spatial heterogeneity of the pore space the soil pores are modelled as nodes of a network connected via links. Specific attributes are assigned to the nodes to describe their physical and chemical conditions. Microbes occupy parts of the network and degrade organic matter that is available to them. Depending on microbial growth new pores can be invaded through the connecting links.
We were able to determine a number of network properties that affect the decomposition efficiency of soil microbes. While high clustering of nodes enables nearly complete decomposition of substrate, the presence of highly connected nodes (hubs) can decrease the efficiency of decomposition and lead to higher amount of substrate that remains undegraded. While the presence of hubs generally does not impact the time needed for decomposition, high clustering slows down decomposition. The impact of the clustering is not affected by the

initial substrate concentration, whereas the presence of hubs particularly in low substrate regimes leads to large amounts of initial substrate remaining undegraded.Regarding microbial growth parameters, the system showes a threshold behaviour. For too low microbial growth, microbes live only in the initially occupied pores and are not able to invade new pores. When the substrate concentration or the growth rate reaches a threshold value, there is a jump to large-scale invasion of all reachable pores in the network and much higher efficiency in the decomposition. In addition, high heterogeneity in pore properties lead to lower invasion efficiency, lower decomposition rate and a higher amount of substrate that is left at the end. These findings allow for better understanding of the impact of soil pore network architecture on microbial processes and further for more accurate assessment of the impact of climate change on soil microbial processes.

Chapter 8

Zusammenfassung

Die Zersetzung organischen Materials durch Mikroorganismen im Boden ist die Grundlage des Nährstoff- und Kohlenstoffkreislaufs in terrestrischen Ökosystemen. Ein beträchtlicher Teil der Forschung ist dem Verständnis der miteinander verbundenen physikalischen, chemischen und biologischen Prozesse im Zusammenhang mit der mikrobiellen Aktivität des Bodens gewidmet, die für einige der dringlichsten gesellschaftlichen Probleme von heute, wie die Emission von Treibhausgasen oder die primäre Pflanzenproduktion, von entscheidender Bedeutung sind. Böden sind aufgrund ihres hierarchischen Aufbaus aus Bodenaggregaten, die ein komplexes Porensystem bilden, sehr heterogene Lebensräume. Eine große Vielfalt von Mikroorganismen besiedelt diesen physikalisch und chemisch heterogenen Porenraum. Obwohl schon seit einigen Jahrzehnten weitestgehender Konsns darüber besteht, dass mikrobielle Prozesse stark von der räumlich heterogenen Architektur des Bodenporenraums und der ungleichmäßigen Verteilung des Substrats beeinflusst werden, werden die Eigenschaften des Porennetzes nur selten in Modellen des mikrobiellen Abbaus von organischen Material berücksichtigt.
Wir verwenden einen agentenbasierten Modellierungsansatz, um die folgenden Fragen zu beantworten:

1. Wie beeinflusst die Netzwerkarchitektur die Effizienz des Abbaus organischen Materials?

2. Wie wirken sich Netzwerkeigenschaften wie *'average node degree'*, *'shortest path length'* und *'clustering coefficient'* auf die Effizienz des Abbaus organischen Materials aus?

3. Kann zusätzliche Heterogenität hinsichtlich der Poreneigenschaften die Effizienz des Abbaus beeinflussen?

Um die räumliche Heterogenität des Porenraums darzustellen, werden die Bodenporen als Knoten (*'nodes'*) eines über Kanten (*'links'* verbundenen Netzwerks modelliert. Den Knoten werden spezifische Attribute zugewiesen, um ihre physikalischen und chemischen Bedingungen zu beschreiben. Mikroorganismen bewohnen Teile des Netzwerks und bauen organisches Material ab, das ihnen zur Verfügung steht. Abhängig vom mikrobiellen Wachstum können benachbarte Poren über die verbindenden Kanten erreicht werden.

Wir konnten eine Reihe von Netzwerkeigenschaften bestimmen, die sich auf die Effizienz des Abbaus durch Bodenmikroorganismen auswirken. Während eine starke Clusterbildung der Knoten eine nahezu vollständige Zersetzung des Substrats ermöglicht, kann das Vorhandensein weniger, sehr vernetzter Knoten (*'hubs'*) die Effizienz des Abbaus verringern und dazu führen, dass ein größerer Anteil des Substrats unzersetzt bleibt. Während das Vorhandensein von *hubs* im Allgemeinen keinen Einfluss auf die Dauer des Abbaus hat, verlangsamt eine starke Clusterbildung den Abbau. Die Auswirkungen der Clusterbildung werden durch die anfängliche Substratkonzentration nicht beeinflusst, während das Vorhandensein von *hubs* insbesondere bei niedrigen Substratkonzentrationen dazu führt, dass große Mengen des anfänglichen Substrats unzersetzt bleiben. Was die mikrobiellen Wachstumsparameter betrifft, so zeigt das System ein Schwellenverhalten. Bei zu geringem mikrobiellen Wachstum leben die Mikroorganismen nur in den ursprünglich besetzten Poren und sind nicht in der Lage, in neue Poren vorzudringen. Wenn die Substratkonzentration oder die Wachstumsrate einen Schwellenwert erreicht, kommt es zu einem sprunghaften Anstieg der Invasion in alle erreichbaren Poren des Netzwerks und zu einer wesentlich höheren Effizienz bei der Zersetzung. Außerdem führt zusätzliche Heterogenität in anderen Poreneigenschaften zu einer geringeren Invasionseffizienz, einer geringeren Zersetzungsrate und einer größeren Menge an Substrat, die am Ende übrig bleibt.
Diese Ergebnisse ermöglichen ein besseres Verständnis des Einflusses der Architektur des Bodenporennetzes auf mikrobielle Abbau-Prozesse und darüber hinaus eine bessere Abschätzung der Auswirkungen des Klimawandels auf mikrobielle Prozesse im Boden.

Chapter 9

References

Steven D. Allison. Cheaters, diffusion and nutrients constrain decomposition by microbial enzymes in spatially structured environments. *Ecology letters*, 8(6):626–635, 2005. doi: 10.1111/j.1461-0248.2005.00756.x.

Marc Barthélemy. Spatial networks. *Physics Reports*, 499(1-3):1–101, 2011. ISSN 03701573. doi: 10.1016/j. physrep.2010.11.002.

Philippe C. Baveye, Wilfred Otten, Alexandra Kravchenko, María Balseiro-Romero, Éléonore Beckers, Maha Chalhoub, Christophe Darnault, Thilo Eickhorst, Patricia Garnier, Simona Hapca, Serkan Kiranyaz, Olivier Monga, Carsten W. Mueller, Naoise Nunan, Valérie Pot, Steffen Schlüter, Hannes Schmidt, and Hans-Jörg Vogel. Emergent properties of microbial activity in heterogeneous soil microenvironments: Different research approaches are slowly converging, yet major challenges remain. *Frontiers in microbiology*, 9:1929, 2018. ISSN 1664-302X. doi: 10.3389/fmicb.2018.01929.

Jennifer K. Carson, Vanesa Gonzalez-Quiñones, Daniel V. Murphy, Christoph Hinz, Jeremy A. Shaw, and Deirdre B. Gleeson. Low pore connectivity increases bacterial diversity in soil. *Applied and environmental microbiology*, 76(12):3936–3942, 2010. doi: 10.1128/AEM.03085-09.

P. Ciais, C. Sabine, G. Bala, L. Bopp, V. Brovkin, J. Canadell, A. Chhabra, R. DeFries, J. Galloway, M. Heimann, C. Jones, C. Le Quéré, R.B. Myneni, S. Piao, and P. Thornton. Carbon and other biogeochemical cycles. In D. Qin G.-K. Plattner M. Tignor S.K. Allen J. Boschung A. Nauels Y. Xia V. Bex Stocker, T.F. and P.M. Midgley, editors, *Climate Change 2013: The Physical Science Basis. Contribution of Working Group I to the Fifth Assessment Report of the Intergovernmental Panel on Climate Change*. Cambridge University Press, Cambridge, United Kingdom and New York, NY, USA, 2013.

Alexandre Coche, Tristan Babey, Alain Rapaport, Laure Vieublé Gonod, Patricia Garnier, Naoise Nunan, and Jean-Raynald de Dreuzy. *Competition within low-density bacterial populations as an unexpected factor regulating carbon decomposition in bulk soil*. 2020. doi: 10.1101/2020.11.16.384735.

D. E. Contois. Kinetics of bacterial growth: relationship between population density and specific growth rate of continuous cultures. *Journal of general microbiology*, 21:40–50, 1959. ISSN 0022-1287. doi: 10.1099/00221287-21-1-40.

T. W. Crowther, K. E. O. Todd-Brown, C. W. Rowe, W. R. Wieder, J. C. Carey, M. B. Machmuller, B. L. Snoek, S. Fang, G. Zhou, S. D. Allison, J. M. Blair, S. D. Bridgham, A. J. Burton, Y. Carrillo, P. B. Reich, J. S. Clark, A. T. Classen, F. A. Dijkstra, B. Elberling, B. A. Emmett, M. Estiarte, S. D. Frey, J. Guo, J. Harte, L. Jiang, B. R. Johnson, G. Kröel-Dulay, K. S. Larsen, H. Laudon, J. M. Lavallee, Y. Luo, M. Lupascu, L. N. Ma, S. Marhan, A. Michelsen, J. Mohan, S. Niu, E. Pendall, J. Peñuelas, L. Pfeifer-Meister, C. Poll, S. Reinsch, L. L. Reynolds, I. K. Schmidt, S. Sistla, N. W. Sokol, P. H. Templer, K. K. Treseder, J. M. Welker, and M. A. Bradford. Quantifying global soil carbon losses in response to warming. *Nature*, 540(7631):104–108, 2016. doi: 10.1038/nature20150.

Jennifer A. J. Dungait, David W. Hopkins, Andrew S. Gregory, and Andrew P. Whitmore. Soil organic matter turnover is governed by accessibility not recalcitrance. *Global Change Biology*, 18(6):1781–1796, 2012. ISSN 13541013. doi: 10.1111/j.1365-2486.2012.02665.x.

Ali N. Ebrahimi and Dani Or. Microbial dispersal in unsaturated porous media: Characteristics of motile bacterial cell motions in unsaturated angular pore networks. *Water Resources Research*, 50(9):7406–7429, 2014. ISSN 00431397. doi: 10.1002/2014 WR015897.

Ali N. Ebrahimi, Saeid Jamshidi, Stefan Iglauer, and Ramin B. Boozarjomehry. Genetic algorithm-based pore network extraction from micro-computed tomography images. *Chemical Engineering Science*, 92:157–166, 2013. ISSN 00092509. doi: 10.1016/j.ces.2013.01.045.

Pete Falloon, Chris D. Jones, Melanie Ades, and Keryn Paul. Direct soil moisture controls of future global soil carbon changes: An important source of uncertainty. *Global Biogeochemical Cycles*, 25(3):n/a–n/a, 2011. ISSN 08866236. doi: 10.1029/2010GB003938.

Noah Fierer. Embracing the unknown: disentangling the complexities of the soil microbiome. *Nature reviews. Microbiology*, 15(10):579–590, 2017. doi: 10.1038/nrmicro.2017.87.

Amir Golparvar, Matthias Kästner, and Martin Thullner. Pore–scale modeling of microbial activity: What we have and what we need. *Vadose Zone Journal*, 20(1), 2021. ISSN 1539-1663. doi: 10.1002/vzj2.20087.

Martin Heimann and Markus Reichstein. Terrestrial ecosystem carbon dynamics and climate feedbacks. *Nature*, 451(7176):289–292, 2008. doi: 10.1038/nature06591.

Julian Heitkötter and Bernd Marschner. Soil zymography as a powerful tool for exploring hotspots and substrate limitation in undisturbed subsoil. *Soil Biology and Biochemistry*, 124:210–217, 2018. ISSN 00380717. doi: 10.1016/j. soilbio.2018.06.021.

Christina Kaiser, Oskar Franklin, Ulf Dieckmann, and Andreas Richter. Microbial community dynamics alleviate stoichiometric constraints during litter decay. *Ecology letters*, 17(6):680–690, 2014. doi: 10.1111/ele.12269.

Christina Kaiser, Oskar Franklin, Andreas Richter, and Ulf Diekmann. Social dynamics within decomposer communities lead to nitrogen retention and organic matter build-up in soils. *Nature communications*, 6:8960, 2015. doi: 10.1038/ncomms9960.

Matt J. Keeling and Ken T. D. Eames. Networks and epidemic models. *Journal of the Royal Society, Interface*, 2(4):295–307, 2005. ISSN 1742-5689. doi: 10.1098/rsif.2005.0051.

M. Kleber, P. Sollins, and R. Sutton. A conceptual model of organo-mineral interactions in soils: self-assembly of organic molecular fragments into zonal structures on mineral surfaces. *Biogeochemistry*, 85(1):9–24, 2007. ISSN 0168-2563. doi: 10.1007/s10533-007-9103-5.

Sara König, Hans-Jörg Vogel, Hauke Harms, and Anja Worrich. Physical, chemical and biological effects on soil bacterial dynamics in microscale models. *Frontiers in Ecology and Evolution*, 8, 2020. doi: 10.3389/fevo.2020.00053.

A. N. Kravchenko, A. N. W. Wang, A. J. M. Smucker, and M. L. Rivers. Long-term differences in tillage and land use affect intra-aggregate pore heterogeneity. *Soil Science Society of America Journal*, 75(5):1658–1666, 2011. ISSN 03615995. doi: 10.2136/sssaj2011.0096.

A. N. Kravchenko, A. K. Guber, B. S. Razavi, J. Koestel, M. Y. Quigley, G. P. Robertson, and Y. Kuzyakov. Microbial spatial footprint as a driver of soil carbon stabilization. *Nature communications*, 10(1):3121, 2019. doi: 10.1038/s41467-019-11057-4. URL `https://www.nature.com/articles/s41467-019-11057-4citeas`.

Stefano Manzoni, Philip Taylor, Andreas Richter, Amilcare Porporato, and Göran I. Ågren. Environmental and stoichiometric controls on microbial carbon-use efficiency in soils. *The New phytologist*, 196(1):79–91, 2012. doi: 10.1111/j.1469-8137.2012.04225.x.

Bruno Mbé, Olivier Monga, Valérie Pot, Wilfred Otten, Frédéric Hecht, Xavier Raynaud, Naoise Nunan, Claire Chenu, Philippe C. Baveye, and Patricia Garnier. Scenario modelling of carbon mineralization in 3d soil architecture at the microscale: Toward an accessibility coefficient of organic matter for bacteria. *European Journal of Soil Science*, 73(1), 2022. ISSN 1351-0754. doi: 10.1111/ejss.13144.

Manoj Menon, Tinashe Mawodza, Arash Rabbani, Aimeric Blaud, Georg J. Lair, Masoud Babaei, Milena Kercheva, Svetala Rousseva, and Steven Banwart. Pore system characteristics of soil aggregates and their relevance to aggregate stability. *Geoderma*, 366:114259, 2020. ISSN 00167061. doi: 10.1016/j. geoderma.2020.114259.

Joel C. Miller. Epidemic size and probability in populations with heterogeneous infectivity and susceptibility. *Physical review. E, Statistical, nonlinear, and soft matter physics*, 76 (1 Pt 1):010101, 2007. ISSN 1539-3755. doi: 10.1103/PhysRevE.76.010101.

O. Monga, P. Garnier, V. Pot, E. Coucheney, N. Nunan, W. Otten, and C. Chenu. Simulating microbial degradation of organic matter in a simple porous system using the 3-d diffusion-

based model mosaic. *Biogeosciences*, 11(8):2201–2209, 2014. doi: 10.5194/bg-11-2201-2014.

Olivier Monga, Mamadou Bousso, Patricia Garnier, and Valérie Pot. 3d geometric structures and biological activity: Application to microbial soil organic matter decomposition in pore space. *Ecological Modelling*, 216(3-4):291–302, 2008. ISSN 03043800. doi: 10.1016/j.ecolmodel.2008.04.015.

P. Nannipieri, J. Ascher, M. T. Ceccherini, L. Landi, G. Pietramellara, and G. Renella. Microbial diversity and soil functions. *European Journal of Soil Science*, 54(4):655–670, 2003. ISSN 1351-0754. doi: 10.1046/j.1351-0754.2003.0556.x.

P. Nannipieri, J. Ascher, M. T. Ceccherini, L. Landi, G. Pietramellara, and G. Renella. Microbial diversity and soil functions. *European Journal of Soil Science*, 68(1):12–26, 2017. ISSN 1351-0754. doi: 10.1111/ejss.4 _12398.

Mark Needham and Amy E. Hodler. *Graph algorithms: Practical examples in Apache Spark and Neo4j*. O'Reilly Media, Sebastopol and Beijing and Boston and Farnham and Tokyo, first edition edition, 2019. ISBN 9781492047681.

Joseph Nesme, Wafa Achouak, Spiros N. Agathos, Mark Bailey, Petr Baldrian, Dominique Brunel, Åsa Frostegård, Thierry Heulin, Janet K. Jansson, Edouard Jurkevitch, Kristiina L. Kruus, George A. Kowalchuk, Antonio Lagares, Hilary M. Lappin-Scott, Philippe Lemanceau, Denis Le Paslier, Ines Mandic-Mulec, J. Colin Murrell, David D. Myrold, Renaud Nalin, Paolo Nannipieri, Josh D. Neufeld, Fergal O'Gara, John J. Parnell, Alfred Pühler, Victor Pylro, Juan L. Ramos, Luiz F. W. Roesch, Michael Schloter, Christa Schleper, Alexander Sczyrba, Angela Sessitsch, Sara Sjöling, Jan Sørensen, Søren J. Sørensen, Christoph C. Tebbe, Edward Topp, George Tsiamis, Jan Dirk van Elsas, Geertje van Keulen, Franco Widmer, Michael Wagner, Tong Zhang, Xiaojun Zhang, Liping Zhao, Yong-Guan Zhu, Timothy M. Vogel, and Pascal Simonet. Back to the future of soil metagenomics. *Frontiers in microbiology*, 7:73, 2016. ISSN 1664-302X. doi: 10.3389/fmicb.2016.00073.

M. E. J. Newman. Properties of highly clustered networks. *Physical review. E, Statistical, nonlinear, and soft matter physics*, 68(2 Pt 2):026121, 2003. ISSN 1539-3755. doi: 10.1103/PhysRevE.68.026121.

Mark Newman. *Networks*. Oxford University Press USA - OSO, Oxford, 2nd ed. edition, 2018. ISBN 9780192527493.

Ndeye Fatou Ngom, Patricia Garnier, Olivier Monga, and Stephan Peth. Extraction of three-dimensional soil pore space from microtomography images using a geometrical approach. *Geoderma*, 163(1-2):127–134, 2011. ISSN 00167061. doi: 10.1016/j.geoderma.2011.04.013.

Naoise Nunan, Kejian Wu, Iain M. Young, John W. Crawford, and Karl Ritz. Spatial distribution of bacterial communities and their relationships with the micro-architecture of soil.

FEMS microbiology ecology, 44(2):203–215, 2003. doi: 10.1016/S0168-6496(03)00027-8.

Romualdo Pastor-Satorras, Claudio Castellano, Piet van Mieghem, and Alessandro Vespignani. Epidemic processes in complex networks. *Reviews of Modern Physics*, 87 (3):925–979, 2015. ISSN 0034-6861. doi: 10.1103/RevModPhys.87.925. URL `http://arxiv.org/pdf/1408.2701v2`.

F. J. Pérez-Reche, S. N. Taraskin, W. Otten, M. P. Viana, L. F. Da Costa, and C. A. Gilligan. Prominent effect of soil network heterogeneity on microbial invasion. *Physical review letters*, 109(9):098102, 2012. doi: 10.1103/PhysRevLett.109.098102.

S. Peth, R. Horn, F. Beckmann, T. Donath, J. Fischer, and A. J. M. Smucker. Three-dimensional quantification of intra-aggregate pore-space features using synchrotron-radiation-based microtomography. *Soil Science Society of America Journal*, 72(4):897–907, 2008. ISSN 03615995. doi: 10.2136/sssaj2007.0130.

Janna Pietikäinen, Marie Pettersson, and Erland Bååth. Comparison of temperature effects on soil respiration and bacterial and fungal growth rates. *FEMS microbiology ecology*, 52 (1):49–58, 2005. doi: 10.1016/j. femsec.2004.10.002.

V. Pot, S. Peth, O. Monga, L. E. Vogel, A. Genty, P. Garnier, L. Vieublé-Gonod, M. Ogurreck, F. Beckmann, and P. C. Baveye. Three-dimensional distribution of water and air in soil pores: Comparison of two-phase two-relaxation-times lattice-boltzmann and morphological model outputs with synchrotron x-ray computed tomography data. *Advances in Water Resources*, 84:87–102, 2015. ISSN 03091708. doi: 10.1016/j. advwatres.2015.08.006.

Valérie Pot, Xavier Portell, Wilfred Otten, Patricia Garnier, Olivier Monga, and Philippe C. Baveye. Accounting for soil architecture and microbial dynamics in microscale models: Current practices in soil science and the path ahead. *European Journal of Soil Science*, 73(1), 2022. ISSN 1351-0754. doi: 10.1111/ejss.13142.

Matthias C. Rillig, Ludo Ah Muller, and Anika Lehmann. Soil aggregates as massively concurrent evolutionary incubators. *The ISME journal*, 11(9):1943–1948, 2017. doi: 10.1038/ismej.2017.56.

Erin C. Rooney, Vanessa L. Bailey, Kaizad F. Patel, Maria Dragila, Anil K. Battu, Alexander C. Buchko, Adrian C. Gallo, Jeffery Hatten, Angela R. Possinger, Odeta Qafoku, Loren.R. Reno, Michael SanClements, Tamas Varga, and Rebecca A. Lybrand. Soil pore network response to freeze-thaw cycles in permafrost aggregates. *Geoderma*, 411:115674, 2022. ISSN 00167061. doi: 10.1016/j. geoderma.2021.115674.

Joshua Schimel and Michael N. Weintraub. The implications of exoenzyme activity on microbial carbon and nitrogen limitation in soil: A theoretical model. *Soil Biology Biochemistry*, (35):549–563, 11 2003.

Joshua P. Schimel and Sean M. Schaeffer. Microbial control over carbon cycling in soil. *Frontiers in microbiology*, 3:348, 2012. ISSN 1664-302X. doi: 10.3389/fmicb.2012.00348.

Michael Schloter, Paolo Nannipieri, Søren J. Sørensen, and Jan Dirk van Elsas. Microbial indicators for soil quality. *Biology and Fertility of Soils*, 54(1):1–10, 2018. ISSN 0178-2762. doi: 10.1007/s00374-017-1248-3.

Onkur Sen and Sandip Sen. Effects of social network topology and options on norm emergence. In David Hutchison, Takeo Kanade, Josef Kittler, Jon M. Kleinberg, Friedemann Mattern, John C. Mitchell, Moni Naor, Oscar Nierstrasz, C. Pandu Rangan, Bernhard Steffen, Madhu Sudan, Demetri Terzopoulos, Doug Tygar, Moshe Y. Vardi, Gerhard Weikum, Julian Padget, Alexander Artikis, Wamberto Vasconcelos, Kostas Stathis, Viviane Torres Da Silva, Eric Matson, and Axel Polleres, editors, *Coordination, Organizations, Institutions and Norms in Agent Systems V*, volume 6069 of *Lecture Notes in Computer Science*, pages 211–222. Springer Berlin Heidelberg, Berlin, Heidelberg, 2010. ISBN 978-3-642-14961-0. doi: 10.1007/978-3-642-14962-7 _14.

Robert L. Sinsabaugh, Stefano Manzoni, Daryl L. Moorhead, and Andreas Richter. Carbon use efficiency of microbial communities: stoichiometry, methodology and modelling. *Ecology letters*, 16(7):930–939, 2013. doi: 10.1111/ele.12113.

Robin Tecon and Dani Or. Bacterial flagellar motility on hydrated rough surfaces controlled by aqueous film thickness and connectedness. *Scientific reports*, 6:19409, 2016. doi: 10.1038/srep19409.

Laure E. Vogel, David Makowski, Patricia Garnier, Laure Vieublé-Gonod, Yves Coquet, Xavier Raynaud, Naoise Nunan, Claire Chenu, Ruth Falconer, and Valérie Pot. Modeling the effect of soil meso- and macropores topology on the biodegradation of a soluble carbon substrate. *Advances in Water Resources*, 83:123–136, 2015. ISSN 03091708. doi: 10.1016/j. advwatres.2015.05.020.

Gangsheng Wang, Wilfred M. Post, Melanie A. Mayes, Joshua T. Frerichs, and Jagadamma Sindhu. Parameter estimation for models of ligninolytic and cellulolytic enzyme kinetics. *Soil Biology and Biochemistry*, 48:28–38, 2012. ISSN 00380717. doi: 10.1016/j. soilbio.2012.01.011.

Ulrich Weller, Lukas Albrecht, Steffen Schlüter, and Hans-Jörg Vogel. An open soil structure library based on x-ray ct data. *SOIL*, 8(2):507–515, 2022. doi: 10.5194/soil-8-507-2022.

U. Wilensky. Netlogo, 1999.

Regina L. Wilpiszeski, Jayde A. Aufrecht, Scott T. Retterer, Matthew B. Sullivan, David E. Graham, Eric M. Pierce, Olivier D. Zablocki, Anthony V. Palumbo, and Dwayne A. Elias. Soil aggregate microbial communities: Towards understanding microbiome interactions at biologically relevant scales. *Applied and environmental microbiology*, 85(14), 2019. doi: 10.1128/AEM.00324-19.

Zhuoting Wu, Paul Dijkstra, George W. Koch, Josep Peñuelas, and Bruce A. Hungate. Responses of terrestrial ecosystems to temperature and precipitation change: a meta-

analysis of experimental manipulation. *Global Change Biology*, 17(2):927–942, 2011. ISSN 13541013. doi: 10.1111/j.1365-2486.2010.02302.x.

V. V. Zelenev, A.H.C. van Bruggen, and A. M. Semenov. Modeling wave-like dynamics of oligotrophic and copiotrophic bacteria along wheat roots in response to nutrient input from a growing root tip. *Ecological Modelling*, 188(2-4):404–417, 2005. ISSN 03043800. doi: 10.1016/j. ecolmodel.2005.01.046.

Hu Zhou, Huan Fang, Sacha Jon Mooney, and Xinhua Peng. Effects of long-term inorganic and organic fertilizations on the soil micro and macro structures of rice paddies. *Geoderma*, 266:66–74, 2016. ISSN 00167061. doi: 10.1016/j. geoderma.2015.12.007.